Characterization of human Neuropsin (hOPN5) and development of new mutants for optogenetic stimulation of the G_q signaling cascade

Dissertation

for the award of the degree

"Doctor rerum naturalium" (Dr.rer.nat.)

of the Georg-August-Universität Göttingen

within the doctoral program Cardiovascular Science

of the Georg-August University School of Science (GAUSS)

submitted by

Udhaya Bhaskar Sathya Narayanan

born in

Coimbatore, India

Göttingen, 2023

Members of the Thesis Committee

Prof. Dr. med. Dr. rer. nat. Tobias Brügmann
Institute of Cardiovascular Physiology, University Medical Center, Göttingen

Prof. Dr. med. Tobias Moser
Institute for Auditory Neuroscience and Inner ear laboratory, University Medical Center, Göttingen

Prof. Dr. rer. nat. Ralph Kehlenbach
Department of Molecular Biology, University Medical Center, Göttingen

Members of the Examination Board

Reviewer: Prof. Dr. Dr. Oliver Schlüter
Department of Psychiatry and Psychotherapy, University Medical Center, Göttingen

Second Reviewer: Prof. Dr. rer. nat. Susanne Lutz
Department of Pharmacology and Toxicology, University Medical Center, Göttingen

Additional Reviewer: Prof. Dr. Tim Gollisch
Department of Sensory Processing in the Retina, University Medical Center, Göttingen

Date of the thesis submission: 30th June 2023

Date of the oral examination: 21st August 2023

dedicated

- to my beloved wife -

- to my parents -

List of publications

Wagdi, A., Malan, D., **Sathyanarayanan, U**. et al. Selective optogenetic control of G_q signaling using human Neuropsin. **Nat Commun** 13, 1765 (2022). https://doi.org/10.1038/s41467-022-29265-w

Abstract

G_q signaling plays a pivotal role in the physiological adaptation of cellular behavior based on the individual body's needs and it is also involved in the pathogenesis of many diseases including cancer, autoimmunity, pathological cardiac hypertrophy, and heart failure. However, the transition between physiological and pathological signaling and the underlying kinetics is not well understood since current approaches with pharmacological stimulation and genetic modulation lack spatiotemporal precision. In striking contrast, optogenetic G protein-coupled receptor (GPCR) stimulation offers an unprecedented advantage of high temporal and spatial precision with the chance of cell-specific expression. Therefore, an optogenetic GPCR would be an ideal tool to study the transitions between physiological and pathological G_q signaling and the underlying kinetics.

In this thesis, I characterized wild-type (WT) Neuropsin (OPN5), an ultra-violet (UV) light-sensitive bistable GPCR, to prove its selective activation of the G_q pathway in heterologous expression systems and a transgenic mouse model. UV light-induced Inositol 1,4,5 trisphosphate (IP_3) production as well as the activation of transient receptor potential canonical cation channel 6 (TRPC6) channels by Diacylglycerol (DAG) was demonstrated in transgenic HEK293 hOPN5 (WT) cells. Using Ca^{2+} imaging, with red-shifted Xanthene-based rhodamine like Ca^{2+} fluorescent indicator-1 (X-Rhod-1, 1.5 µM), the light sensitivity (3.26 ± 0.17 µW/mm^2, n=17) and the most efficient wavelength for activation (388 ± 2.7 nm, n=14) were determined for hOPN5 (WT). I further compared light with pharmacological stimulation and also proved that light-stimulated Ca^{2+} transients were abolished in $G_{q/11}$ knock-out (KO) cells while the Ca^{2+} transients were preserved in G_i KO cells. G protein activated inward rectifying K^+ (GIRK) channel assay excluded the promiscuous G_i coupling of hOPN5 (WT) in HEK293 cells.

By combining structural modeling and sequence alignments, a few mutations were predicted around the 8 Å region of the retinal chromophore to alter the photo-excited state, thereby having a fine-tuned activation spectrum and altered kinetics. The expression rate and expression strength of the transgenic hOPN5 mutant cells along with chicken OPN5 (cOPN5) cells were analyzed. They were further characterized using Ca^{2+} imaging. The light sensitivities were ranging from (eLi50 in µW/mm^2) 160 to 2. The most efficient wavelength for activation was shifted maximally from 388 ± 2.7 (hOPN5 (WT), n=10) to 406 ± 2.5 (cOPN5, n=10). Investigation of the retinal dependence among OPN5s hinted at the importance of threonine to alanine mutation.

Taken together, hOPN5 is a selective optogenetic tool to control G_q signaling in cells, tissues, and organs. Further, the development of new hOPN5 mutants which are expected to have altered spectral properties would pave the way for a foundation to better understand the structural

properties and important amino acid positions of OPN5 with the aid of Molecular dynamics (MD) simulations. Finally, the goal is to develop enhanced and highly efficient OPN5-based optogenetic tools in the future to control organ function.

Table of contents

List of figures

List of tables

Abbreviations

°C	Degree Celsius
µg	microgram
µs	microseconds
µW	microwatt
Å	Angstrom
A1 AR	A1 Adenosine receptors
ACRs	Anion channelrhodopsins
AdoCbl	Adenosylcobalamin
AM	acetoxy methyl ester
ATP	Adenosine triphosphate
ATR	all-trans-retinal
BAPTA	1,2-bis-(o-aminophenoxy)-ethane-N, N, N′, N′-tetra acetic acid
BLUF	Blue light utilizing flavin adenine dinucleotide
BRET	Bioluminescence resonance energy transfer
BRs	Bacteriorhodopsins
Ca^{2+}	Calcium
$CaCl_2$	Calcium chloride
CAG	chicken beta-actin promoter
cAMP	Cyclic adenosine monophosphate
CCh	Carbamoylcholine chloride
CCRs	Cation Channel rhodopsins
CD	Cytoplasmic domain
cGMP	Guanosine 3',5'-cyclic monophosphate
ChEMBL	Chemegenomics European Molecular Biology Laboratory databases
ChR2	Channelrhodopsin-2
ClRs	Chloride-pumping rhodopsins
CNO	Clozapine-N-oxide
COS-1	CV-1 (kidney cells from simian) in Origin, and carrying the SV40 genetic material 1 cells
CPA	cyclopiazonic acid

CRY	Cryptochrome
CsCl	Cesium chloride
CsOH	Cesium hydroxide
CYG	Cysteine-tyrosine-glycine
DAG	Diacylglycerol
DDM	n-dodecyl β-D-maltoside
ddNTPS	dideoxynucleotide triphosphates
DMB	5,6-dimethylbenzimidazole ribonucleoside
DMEM	Dulbecco's Modified Eagle's Medium
DNA	Deoxyribonucleic acid
dNTPs	deoxynucleotide triphosphates
DREADDs	Designer receptors exclusively activated by designer drugs
DTD	aspartic acid-threonine-aspartic acid
DTE	aspartic acid-threonine-glutamic acid
EC50	Half maximal effective concentration
ECL	Extracellular loops
eLi50	half maximal effective light intensity
ELISA	enzyme-linked immunosorbent assay
ER	Endoplasmic reticulum
eYFP	enhanced Yellow Fluorescent Protein
FAD	Flavin adenine dinucleotide
FCS	Fetal calf serum
FMN	Flavin mononucleotide
FR	FR900359
FRET	Förster resonance energy transfer
FSK	forskolin
G protein	Guanine nucleotide binding protein
G418	Geneticin
GAP	GTPase activating protein
GC	Guanyl cyclase
G-CASE	G protein tri-cistronic activity sensors
GDP	Guanine diphosphate

GEF	Guanine exchange factor
GFP	Green fluorescent protein
GIRK	G-protein coupled inwardly rectifying potassium channel
GPCRs	G-protein coupled receptors
GRAFS	Glutamate, rhodopsin, adhesion, frizzled/taste, secretin
GRKs	G protein receptor kinases
GtoPdb	Guide of Pharmocology database, IUPHAR
GTP	Guanine triphosphate
GTPases	Guanine triphosphatases
Gαβγ	G protein heterotrimer
h	Hours
HEK293	Human embryonic kidney cells 293
HEPES	4-(2-hydroxyethyl)-1-piperazineethanesulfonic acid
HK	Histidine kinase
hOPN5	Human Neuropsin
HRKs	Histidine kinase rhodopsins
HRs	Halorhodopsins
HTRF	Homogenous time-resolved fluorescence
ICL	Intracellular loops
I_{KACh}	Acetylcholine dependent inward rectifier current
IP_1	Inositol monophosphate
IP_3	Inositol (1,4,5) triphosphate
IRES	internal ribosome entry sequence
JellyOp	Jellyfish Opsin
kb	kilobase pair
KCl	Potassium chloride
kHz	kilohertz
KLD	Kinase, Ligase and DpnI
KO	Knock out
KORD	Kappa opioid receptor DREADD
KR2	Krokinobacter rhodopsin 2
LARG	Leukemia-associated RhoGEF

LB	Luria-Bertani broth
LBC	Lymphoid blast crisis RhoGEF
LOV	Light oxygen voltage
M2R	Muscarinic receptors
MAPK	Mitogen-activated protein kinase
mg	milligram
$MgCl_2$	Magnesium chloride
min	minutes
mL	millilitre
mm	millimetre
mM	millimolar
mmol	millimole
ms	milliseconds
mV	millivolt
MΩ	milliohm
Na^+	Sodium
NaCl	Sodium chloride
NaOH	Sodium hydroxide
NaRs	Na^+ pumping rhodopsins
NDQ	asparagine-aspartic acid-glutamine
ng	nanogram
nm	Nanometre
nM	nanomolar
OAG	oleoyl-2-acetyl-sn-glycerol
OCP	Orange carotenoid protein
OD	Optical density
OPN4	Melanopsin
OPN5	Neuropsin
OptoXRs	Opsin-GPCR chimeras
P2Y	purinergic G protein-coupled receptors
PCR	Polymerase chain reaction
PDZ-RhoGEF	PSD-95/Disc-large/ZO-1 homology RhoGEF

pg	picogram
PI3Ks	Phosphatidylinositol 3-kinases
PIP2	Phosphatidylinositol 4,5-bisphosphate
PKA	Protein kinase A
PKC	Protein kinase C
PLC-β	Phospholipase C-β
pmol	picomole
PRs	Proteorhodopsins
PTX	Pertussis toxin
PYP	Photoactive yellow protein
RASSLs	Receptors activated solely by synthetic ligands
RGR	Retinal G-protein coupled receptor
RhoPDEs	Rhodopsin phosphodiesterases
rpm	rotations per minute
RT	Room temperature
SALB	Salvinorin β
SDS	Sodium dodecyl sulphate
s	seconds
SERCA	Sarco/endoplasmic reticulum Ca^{2+} ATPase
SOC	Super optimal broth with catabolite repression medium
SR	Sarcoplasmic reticulum
TM	transmembrane helices
TRECs	Therapeutic receptor effector complexes
TRPC6	Transient receptor potential, canonical 6
UV	Ultraviolet
UVLamP	Lamprey Parapinopsins
WT	wild-type
X-Rhod-1	Xanthene based rhodamine like Ca^{2+} fluorescent indicator
α2-AR	α2-adrenergic receptors
ΔF/F0	relative change in fluorescence
F114S	Phenylalanine substituted with Serine at position 114
T164A	Threonine substituted with Alanine at position 164

Y174F	Tyrosine substituted with Phenylalanine at position 174
F217I	Phenylalanine substituted with Isoleucine at position 217
F217L	Phenylalanine substituted with Leucine at position 217
F217V	Phenylalanine substituted with Valine at position 217
S218C	Serine substituted with Cysteine at position 218
Y268F	Tyrosine substituted with Phenylalanine at position 268
Y301H	Tyrosine substituted with Histidine at position 301

1 Introduction

1.1. G-protein coupled receptors (GPCRs)

GPCRs form the largest and the most abundant superfamily of membrane proteins that are key regulators of cellular behavior. GPCRs are an evolutionarily preserved protein class expressed in all eukaryotes, from yeast and other unicellular metazoan to mammalians and humans (King et al., 2003). GPCRs act as signal mediators transducing signals on the extracellular site leading to intracellular activation of specific signaling cascades. These signaling cascades further form a network that regulates the downstream metabolic enzymes, ion channels, transporters and other components of the cellular machinery. Each GPCR reacts to a specific group of activators which range from odorants, nucleotides, amines, peptides, proteins, lipids, and photons (in the case of opsins) while some also can also sense ion concentrations, membrane stretch and voltage (Schiöth and Fredriksson, 2005). Only in the human genome, over 800 GPCRs have been identified by genome sequencing data (Lander et al., 2001; Venter et al., 2001). The presence and functioning of GPCRs are vital for many physiological functions and malfunctioning of the GPCRs lead to severe pathophysiological conditions. Hence, the GPCR family of proteins are by far the most targeted and the largest family of proteins for approved drugs. Approximately, thirty percent of approved drugs available in the market target GPCRs (Figure 1). Thus, they are of high pharmacological importance (Sriram and Insel, 2018). Therefore, a thorough and concrete understanding of GPCRs and their signaling cascades is a pre-requisite to comprehend their role in physiological processes and diseases, for controlling them pharmacologically and development of new drugs targeting specific GPCRs of interest and their pathways.

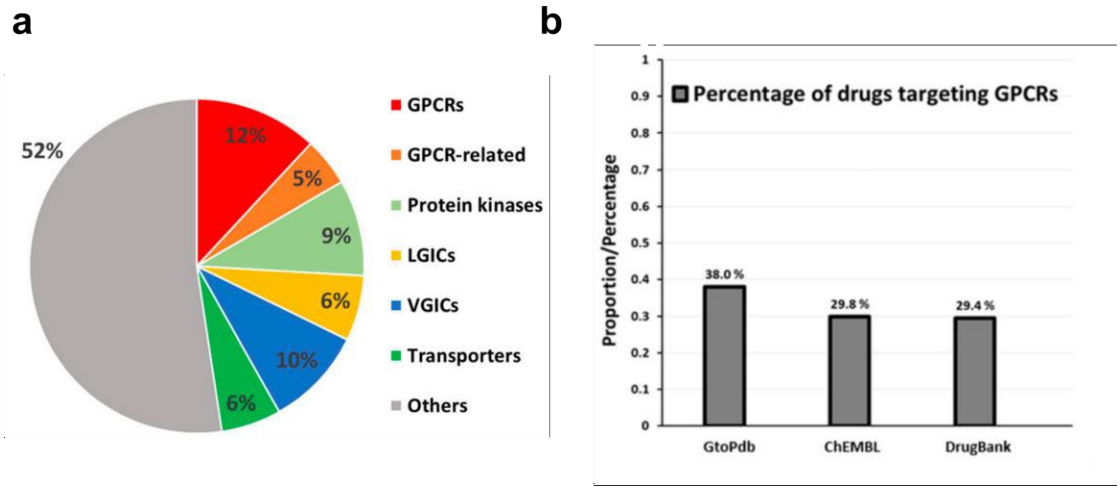

Figure 1: GPCR family - major drug targets.
a. An estimated proportion of different protein families that are targets for approved drugs. b. The percentage of approved drugs that target GPCRs analysed in three different databases. GtoPdb (Guide to Pharmacology database, IUPHAR), ChEMBL (Chemgenomics European Molecular Biology Laboratory database) and DrugBank (data base from University of Alberta, Canada). Adapted from Sriram and Insel, 2018.

1.1.1. General classification and structure of GPCRs

One of the GPCR classification systems is based on amino acid sequences and functional correlations between GPCRs identified in both vertebrates and invertebrates. They were grouped into six major families: rhodopsin-like (family A), secretin-like (family B), glutamate-like (family C), fungal mating pheromone (family D), cAMP (family E), and frizzled/smoothened (family F) GPCRs. Classes D and E are not expressed in the mammalian system (Attwood and Findlay, 1994). Later, an alternative GPCR classification based on genome wide phylogenetic analysis of human GPCRs was established which classified them into the GRAFS (glutamate, rhodopsin, adhesion, frizzled/ taste, secretin) system (Fredriksson et al., 2003). This classification system was further extended for grouping GPCRs from all other organisms. The two GPCR classification methods are quite similar and the main difference is the further division of class B into two families, Secretin (S) and Adhesion (A) based on their evolutionary history (Schiöth and Fredriksson, 2005).

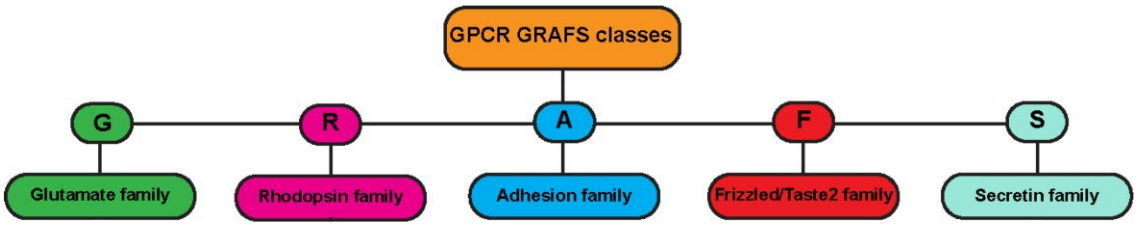

Figure 2: GRAFS classification of GPCRs.
GPCR classification based on their phylogenetic analysis in humans. GPCRs are divided into five families: glutamate-like family (G, green), rhodopsin-like (R, pink), adhesion-like family (A, blue), frizzle/taste2-like family (F, red) and secretin-like family (S, cyan) (Adpated from Liccardo, Luini and Di Martino, 2022).

GPCRs are characterized by seven transmembrane domains with each transmembrane domains consisting of at least 25 lipophilic amino acids (Schiöth and Fredriksson, 2005). The transmembrane helices (TM) are linked by three extracellular loops (EL1, EL2, EL3) and three intracellular loops (IL1, IL2 and IL3) along with the presence of extracellular N-terminal region and intracellular C-terminal region. Generally, the N-terminal region, TM1 to 7 and ECL1 to 3 are associated with ligand binding and receptor activation, whereas ICL1 to 3 and the C-terminal region contain residues that regulate downstream effectors, especially G proteins (Figure 3). Thus, the amino acid residues of each region distinguish the different classes of GPCRs and are especially important for the selectivity of activators and downstream effectors.

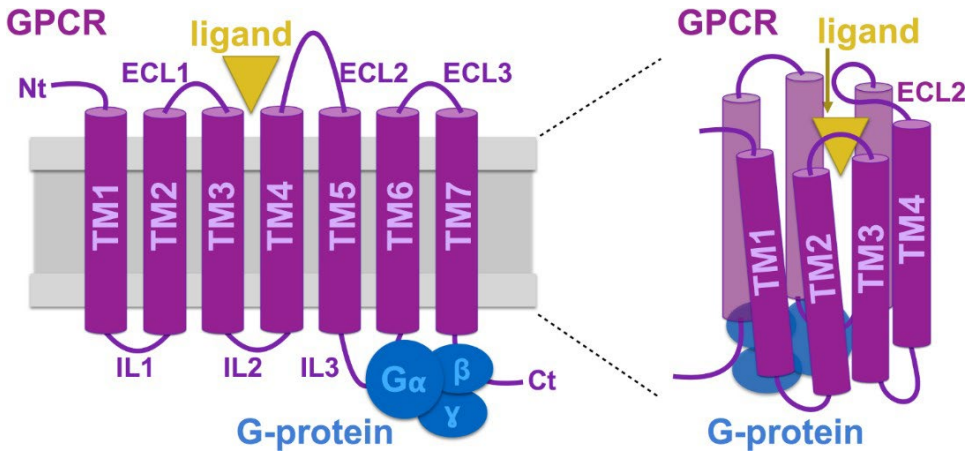

Figure 3: Schematic 2D (left) and 3D (right) representations of the structure of GPCRs.
Each GPCR comprises seven transmembrane helices (TM) connected by intracellular (ICL) and extracellular (ECL) loops C and N terminal regions (Schneider et al., 2018).

1.1.2. GPCR and G proteins interaction

G proteins belong to the large group of GTPases consisting of three subunits. The G protein heterotrimer ($G_{\alpha\beta\gamma}$) acts as the first interactor of the GPCRs on the intracellular side after the activation of the GPCR. In this combination of GPCR and the G protein heterotrimer, the GPCR acts as the Guanine exchange factor (GEF) and the G_{α} subunit is the GTPase activating protein (GAP) (Bos et al., 2007). The G_{α} subunit binds to an energy carrier guanosine triphosphate (GTP) and hydrolyses it to Guanosine diphosphate (GDP), this phenomenon dictates the switching between the active and the inactive states. The G_{α} subunit in its resting state is bound to a GDP along with the $G_{\beta\gamma}$ subunits which form a stable heterotrimer. Upon activation of the GPCR, a conformational change triggers the bound inactive G_{α} subunit to release GDP and exchange it with a GTP owing to the sheer concentration difference between the two nucleotides in the cytoplasm. The GTP bound active G_{α} subunit then dissociates from the GPCR and eventually from the $G_{\beta\gamma}$ dimer to further interact with other effector proteins downstream. Both the G_{α} and G_{γ} subunits have membrane anchoring residues often being N-terminally palmitoylated or myristoylated (Vögler et al., 2008). Later, due to the intrinsic GTPase activity of the G_{α} subunit, the GTP gets hydrolyzed to GDP forcing it to return to the inactive state along with the reassociation with the $G_{\beta\gamma}$ subunits completing the $G_{\alpha\beta\gamma}$ protein heterotrimer. The G_{α} subunit depending on its structure and amino acid residues interacts with different downstream effector enzymes and modulates the activity of them. Thus, the different G_{α} and $G_{\beta\gamma}$ subunits combine in multiple possible ways to produce a diverse family of G protein heterotrimers. In essence, the G protein heterotrimer function as a dimer as signal relays can be started either by the G_{α} subunit or by the $G_{\beta\gamma}$ complex modulating its targeted downstream effector proteins. The active GPCR is phosphorylated by the soluble G protein receptor kinases (GRKs) which leads to reduced coupling of GPCR to the G protein heterotrimer (Gurevich and Gurevich, 2019). The arrestins target the phosphorylated GPCR and render the complete blockage of the G protein signaling by merely outcompeting the G protein heterotrimer in the vicinity. The binding of arrestins leads to the recruitment of trafficking proteins and ubiquitination related proteins which leads to internalization, trafficking to other organelles, and lysis or trafficking back to the membrane (Figure 4) (Gurevich and Gurevich, 2015).

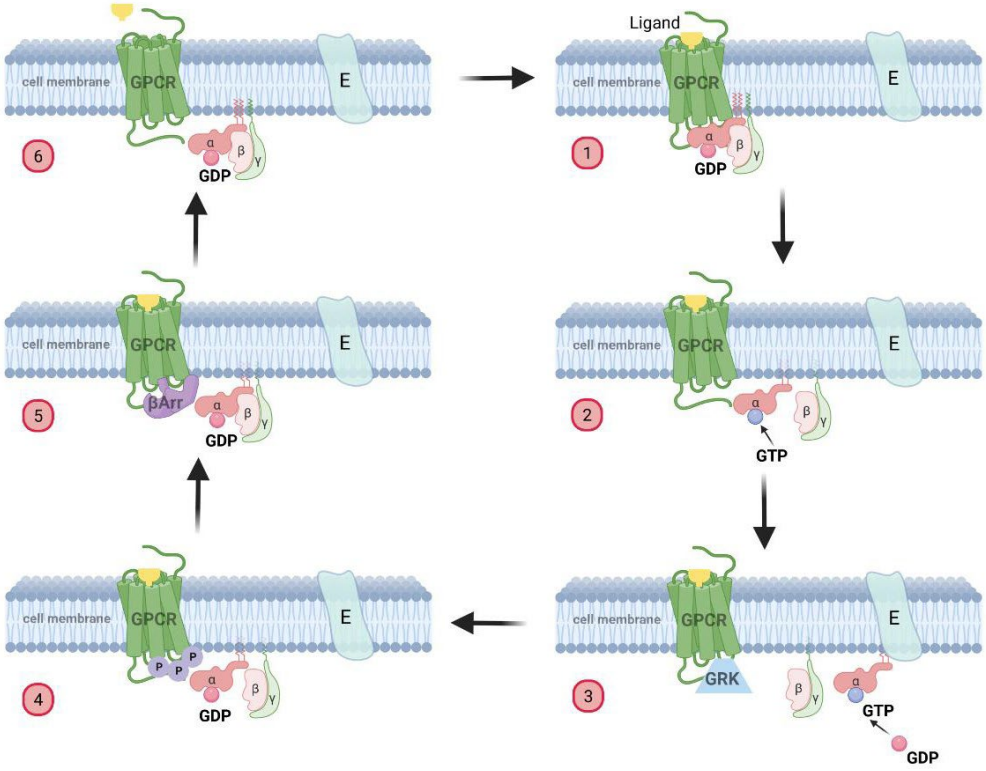

Figure 4: GPCR activation cycle.
1) The GPCR activated by the ligand undergoes a conformation change and acts as a GEF for the G_{α}. 2) Exchange of GDP by GTP induces the separation of G_{α} and $G_{\beta\gamma}$ subunits leading to the interaction with their respective effector proteins. 3) The intrinsic GTPase activity of G_{α} leads to the hydrolysis of GTP to GDP and on the other hand the GPCR is phosphorylated by GRKs. 4) The phosphorylation leads to inactivation of the GPCR. 5) Further, β-arrestins binding leads to internalization of the GPCR followed by degradation or the GPCR is directed back to the membrane. 6) In parallel, the $G_{\alpha\beta\gamma}$ heterotrimer re-associates and becomes available for the next cycle. Generated using BioRender.com

1.1.3. G proteins signaling pathways

On the basis of structural similarity, Gα subunits have been classified into four families which drive the regulation of its specific downstream effector proteins (Neves et al., 2002). The four different G_{α} families consists of G_s, $G_{i/o}$, G_q, and $G_{12/13}$. The G_{α} subunit has a size of approximately 40 kDa and contains the guanine nucleotide-binding pocket along with the intrinsic GTPase activity. The 35 kDa G_{β} subunit and the 10 kDa G_{γ} subunits are tightly associated with each other and are often referred to as a single entity, $G_{\beta\gamma}$ subunit modulating their effector proteins together (Simon et al., 1991; Hepler and Gilman, 1992; Conklin and Bourne, 1993). Currently there are 23 known G_{α}, 5 G_{β}, and 12 G_{γ} subunits (Liccardo et al., 2022).

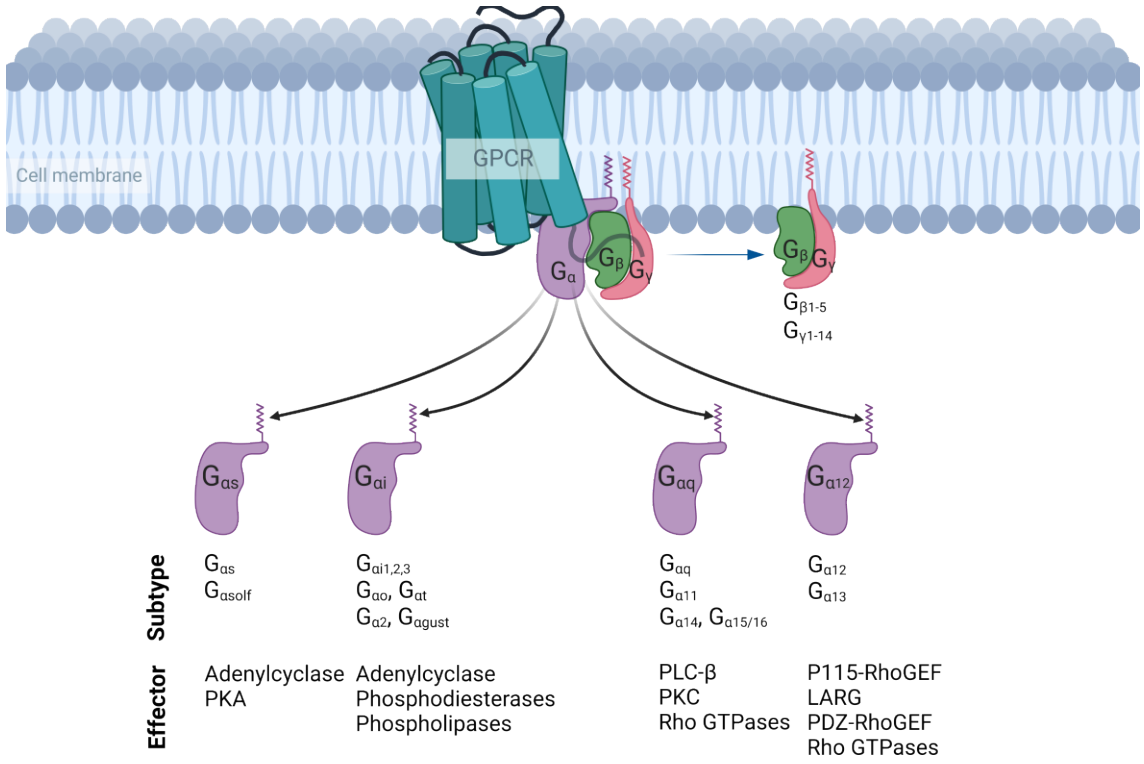

Figure 5: Classification of G_α proteins.
G_α proteins are classified based on which G protein signaling cascades they initiate by activating their specific downstream effectors. Effector proteins activated by G_s signaling are adenyl cyclases and protein kinase A (PKA). Effector proteins inactivateded by G_i signaling includes adenyl cyclases, phosphodiesterases, and phospholipases. Effectors activated by G_q signaling are phospholipase C-β (PLC-β), protein kinase C (PKC) and RhoGTPases. Effector proteins activated by $G_{12/13}$ pathway include RhoGEF family members such as p115-RhoGEF, PSD-95/Disc-large/ZO-1 homology RhoGEF (PDZ-RhoGEF), leukemia-associated RhoGEF (LARG), lymphoid blast crisis RhoGEF (LBC) and Rho GTPases (Neves et al., 2002). Generated using BioRender.com.

1.1.3.1 G_s signaling cascade

The $G_{\alpha s}$ family comprises $G_{\alpha s}$ and $G_{\alpha olf}$. The G_s signaling pathway was the first to be described among the GPCR signaling pathways and is called G_s (stimulatory) based on the stimulation of adenylyl cyclase activity by the $G_{\alpha s}$ subunit. The stimulated adenyl cyclase produces cAMP, leading to the activation of downstream effector proteins, such as protein kinase A (PKA) and cyclic nucleotide-gated channels. PKA is a serine/threonine kinase that phosphorylates several downstream proteins, leading to the regulation of several physiological processes, such as metabolism, gene expression, cell growth, and differentiation. The G_s signaling pathway is one of the key regulators of cardiac contractility (Rockman et al., 2002). β-adrenergic receptor activation by adrenaline and noradrenaline leads to cAMP-dependent PKA mediated phosphorylation of myocyte proteins including the voltage-gated L-type Ca^{2+} channels, the cardiac ryanodine receptors 2, phospholamban, and troponin-I. The activation of

G_s signaling leads to increased ionotropic (increased contractility), chronotropic (increased heart rate), dromotropic (enhanced conduction of electrical impulse from SA node to AV node), bathmotropic (enhanced cardiac muscle stimulation) and lusitropic (enhanced relaxation of cardiomyocytes) effects which modulate physiological status of the heart thereby improving heart rate, stroke volume, and cardiac output (Salazar et al., 2007; Xiang and Kobilka, 2003). G_s signaling also plays a pivotal role in case of regulation of hormone secretion from endocrine glands, such as the pituitary gland, thyroid gland, and adrenal gland. It is further involved in the regulation of neurotransmitter release from neurons including the release of adrenaline and noradrenaline from the adrenal medulla, which plays an important role in the sympathetic nervous system (Cunha and Ribeiro, 2000).

1.1.3.2. $G_{i/o}$ signaling cascade

$G_{i/o}$ signaling cascade was originally identified as the signaling cascade opposing the G_s cascade by inhibition of adenylyl cyclases and reducing the subsequent production of cAMP and the downstream effects. The $G_{i/o}$ family includes $G_{\alpha i1}$, $G_{\alpha i2}$, $G_{\alpha i3}$, $G_{\alpha t\text{-}rod}$, $G_{\alpha t\text{-}cone}$, $G_{\alpha oA}$, $G_{\alpha oB}$, and $G_{\alpha z}$. In this signaling cascade, both G_α and $G_{\beta\gamma}$ subunits can relay signals. In the heart, A1 adenosine receptors, M2 muscarinic receptors, and α2 adrenergic receptors in the heart couple to the G_i signaling cascade (Salazar et al., 2007). G_i signaling leads to a reduction in L-type Ca^{2+} currents which inhibits the force of contraction in myocytes (Brodde and Michel, 1999). Also, G_i signaling cascade plays key physiological functions such as muscarinic regulation of pacemaker activity in the heart which occurs via M2 receptors leading to negative chronotropic effect by $G_{\alpha i}$, while a negative chronotropic effect mediated by release of a $G_{\beta\gamma}$ subunit by activating I_{KACh} channels (Logothetis et al., 1987; Pierce et al., 2002). The release of many important hormones and neurotransmitters, including epinephrine, acetylcholine, dopamine, and serotonin is tightly modulated by the G_i cascade. Especially, presynaptic α2 adrenergic receptors regulate the suppression of neurotransmitter release from synaptic terminals to the heart which attenuates the adrenergic drive thereby providing a cardio protective effect. $G_{\beta\gamma}$ subunits also directly couples to specific isoforms of PLC-βs, GIRK channels, adenylyl cyclases, and phosphatidylinositol 3-kinases (PI3Ks) and also plays an important role in receptor desensitization via β-arrestin mediated pathways. Although, not directly related to cause cardiomyopathies increased G_i protein levels were found during dilated cardiomyopathies leading to heart failure (Bohm et al., 1990; Flesch et al., 1996).

1.1.3.3. G_q signaling cascade

The $G_{\alpha q}$ family consists of $G_{\alpha q}$, $G_{\alpha 11}$, $G_{\alpha 14}$, $G_{\alpha 15}$ and $G_{\alpha 16}$ and all of them stimulate the phosphoinositide-specific phospholipase C- β (PLC-β). The stimulated PLC-β

lyses phosphatidylinositol 4,5-bisphosphate (PIP_2) producing two intracellular second messengers free floating inositol trisphosphate (IP_3) and membrane bound diacylglycerol (DAG). IP_3 triggers the release of calcium from intracellular stores by binding to IP_3 receptors present on the endoplasmic reticulum (ER) or sarcoplasmic reticulum (SR), and DAG triggers the recruitment of protein kinase C (PKC) to the cell membrane via the C1 DAG or phorbol ester sensing domain and further triggers its activation in the cell membrane (Das and Rahman, 2014). The intracellular Ca^{2+} release activates the store-operated Ca^{2+} channels found in the cell membrane to cause the influx of extracellular Ca^{2+} into the cytosol in all types of contractile cells. $G_{\alpha q}$ also directly working through PKC appears to regulate various isoforms of phospholipase D (Xie et al., 2002). Especially, the role of G_q signaling in the heart is important which regulates cardiac growth responses, myocyte apoptosis, and cardiac hypertrophy (Hubbard and Hepler, 2006). Of note, acetylcholine stimulation of G_q coupled muscarinic receptors modulate heart rate, conduction velocity, and contractility (Huizhen Wang et al., 2001). However, dysregulation of the G_q signaling cascade can contribute to hypertrophy, fibrosis, cardiac cell apoptosis. They further lead to the development of arrhythmias, heart failure and increased mortality.

1.1.3.4. $G_{12/13}$ signaling cascade

$G_{12/13}$ family comprises the G_α subunits $G_{\alpha12}$ and $G_{\alpha13}$. Their existence was first reported in 1991 and was shown to have a ubiquitous expression in most tissues (Strathmann and Simon, 1991). They play a prominent role in many vital processes, including embryonic development, angiogenesis, cell growth, cell migration, platelet activation, immune responses, neuronal responses and cell apoptosis (Suzuki et al., 2009). Improper regulation of $G_{12/13}$ signaling is involved in multiple pathophysiological conditions such as cancer, cardiovascular diseases, arterial and pulmonary hypertension, and bronchial asthma (Dhanasekaran and Dermott, 1996; Offermanns et al., 1997; Suzuki et al., 2009; Xu et al., 1994). $G_{12/13}$ proteins activate specific RhoGEF family members such as p115-RhoGEF, PSD-95/Disc-large/ZO-1 homology RhoGEF, leukemia-associated RhoGEF and lymphoid blast crisis RhoGEF (Dutt et al., 2004; Fukuharaa et al., 2001). The activation of RhoGEFs lead to activation of the RhoA which further leads to the activation of downstream signaling pathways including the activation of Rho kinases like ROCK1/2 (Leung et al., 1995). In cardiomyocytes, it has been reported that α1-adrenergic receptor-induced hypertrophic responses are mediated in part by a $G_{12/13}$-Rho-JNK pathway (Maruyama et al., 2002).

Despite the prevailing fundamental knowledge of GPCRs and their physiological role in biology, only a minimal understanding of the receptor dynamics exists. Specifically, differences between pulsatile and tonic activation of GPCRs and the subsequent

signal integration to different effector proteins are poorly understood. Also, the information on pathological GPCR signaling and the timescale at which a physiological signaling process becomes pathophysiological remains elusive. Therefore, one of the major challenges that exists is to perform a direct manipulation and sensing of GPCRs in specific cell types with high spatiotemporal precision without activating other nonspecific responses in due process.

1.1.4. Chemogenetic approach to study GPCR signaling

Chemogenetics is one such approach which partially addresses the problems previously discussed. It is based on the bioengineering of GPCRs to previously unrecognized small molecules without affecting the activity of other GPCRs. The modified GPCRs can be targeted to specific cell types with the aid of cell specific promoters. This approach paved the way for a better understanding of the signal transduction that occurs downstream of the GPCR without affecting the endogenous GPCR signaling. An ideal chemogenetic GPCR was conceptualized as a GPCR that is unresponsive to the native ligands, has affinity and responds only to the specific small molecules that does not affect endogenous signaling. In the attempt to create the engineered GPCRs/ligand pairs for each of the four signaling cascades, several approaches were created which includes receptors activated solely by synthetic ligands (RASSLs), therapeutic receptor-effector complexes (TRECs), neoceptors, and designer receptors exclusively activated by designer drugs (DREADDs) (Conklin et al., 2008; Miura et al., 2022). The first engineered GPCR was the outcome of the pioneering work done by Strader *et al.*, 1991. They performed a single amino acid mutation in the G_s coupled β-adrenergic receptor that led to the inability to bind native ligands but improved binding to catechol esters or ketone ligands such as synthesized butanone derivatives. These receptors displayed very low receptor activation potency, which rendered it impractical for its use.

The first RASSL was engineered by replacing the second extracellular loop of G_i coupled kappa opioid receptor with that of the corresponding loop from delta opioid receptor in addition to a single mutation to enhance the binding of the potent synthetic ligand spiradoline (Coward et al., 1998). New RASSLs emerged for G_s coupled receptors like $5HT_4$ Serotonin, MC4 melanocortin (Claeysen et al., 2003; Srinivasan et al., 2007) and a G_q coupled H1 histamine receptor (Bruysters et al., 2005). The biggest disadvantage of RASSLs is off-target effects. The small molecule ligands can bind to other native receptors for example other endogenous opioid receptors. Also, the RASSLs exhibited high levels of constitutive activity, making them less desired.

In 2001, Liggett's group created a new approach called as highly modified therapeutic receptor-effector complex (TREC), for which they used a G_s coupled β2 adrenergic

receptor and performed 19 modifications. The modified receptor had its agonist sensitivity tailored to non-biogenic synthetic amine ligands, altered target phosphorylation sites of GPCR kinases, PKA, PKC responsible for receptor down regulation and fused $G_{\alpha s}$ subunit to the C-terminus of the receptor. Thus, the TREC yielded a strong targeted activation of the G_s pathway with a synthetic ligand. The heavy modifications of the GPCR along with the strong activation capabilities of these receptors mimicked certain G_s signaling linked pathological states. TRECs remain to be engineered for other G protein signaling pathways (Small et al., 2001).

In 2001, Jacobson *et al.*, proposed a new approach to study GPCRs by the name of neoceptors. It involved the engineering of desired GPCRs according to the molecular complementarity of a synthetic neoligand to attain a highly selective ligand-receptor combination while preserving their downstream G protein signaling. Also, the modified neoligands do not affect the endogenous receptors. There is only one neoceptor which was engineered based on the G_q/G_i coupled adenosine 3 receptor by enhancing the neoligand binding regions. For the first time, the use of a neoceptor-neoligand pair in the GPCR research did not lead to any undesirable and non-selective endogenous receptor activation. Neoceptors still remain to be engineered for specific G protein signaling pathways (Jacobson et al., 2007; Pottie et al., 2020).

Armbruster *et al.*, in 2007 created the first set of Designer receptors exclusively activated by designer drugs (DREADDs) based on human muscarinic receptors which addressed the shortcomings of the previously engineered receptors and ligand pairs. The primary advantage of DREADDs is their insensitivity to endogenous ligands with low constitutive activity and very miniscule off-target effects of their specific synthetic ligands. Engineered human muscarinic receptors $hM1D_q$, $hM3D_q$, and $hM5D_q$ are G_q coupled receptors with $hM3D_q$ being widely used (Armbruster et al., 2007). G_i coupled DREADDs include modified human muscarinic GPCRs hM2Di and $hM4D_i$. Also, a modified human kappa opioid receptor DREADD called KORD (Vardy et al., 2015) paved the way for multiplexed use along with the G_q muscarinic based DREADDs due to their specific affinities to their corresponding synthetic ligands. For the G_s signaling cascade, $rM3D_s$ was created by exchanging the corresponding intracellular region of a turkey erythrocyte β-adrenergic receptor with a rat M3 muscarinic receptor (Guettier et al., 2009). For $G_{12/13}$ signaling cascade, $hM3D_{12}$ and $hM4D_{12}$ were engineered based on the human muscarinic receptors and G_{12} coupled GPR132 (or GPR183) and specifically activated only $G_{\alpha 12}$ proteins (Inoue et al., 2019). DREADDs were also engineered to couple to β-arrestins to activate noncanonical GPCR signaling independent of G proteins. R_q (R165L) is one such DREADD based on the human M3 muscarinic receptor (Nakajima and Wess, 2012). All the muscarinic based DREADDs were designed to be potently activated by clozapine-N-oxide (CNO). But it was later revealed to be converted *in vivo* to

clozapine which presents off-target effects. Ligands with structures similar to CNO including deschloroclozapine, compound 21, perlapine, and olanzapine have been investigated as alternative ligands for muscarinic receptors based DREADDs (Chen et al., 2015; Nagai et al., 2020; Thompson et al., 2018). The kappa opioid based GPCR, KORD is only activated by salvinorin B (Vardy et al., 2015).

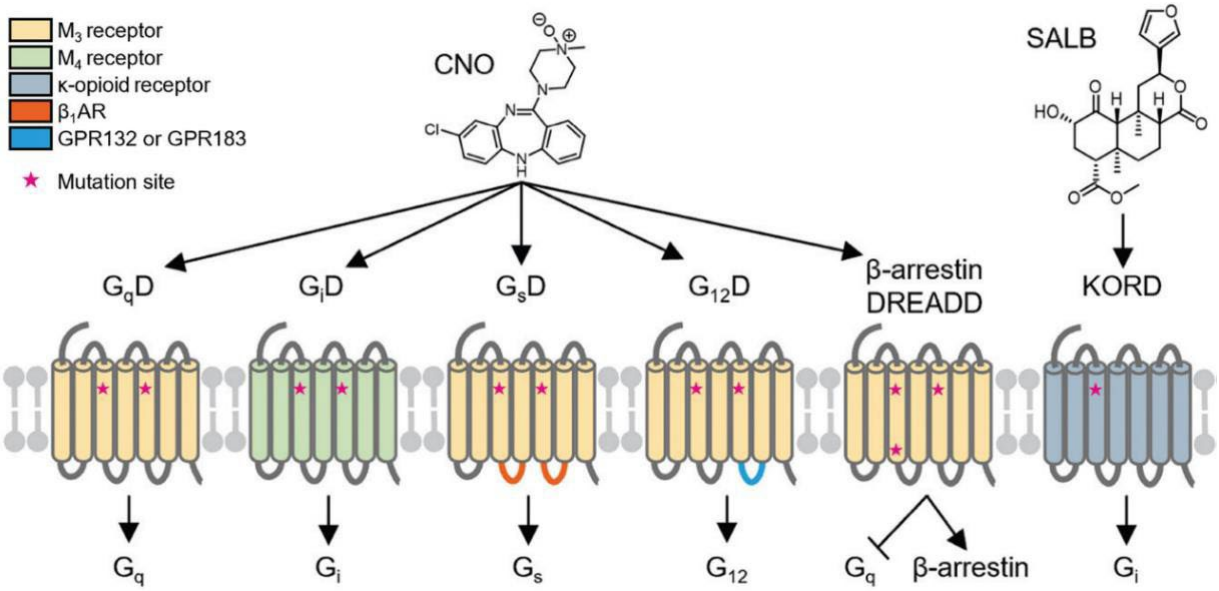

Figure 6: Different DREADDs for each of the G protein signaling cascades with corresponding potent synthetic ligands.
All engineered DREADDs are unable to bind to the endogenous agonists and are specific for their synthetic ligands. Modified from (Miura et al., 2022).

Chemogenetic approaches allowed to assess the consequences of GPCR signaling cascades *in vivo* in specific cell types but they still lack precise spatiotemporal control. Therefore, the quest for an approach which satisfies the criteria for an ideal GPCR tool is highly in demand.

1.2. Optogenetics

Optogenetics is an elegant technique that integrates genetic engineering and optical technology to alter and regulate the biological functions and the subsequent bioprocesses of cells, tissues, organs, or organisms that express the desired light-sensitive proteins. It is a better alternative to traditional methods of electrical or chemical manipulation used in conventional research due to its unprecedented capabilities of precise stimulation with temporal resolution in µs range and spatial resolution in nm range. It is also being used in

combination with genetic manipulation to provide a cell specific high spatiotemporal resolution which is almost impossible to achieve by other conventional methods.

1.2.1. History of optogenetics

In 1979, Francis Crick wrote about the imminent need for a technology that can control certain cell types of the brain that can be manipulated with spatial and temporal precision while leaving the other cell types unaffected. This suggestion hinted at the utility of light to control the biological activity of cells expressing light-sensitive proteins (Crick, 1979). As early as the 1970s, some microbiologists were already familiar with the existence of light-sensitive proteins that regulate the movement of ions across the plasma membrane in some microorganisms (Kaneko et al., 1975; Murphy & Lanier, 1978). The idea of using light to activate mammalian cells was first proved by the work of Nagel *et al.,* demonstrating the utility of microbial opsin Channelrhodopsin-2 (ChR2). It is a non-selective cation channel which enables fast, light- induced cell depolarization (Kateriya et al., 2004; Nagel et al., 2003). These light sensitive ion channels have made a significant impact in the field of neuroscience and offers more precise spatiotemporal control compared to electrical stimulation (Boyden et al., 2005; Chow et al., 2010; Yizhar et al., 2011). The successful and straightforward use of these optogenetic proteins triggered the efforts for the discovery of new members with distinct properties that can be used for specific purposes. Recently, the potential of optogenetics in restoring auditory signaling was proved and has also been shown in the restoration of sinus rhythm after atrial fibrillation (Joshi et al., 2020; Zhang et al., 2022). Also, recently optogenetic stimulation with the use of G_s specific optogenetic GPCR was used to study the role of G_s signaling in the heart (Makowka et al., 2019). In the G protein signaling research, the use of optogenetic GPCRs which couple to specific G protein signaling cascade has proven to be more advantageous than conventional methods like pharmacological strategies and chemogenetic strategies including DREADDs to control a focused group of cells or organs, as optogenetic proteins provide a high spatiotemporal resolution for the precise control of the desired G protein signaling pathways. Also, direct optogenetic stimulation would provide new insights into its intricate temporal signaling aspects and its downstream cascades exploring its biological consequences.

1.2.2. Light sensitive proteins

The light sensitive proteins or photoreceptors are evolutionarily specialized proteins which convert light into an intracellular biochemical cascade to evoke an appropriate response in their natively expressed cells or organisms. They are bound to an organic chromophore molecule making them receptive to photons. Organic chromophores consist of

unsaturated molecules with a delocalized π electron system that absorb light at specific wavelengths. Upon light illumination, the chromophore goes through a series of intermediary states due to electron transfers leading to cis-trans isomerization or bond formation/disruption with the photoreceptor which alters the conformation of the protein. The series of changes the chromophore bound protein endures upon light excitation is called a photocycle. Currently, the light sensitive proteins have been classified based on the chromophore and its host photosensory protein domain. Most known chromophores like flavin mononucleotide (FMN), flavin adenine dinucleotide (FAD), p-coumaric acid, and keto-carotenoids absorb in the blue light region from 400 - 500 nm. Chromophores like retinal and coenzyme B_{12} cover a broader range from UV to green light from 300 - 570 nm, while biliverdin and phycocyanobilin cover the red/far-red light from 620 - 750 nm (Jost et al., 2015; Seong and Lin, 2021; Shcherbakova et al., 2015). In current optogenetic research, the flavin and retinal based proteins have gained a lot of interest and are currently being explored for their applicability in optogenetic applications. Therefore, these photoreceptors are described extensively in the next paragraphs.

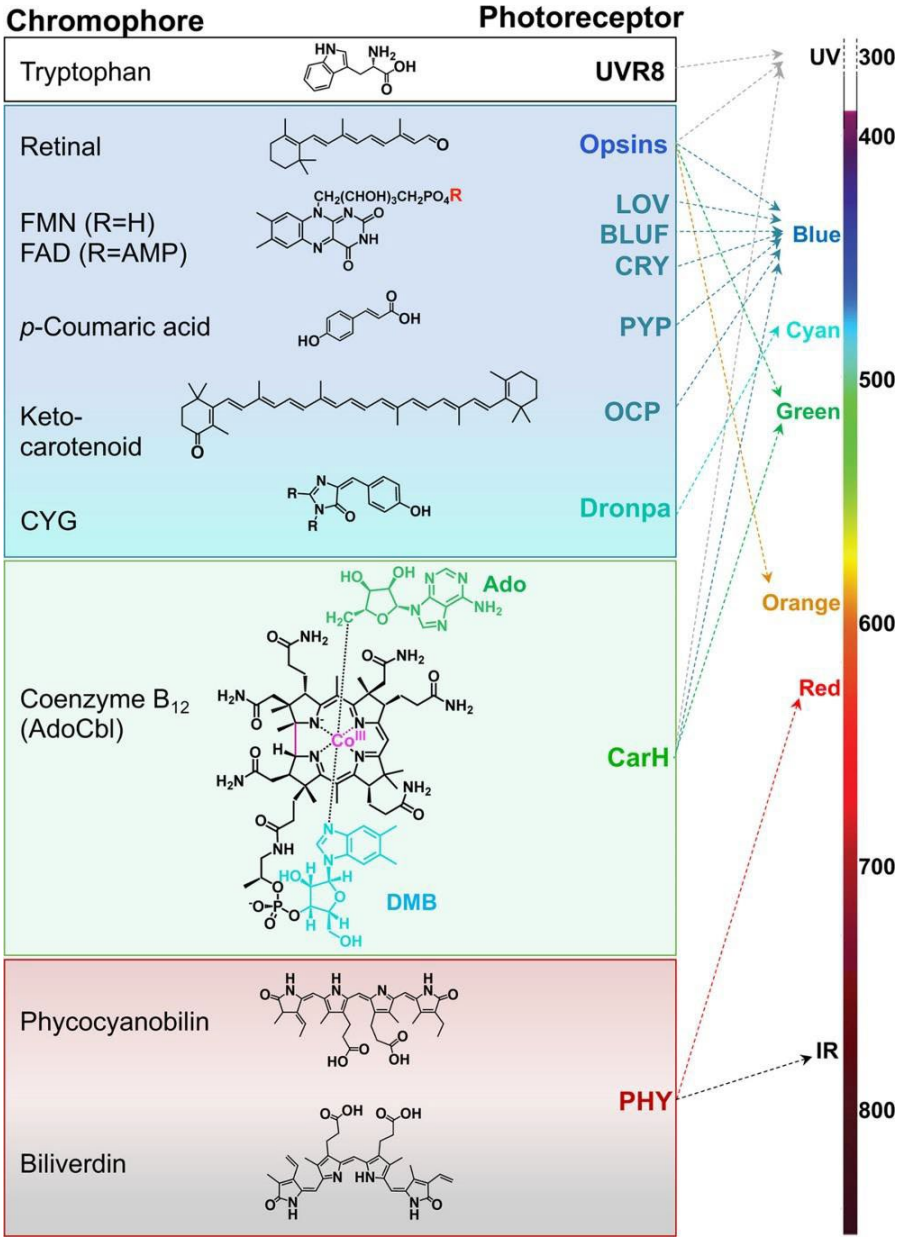

Figure 7: Photoreceptors and their chromophores.
All known photoreceptors and their specific chromophores. Chromophores - photoreceptor: Tryptophan - UVR8; Retinal - Opsins; flavin mononucleotide (FMN) - Light oxygen voltage sensors (LOV); flavin adenine dinucleotide (FAD) - Blue light utilizing FAD (BLUF); FAD - cryptochrome (CRY); *p*-Coumaric acid - photoactive yellow protein (PYP); keto carotenoid -orange carotenoid protein (OCP); cysteine-tyrosine-glycine (CYG) tripeptide - Dronpa; Coenzyme B_{12} or AdoCbl (5´-deoxyadenosylcobalamin) - CarH transcription factor. Shown in B_{12} are the Ado (5´-deoxyadenosyl group) in green and the DMB (5,6-dimethylbenzimidazole ribonucleoside) in cyan (Padmanabhan et al., 2022).

1.2.2.1 Flavin chromophore-based photoreceptors

The light sensitive proteins that use different riboflavin (Vitamin B_2) derivatives as chromophores form the blue light sensitive flavoproteins or the blue light receptors (Losi and Gärtner, 2011). The Light-oxygen-voltage (LOV) sensors incorporate flavin mononucleotide (FMN) and it was first identified in plant phototropins. N-terminal light sensing domain of the phototropins consists of two LOV sensor domains that bind FMN. Absorption of light in the blue spectral region around 450 nm leads to the formation of a thioether between the FMN and a cysteine residue of the LOV domain (Kottke et al., 2018; Matsuoka et al., 2007; Schleicher et al., 2004). Thereby, it causes a conformational change leading to the activation of the phototropin and its downstream cascades (Christie et al., 2002; Raffelberg et al., 2011). Blue-light utilizing flavin (BLUF) sensors bind to flavin adenine dinucleotide (FAD) and they are widely present in prokaryotes and lower eukaryotes but not in plants. They exist as individual domains or bound to adenylate/guanylate cyclases or phosphodiesterases playing a role in cyclic nucleotide metabolism. Blue light absorption leads to electron transfer to FAD from a tyrosine residue forming a radical intermediate state and triggering an altered electrostatic environment with minimal conformational change. This minimal change is propagated to the effector domains leading to enzyme activity. Cryptochromes bind to FAD using a photolyase-like domain and they are widely distributed in plants and animals. They are primarily involved in circadian entrainment in addition to development and flower induction in plants (Li and Yang, 2007; Shatn et al., 2002). The photochemistry of cryptochromes is similar to BLUF, a radical intermediate is formed which triggers the conformation change. The most studied cryptochromes are from the *Arabidopsis thaliana* (*At*CRY1 and *At*CRY2) acting as light dependent kinases while the other cryptochromes regulate ubiquitin ligases (Özgür and Sancar, 2006; H. Wang et al., 2001; Yang et al., 2000). A major disadvantage with the flavin based photoreceptors is that they display residual dark activity, and just act as light-dependent analogue activity modulators which improve the specific activity. Moreover, their signaling depends likely on thermal relaxation which means no precise temporal control during the experiments (Losi et al., 2018).

1.2.2.2. Retinal chromophore-based photoreceptors

The photosensitive proteins that depend on the retinal, a derivative of Vitamin A form the group of retinal photoreceptors. Retinal serves as the photoreceptor's antenna for light absorption. The retinal chromophore is made of a conjugated polyene chain with an extended π electron system. All opsin members share a seven-helix protein structure forming an internal pocket for a retinal molecule. It is bound to a lysine residue of the seventh helix by

a protonated Schiff's base linkage (Palczewski, 2006; Wald and Hubbard, 1950). The rhodopsin type photoreceptors based on their origin, amino acid sequence and mode of action can be broadly classified into type I (microbial) rhodopsins and type II (animal) rhodopsins (Kato and Nureki, 2013; Shichida and Matsuyama, 2009; Terakita, 2005).

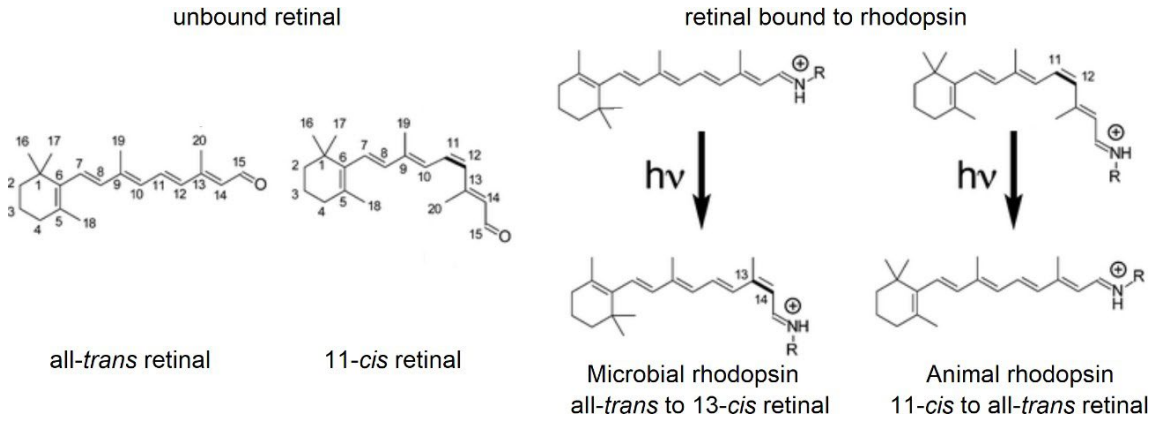

Figure 8: Different isoforms of retinal chromophore of microbial and animal rhodopsins. The ground state or dark state of microbial and animal rhodopsins constitute all-trans retinal and 11-cis retinal as its chromophore, respectively. Retinal moiety is bound to a Lysine residue via a Schiff base, which is normally protonated and exists in the 15-anti configuration. Microbial rhodopsins photoisomerize selectively at the C13=C14 double bond whereas animal rhodopsins at the C11=C12 double bond. Adapted from Ernst *et al.*, 2014.

1.2.2.2.1. Microbial rhodopsins

Microbial rhodopsins consist of structurally similar photoreceptors expressed in prokaryotes, archaea and lower eukaryotes. They are named microbial opsins based on their commonality with the septahelical animal opsins. Upon light absorption, the canonical event of the trans-cis photoisomerization of the retinal around the C13=C14 double bond triggers a conformational change of the photoreceptor. This change leads to the activation of the photoreceptor to perform its specific function. The microbial opsins can be broadly categorized into light driven ion pumping opsins, ion channels and enzyme rhodopsins (Govorunova et al., 2017).

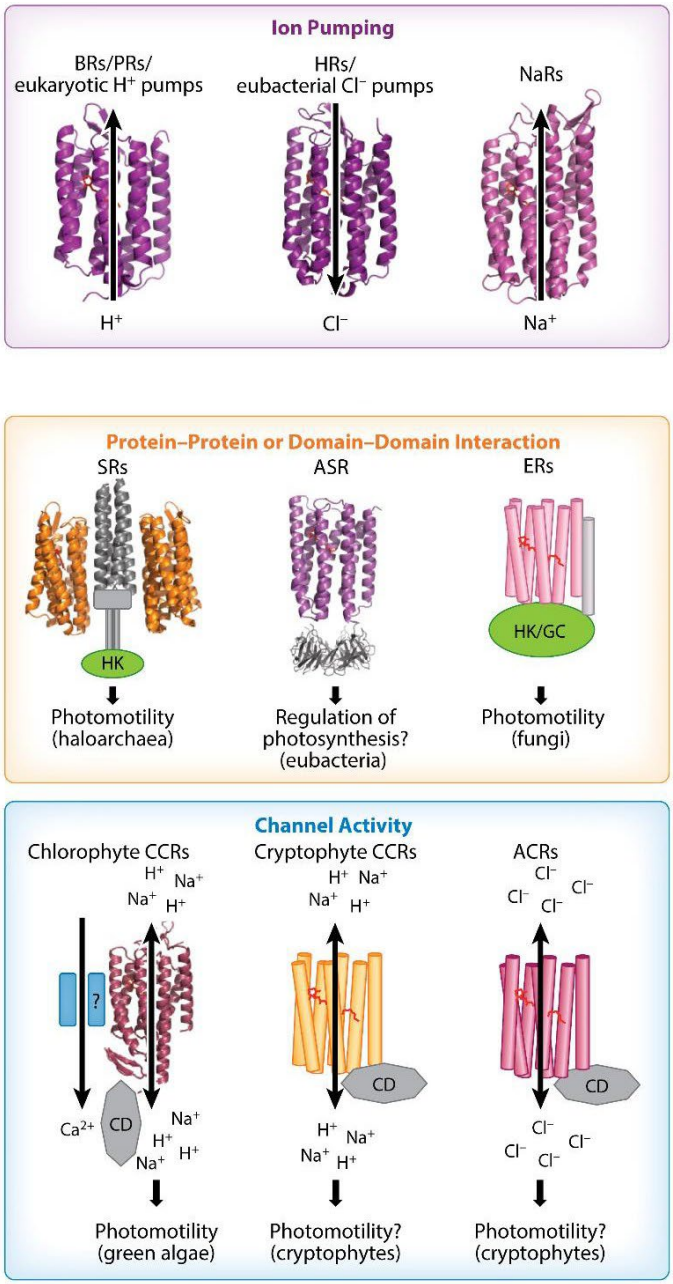

Figure 9: Functional types of microbial opsins.
All opsins are oriented with their extracellular surface pointing upwards. The group of ion pumping opsins includes bacteriorhodopsins (BRs), halorhodopsins (HRs,), and Na^+ pumping rhodopsins (NaRs); Enzyme rhodopsins group includes prokaryotic sensory rhodopsins (PRs) with enzyme domains, Anabaena sensory rhodopsin (ASR), and fungal enzymerhodopsins (ERs) with either guanylyl cyclase (GC) or histidine kinase (HK) domains. The group of channelrhodopsins includes anion channelrhodopsins (ACRs), cation channel rhodopsins (CCRs), and some CCRs with additional cytoplasmic domain (CD). Modified from Govorunova *et al.*, 2017.

1.2.2.2.1.1. Microbial ion pump Opsins

The Ion pump opsins are widespread microbial opsins that function as light-driven pumps to transport specific ions across the microbial cell membranes independent of the electrochemical gradient. This phenomenon driven by light regulates several processes, such as ATP synthesis, transport of nutrients, and cell motility. They are currently classified into proton pumps, chloride pumps, and sodium pumps. The most common light-driven proton pumps include bacteriorhodopdsins (BRs) and proteorhodopsins (PRs) that actively pump protons outside, causing transient hyperpolarization of the microbial cells. They share a conserved DTD and DTE motifs, respectively (Henderson and Unwin, 1975; Oesterhelt and Stoeckenius, 1971; Sanders et al., 1981). These light-driven proton pumps have been used to suppress neural firing by hyperpolarizing the neurons (Chow et al., 2010). The halorhodopsin (HR) and chloride-pumping rhodopsins (ClRs) belong to the inward Cl^- pump microbial opsins. They function by pumping chloride ions inside of the cell and hyperpolarizing the cell (Helgerson and Stoeckenius, 1985; Lanyi, 1986; Schobert and Lanyi, 1982). Few HRs, such as *Np*HR from *Natronomonas pharaonic*, are used as an optogenetic suppressor of neural firing (Gradinaru et al., 2008). The outward-directed Na^+ pumps which are mechanistically closely related to proton pumps, form the family of Na^+ pumping opsins, which currently consists of more than ten homologs. They all display a characteristic conserved NDQ motif and have the ability to pump protons in the absence of Na^+ ions. KR2 from *Krokinobacter eikastus* is the first described and one of the well-characterized Na^+ pumps (Abe-Yoshizumi et al., 2016; Balashov et al., 2014; Inoue et al., 2013; Kato et al., 2015).

1.2.2.2.1.2. Microbial ion channel rhodopsins

The microbial channel rhodopsins are light-gated ion channels that serve as sensory rhodopsins in lower eukaryotes by controlling phototaxis. These channelrhodopsins are predominantly expressed in chlorophyte and cryptophyte algae. They can be categorized into cation and anion-conducting channelrhodopsins (CCRs and ACRs) based on the specificity to certain ions. The first characterized channel rhodopsins were from the unicellular flagellated algae *Chlamydomonas reinhardtii*. It was previously known that they presented phototaxis behavior. This behavior was attributed to the light-sensitive proteins expressed in their eyespot. The heterologous expression of these light-sensitive protein in *Xenopus laevis* oocytes proved them to be photosensitive proteins (Nagel et al., 2002, 2003). The channelrhodopsins can also be used as bistable optical switches photoactivated by one wavelength of light and rapidly reset to the dark state by another wavelength of light (Berndt et al., 2009). The optogenetic potential of these channels soon led to the discovery of several other channelrhodopsins from the

genomic databases with interesting characteristics of conducting certain types of ions, different wavelengths for activation, different on/off kinetics, and enhanced bistable characteristics.

1.2.2.2.1.3. Microbial enzyme rhodopsins

The microbial enzyme rhodopsins found in lower eukaryotes consists of a light sensing domain, an enzymatic domain with or without response regulatory domain connected via a linker (Mukherjee et al., 2019). Histidine kinase rhodopsins (HKRs) are expressed in unicellular flagellated algae, and it was first reported to be expressed in *Chlamydomonas reinhardtii.* HKRs are involved in regulating cyclases and other downstream proteins by phosphorylation. These rhodopsins contain another transmembrane helix in addition to the canonical septahelical light-sensing domain (Kateriya et al., 2004; Luck et al., 2012). Rhodopsin phosphodiesterases (RhoPDEs) are rhodopsins with a C-terminal phosphodiesterase domain commonly found among the choanoflagellates (Brunet et al., 2019; Yoshida et al., 2017). They catalyze the breakdown of the phosphodiester bond in the second messengers like cAMP and cGMP, which plays a major effect in regulating these cyclic nucleotides in these organisms. In the choanoflagellates, RhoPDEs are involved in the collective contractility of the colonies (Brunet et al., 2019). Rhodopsin cyclases are the rhodopsins with the cyclase domains, catalyzing the production of cyclic nucleotides. They are often associated with phototaxis and development in motile zoospores of fungi and algae. They can be either light-activated or light-inhibited cyclases (Avelar et al., 2014; Tian et al., 2018).

1.2.2.2.2. Animal opsins

Animal opsins are the type II rhodopsins that belong to the superfamily of GPCRs. They function by sensing photons and induce conformational change to activate specific G proteins. There is no structural relevance to microbial opsins apart from the seven helical structure. These members form the basis for the visual and non-visual photoreception in the animals in which they are expressed. They can be distinguished by their role as visual opsins, non-visual opsins, or photoisomerases. The animal opsins are broadly classified into eight groups: vertebrate visual & non-visual opsins, encephalopsin, G_q coupled visual opsin & melanopsin, neuropsin, G_o coupled opsin, cnidarian G_s coupled opsin, peropsin and retinochrome & retinal G protein-coupled receptor (RGR) (Nagata and Inoue, 2021). Most animal rhodopsins are known to couple to cyclic nucleotide signaling cascade types like G_t, G_i, G_o, and G_s while some to phosphoinositol-based G_q signaling cascades. Peropsin and retinal

photoisomerase serves to isomerize all-trans-retinal to 11-cis-retinal for the other opsins (Hao and Fong, 1999; Nagata et al., 2018).

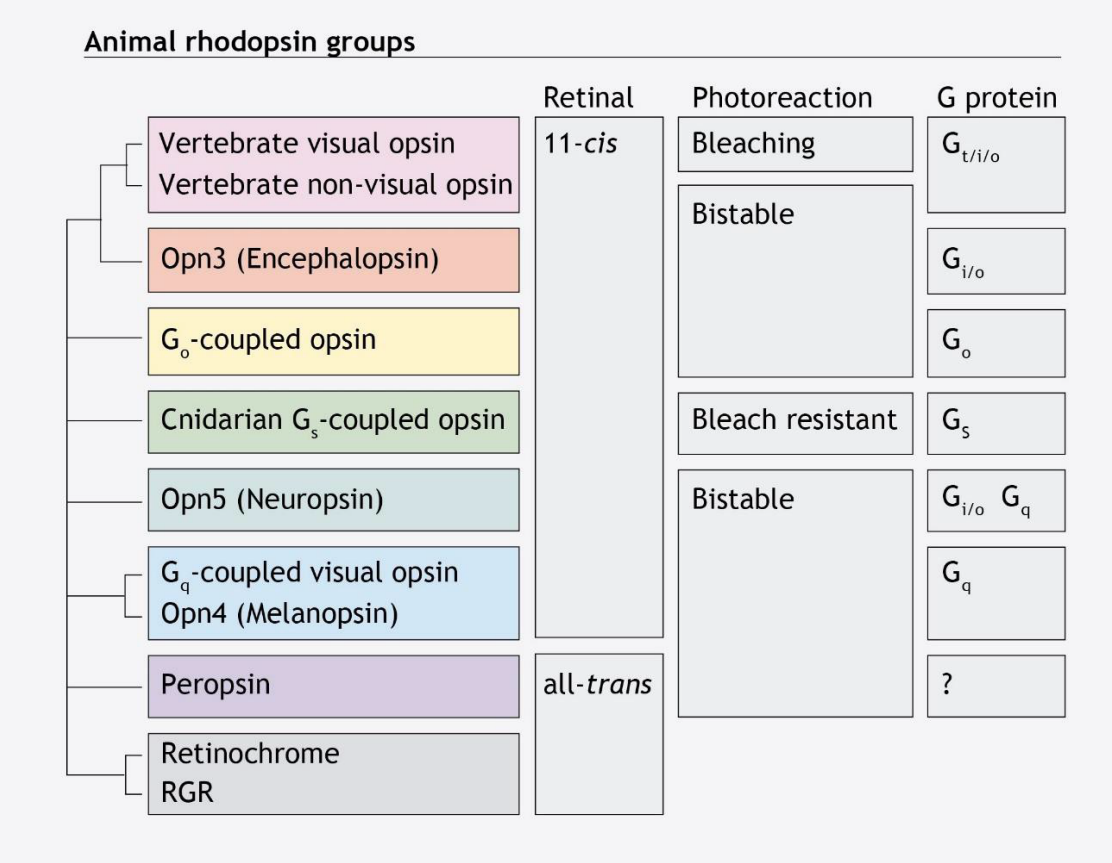

Figure 10: Functional diversity of animal rhodopsins.
The different type II rhodopsins that bind to 11-cis retinal and activate distinct G protein-mediated signaling cascades, which include cyclic nucleotide signaling mediated by G_t protein-coupled, $G_{i/o}$ coupled, G_o coupled, and G_s coupled rhodopsins in addition to phosphoinositol based signaling mediated by G_q-coupled rhodopsins. The type II rhodopsins that bind to all-trans retinal are peropsin and retinal photoisomerases. They photoisomerize all-trans to the 11-cis retinal (Nagata and Inoue, 2021).

In the dark state, bistable and monostable opsins both bind to 11-cis retinal. They are primarily distinguished by their differences in photoreactions. Bistable pigments show a reversible photoconversion of their 11-cis retinal to all-trans retinal, while monostable pigments release retinal after the photoconversion of 11-cis to all-trans retinal. Thereby, the monostable opsins are subjected to bleaching and depend on a retinal supply for continuous functioning (Figure 10). Alternatively, photoisomerases perform light-mediated conversion of all-trans to 11-cis retinal in the retinal pigment epithelium, which supplies 11-cis retinal to replenish monostable opsins present in the rod and cone cells (Tsukamoto and Terakita, 2010). For

visible light absorption, a protonated Schiff base formation between the retinal chromophore and a conserved lysine residue is essential, but it is unstable because of the positive charge within the opsin (Palczewski, 2006). A negatively charged amino acid acts as the counterion to stabilize the protonated Schiff base. Thus, the counterion has a major impact on the spectroscopic and photo-biochemical properties of rhodopsins. Parapinopsin is phylogenetically close to vertebrate visual rhodopsins, and it is a bistable pigment that contains glutamic acid at two positions 113 and 181. Glu181 serves as a counterion, at least in the photoproduct. It is suggested that during the evolution of monostable visual opsins, the amino acid in the counterion position 181 was lost, whereas only the glutamic acid in the position 113 stabilized the retinal, and thereby becoming monostable opsins. In conclusion, the counterion position determines whether an opsin is bistable or monostable (Kojima et al., 2017; Nagata and Inoue, 2021; Tsukamoto and Terakita, 2010b) and the counterion position along with nearby amino acids, affects the electronic resting state of the retinal and thereby the spectral properties.

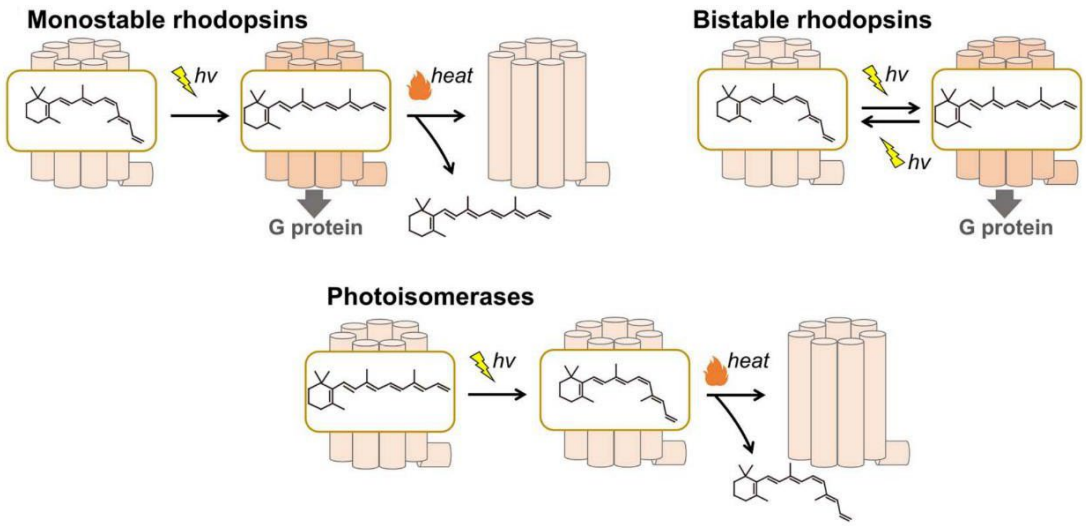

Figure 11: The schematics of photoreaction of animal rhodopsins.
In monostable type II rhodopsins, the photoisomerization of 11-cis to all-trans retinal forms the active state, followed by the release of retinal called bleaching. In bistable type II rhodopsins, reversible photoisomerization occurs between the inactive and active states containing 11-cis and all-trans retinal, respectively. Photoisomerase type II rhodopsins on the other hand, bind exclusively to the all-trans retinal in the dark and photoisomerize all-trans to 11-cis retinal. The 11-cis retinal produced by photoisomerases in the retinal pigment epithelium is supplied to the rhodopsins in cone and rod cells that require 11-cis retinal for their functioning (Kojima and Sudo, 2023).

The type II rhodopsins have the potential to be used as novel molecular tools that can be used to control specific intracellular G protein signaling cascades. The usage of these light-sensitive GPCRs can outcompete the conventional methods of chemical and genetic manipulation to study GPCRs. With current technologies with optics and microscopy, it is

possible to achieve high temporal and spatial resolution. The possibility of mimicking the effects of endogenous pulsatile or tonic activation of GPCRs by neurotransmitters or hormones with both spatial and temporal resolution is made possible with this combination of light-sensitive GPCRs and optical advancements with respect to light illumination. The quest to find a GPCR that selectively couples to a specific G protein also led to the engineering of Opsin-GPCR chimeras in the early years (Airan et al., 2009; Kim et al., 2005). In recent years, with the rapid progression in the field of genomic analyses, a large number of animal rhodopsins from different organisms have been identified. Some of these newly discovered rhodopsins possessed the ability to activate specific G protein signaling pathways, and they are briefly described in the next paragraphs.

1.2.2.2.3. OptoXRs: Opsin-GPCR chimeras

Firstly, the OptoXR is an optogenetic approach that combines the light-sensitive domains of an opsin with the domain responsible for the G protein coupling of a GPCR. This novel idea of benefitting from the creation of chimeras stemmed from the work of Khorana's group, which engineered the chimeric receptor from the bovine rhodopsin and β2-adrenergic receptor (β2-AR) (Kim et al., 2005). They constructed the chimera by replacing each of the cytoplasmic loops of rhodopsin with that of corresponding loops from β2-AR. The most critical part was the size of the third cytoplasmic loop, which determines the extent of chromophore bond formation, stability, and subsequent signal transduction specificity. They engineered a chimeric receptor and demonstrated its novelty in HEK293S and COS-1 cells. The light-induced conformational changes resulted in the activation of the G_s signaling cascade corresponding to the β2-AR. This interesting work led to the development of the OptoGPCR as a new class in *in vivo* physiology tools. Deisseroth's group engineered a G_q coupled human α_{1a} adrenergic receptor (α1a-AR) and the G_s coupled hamster (β2-AR) with bovine rhodopsin and validated the signaling cascades of resulting chimeras in HEK293 cells. Further, the OptoXRs were explored in neurons as well as *in vivo* in mice to modulate their behavior (Airan et al., 2009). There are several problems associated with the use of current OptoXRs. They do not show the predicted functionality as expected or exhibit reduced folding and stability compared to the native GPCR from which the sequences were exchanged. The agonist-mediated interaction vary the activation strength in addition to differences in activation of G protein-dependent and β-arrestin dependent pathways. Receptor dimerization or association with other interactors by the native receptors does not exist, as these are driven by distinct transmembrane sequences or sequences present in the N-terminal region. The overexpression of OptoXRs can compete with endogenous receptors or lead to accumulation due to their problems with folding or stability. Since OptoXRs are based on bovine rhodopsin ciliary type opsins, they have the tendency to lose the retinal molecule after a single activation, which leads to a bleaching effect. So, a

constant replenishment of 11-cis retinal is a prerequisite to use these OptoXRs. The retinal loss also leads to OptoXRs structural instability, which leads to internalization and subsequently targeted for degradation by the endogenous cell machinery. Therefore, the use of OptoXRs for repeated light stimulations would lead to a gradual loss in the magnitude of light-mediated response, which affects the efficacy of OptoXRs use in optogenetic research (Tichy et al., 2019).

1.2.2.2.4. G_s coupling Opsins: Jelly fish Opsin

Jellyfish Opsin (JellyOp) from the box jellyfish visual system was discovered as a green light-sensitive opsin which triggers the G_s signaling cascade (Koyanagi et al., 2008). JellyOp belongs to the group of cnidarian rhodopsins, which are known to regulate vital functions predominantly using cyclic nucleotide-gated channels (Plachetzki et al., 2007). The identification of JellyOp is highly important in G_s signaling research as it is a naturally occurring G_s coupled optogenetic GPCR. Its discovery aids in the investigation of pathological effects caused by varied temporal activation of G_s signaling in desired groups of cells. Members of the Sasse group were the first to use the JellyOp to investigate G_s signaling in the heart. The use of JellyOp in adult mouse hearts made the possibility for the first time to explore the effect of localized and time-restricted G_s protein stimulation (Makowka et al., 2019). The successful use of an optogenetic GPCR to specifically control the G_s signaling cascade paved the way for the investigation of newly discovered optogenetic GPCRs that can be utilized to control other G protein signaling cascades in cardiac research.

1.2.2.2.5. G_i coupling Opsins: Lamprey Parapinopsins

Lamprey Parapinopsin (UVLamP) from Japanese river lampreys is a UV light-sensitive bistable rhodopsin. It is typically expressed in the pineal complex and functions in non-visual photoreception coupled natively to the G_t signaling cascade (Blackshaw and Snyder, 1997; Koyanagi et al., 2004; Wada et al., 2012). In heterologous expression systems like HEK293S, it causes light-mediated inhibition of adenyl cyclases (Kawano-Yamashita et al., 2015; Wada et al., 2018). Members of the Herlitze's group used different strategies in HEK293 expressing UVLamP to prove the G_i specificity and the fast on/off kinetics compared to other commonly used optogenetic GPCRs (Eickelbeck et al., 2019). UVLamP presents it as an attractive G_i coupling optogenetic tool to specifically regulate the G_i signaling cascade in heterologous systems. The bistable nature of UVLamP is an added advantage with fast switching on or off with two different light wavelengths that would allow precise control of the activation duration, making it an ideal optogenetic protein for studying the G_i signaling cascade.

1.2.2.2.6. G_q coupling Opsins: Melanopsin

Melanopsin (OPN4) is expressed in intrinsically photosensitive retinal ganglion cells within the retina of mammals and is involved in a range of non-visual functions, including regulating circadian rhythms, retinal vascular development, and pupillary light response (Hankins et al., 2008; Provencio et al., 1998). Evidence suggests that it belongs to the group of rhabdomeric rhodopsins marked by its distinct phototransduction cascade differing from that of the other visual opsins like rod and cone opsins (Arendt, 2003; Graham et al., 2008; Panda et al., 2005; Provencio et al., 2000). It binds to 11-cis retinal and it is most sensitive to 480 nm wavelength of light. In addition, it has an intrinsic photoisomerase activity to revert all-trans retinal to the cis-retinal upon illumination by a longer wavelength of light displaying its bistable nature. (Bailes and Lucas, 2013; Berson et al., 2002; Melyan et al., 2005). In mice, light activation of photosensitive retinal ganglion cells induces three types of Ca^{2+} responses, i.e. sustained, transient, and repetitive (Jagannath et al., 2015; Sekaran et al., 2003). These differences in these Ca^{2+} responses are most likely due to the activation of different splice variants of OPN4 and may involve the activation of different G_α proteins such as $G_{\alpha q}$, $G_{\alpha 11}$, and $G_{\alpha 14}$ (Chew et al., 2014; Graham et al., 2008; Hughes et al., 2014). In HeLa cells, OPN4 exhibits concurrent activation of both G_i and G_q signaling cascades (Kankanamge et al., 2018). In mouse embryonic stem cells cardiomyocytes, the $G_{q/11}$ signaling cascade was activated by mouse OPN4 upon light illumination (Beiert et al., 2014). Whereas in the adult transgenic mouse heart, the G_i signaling cascade was activated by OPN4 (Wagdi, Malan, Sathyanarayanan et al., 2022). Therefore, OPN4 may activate different signaling pathways concurrently depending on the cell type. Hence, currently there is no specific G_q activating opsin to study the G_q signaling cascade, and this quest leads to the recently discovered Neuropsin.

1.2.2.2.7. Neuropsin

Neuropsin (OPN5) is a UV light-sensitive bistable GPCR. It shares only 25 to 30 % similarity to other known type II rhodopsins (Tarttelin et al., 2003). They are phylogenetically related to RGR-opsins and peropsins based on their similar intron structure, but they displayed very low amino acid similarity (Leung and Montell, 2017). It is expressed in deuterostomes and well conserved in vertebrates from fish to humans. Among mammals, they are extraordinarily conserved, especially the amino acid sequence of mouse and human OPN5. which shows very high similarity and exhibits a strong functional requirement (Tarttelin et al., 2003). Its expression in humans and mice was found in the retina, brain, and spinal cord. Later, also it was found to be expressed in the testes, sperm, skin, and outer ear in mammals (Haltaufderhyde et al., 2015; Kojima et al., 2011; Pérez-Cerezales et al., 2015; Sato et al., 2016; Tarttelin et al., 2003). OPN5 plays a role in the regulation of perinatal vascular development and entrains local circadian clocks of the retina, cornea, and skin independent of the suprachiasmatic nucleus. Also, it is required for local adaption

to the day/night rhythm in mice (Buhr et al., 2015; Díaz et al., 2020; Nguyen et al., 2019; Ota et al., 2018). In mice, OPN5 involvement in energy metabolism and regulation of brown adipose tissue thermogenesis was reported, and the evidence of expression in the medial preoptic nucleus of the hypothalamus demonstrates the role as a deep brain photoreceptor (Zhang et al., 2020). In chicken, it is expressed in differentiating ganglion and amacrine cells of embryonic and early hatchings neural retina (Tomonari et al., 2008). In Japanese quail, it is expressed in the paraventricular region of the brain and has been proven to play a role in seasonal reproductive cycles (Nakane et al., 2010). UV light stimulation of human OPN5 led to MAPK phosphorylation in HEK293 cells. MAPK phosphorylation, which occurs downstream of the G_q signaling cascade, leads to the regulation of genes for the production of corticotropin, which is associated with sexual reproduction in birds (Buhr et al., 2015; Sugiyama et al., 2014).

Another attractive characteristic of Neuropsin is the bistable nature of the opsin. It has two stable states, a dark state (inactive state) bound to the 11-cis retinal and after a short wavelength light stimulation covert to a stable photoproduct containing the photo-isomerized all-trans retinal, that reverts to the original dark state after a subsequent long wavelength light absorption (Kojima et al., 2011). Reports from Yamashita et al. and Kojima et al. showed membrane-purified chicken and mouse OPN5 couple to G_i proteins based on radionucleotide filter binding assay, which measures GDP/$GTP_\gamma S$ exchange by G protein at non-physiological conditions of 0 °C (Yamashita et al., 2010). Additionally, a decrease in cAMP levels was observed upon UV light illumination in HEK293 expressing mouse OPN5 (Kojima et al., 2011). Nakane et al. also reported a high level of expression levels of $G_{\alpha q}$ protein in the paraventricular region of quail in addition to OPN5 expression, suggesting that it might couple to the G_q signaling cascade (Nakane et al., 2010). Retinal ganglion cell line 5 and immortalized human müller cells from the retina, which have endogenous OPN5 expression, displayed an increase in Ca^{2+} levels observed upon light stimulation (Hollborn et al., 2011; Nieto et al., 2011). Sugiyama and colleagues expressed human OPN5 in HEK293 and mouse neuroblastoma Neuro-2a cells and observed a UV light-mediated increase in Ca^{2+} and a decrease in cAMP levels. They suggested OPN5 to be $G_{i/o}$ coupled, as it causes cAMP decrease by adenyl cyclase inhibition that increases Ca^{2+} in the cytosol from Ca^{2+} stores. The coupling selectivity of OPN5 was not clear, as the previous reports on OPN5 provided mixed information on G protein coupling, with many reports suggesting G_i coupling. The quest to find an optogenetic tool that selectively activates the G_q signaling cascade and to clarify the prevailing information of hOPN5 coupling selectivity together led to the characterization of OPN5.

1.3. Scope and Aims of the Thesis

In mammalian cells, GPCRs form the most abundant superfamily of membrane proteins, which act as key regulators of cellular behavior. Activation by specific stimuli is transposed into intracellular signaling by triggering distinct G_α proteins. G_q signaling is one of the four major G protein signaling cascades, which plays a pivotal role in many physiological processes. Improper functioning leads to many pathophysiological conditions, such as cancer, auto-immunity, and cardiac hypertrophy. Even though prevailing technologies utilizing pharmacologic and genetic manipulation provided many insights into GPCR's signaling, the dynamics and encoding of extracellular activation into intracellular processing are not understood yet. Specifically, it was so far not possible to mimic the precise spatiotemporal aspects of the pulsatile or tonic release happening during the synaptic release of transmitters or hormones, respectively. Optogenetic stimulation has the capability to accomplish nearly endogenous levels of temporal precision in the ms range and spatial precision in the nm range. Research in Optogenetics has discovered many light-sensitive GPCRs that trigger specific G protein signaling cascades. But currently, there is a lack of light-sensitive GPCRs which can selectively trigger the G_q signaling cascade.

The aims of this project are 1) Characterization of the wild type (WT) hOPN5 using assays that sequentially address each of the second messengers produced during the activation of the Gq signaling cascade and to prove its specificity. 2) To create a foundation to develop new OPN5 variants in the long term for specific optogenetic applications. With the focus on engineering enhanced properties, including peak wavelength shifts for both activation and deactivation, improved retinal retention, improved receptor kinetics, and red-shifted variants.

2 Materials and Methods

2.1. Materials

Table 1: List of reagents

Reagent	Article no.	Company
1,2-Bis-(2-Aminophenoxy)-ethane-*N, N, N′, N′*-tetra acetic acid (BAPTA)	A4926	Sigma Aldrich
1-Oleoyl-2-acetyl-sn-glycerol	O6754	Sigma Aldrich
2-Propanol	6752.4	Carl Roth
4-(2-hydroxyethyl)-1-piperazineethanesulphonic acid (HEPES)	9105.3	Carl Roth
4′,6-diamidino-2-phenylindole (DAPI)	0018860.01	Th. Geyer
Adenosine 5`-triphosphate magnesium salt (MgATP)	A9187	Sigma Aldrich
Agarose Broad range	T846.3	Carl Roth
All-trans retinal	R2500	Sigma Aldrich
Aqua Pro	2351744	Braun
Calcium Chloride ($CaCl_2$)	CN93.1	Th. Geyer
Carbamoylcholine chloride	C4382	Sigma Aldrich
Cellmask Deep Red Plasma Membrane	C10046	Life Technologies
Cesium Chloride ($CsCl_2$)	C4036	Sigma Aldrich
CIAP 20 U/µL (alkaline Phosphatase)	18009019	Life Technologies
Cyclopiazonic acid	BML-CA415-0010	Enzo Life Sciences
Deoxyribose nucleotide triphosphate (dNTP) Solution Set	N0446S	New England Biolabs
D-Glucose	G8270	Sigma Aldrich
Dimethyl sulphoxide (DMSO)	D5879	Th. Geyer
Dithiothreitol (DTT)	10708984001	Sigma Aldrich
DMEM, high glucose	41965062	Life Technologies
Ethylene glycol-bis-(β-aminoethyl ether)-N,N,N′,N′-tetraacetic acid (EGTA)	E4378	Sigma Aldrich

Ethylenediamine tetraacetic acid disodium salt dihydrate (EDTA)	8043.2	Carl Roth
FBS Superior	S0615	Sigma Aldrich
Fibronectin from bovine	F1141	Sigma Aldrich
Formaldehyde (4%)	2134	Th. Geyer
FuGene HD	E2311	Promega
Gene Ruler DNA Ladder Mix	SM0333	ThermoFischer
Glycerine (99.5%)	3783.2	Carl Roth
Guanosine-5`-triphosphate Disodium salt Dihydrate (Na_2GTP)	G8877	Sigma Aldrich
KLD Enzyme Mix	M0554S	New England Biolabs
Lipofectamine 3000	L3000015	Life Technologies
Luria-Bertani (LB) Agar	X969.2	Carl Roth
Luria-Bertani (LB) Medium	X968.2	Carl Roth
Magnesium Chloride ($MgCl_2$)	KK36.2	Carl Roth
n-dodecyl-β-D-maltoside (DDM)	850520P	Sigma Aldrich
Panserin 401	P04-710401	PAN biotech
PBS w/o Ca^{2+}, Mg^{2+}	D8537	Sigma Aldrich
Pertussis Toxin Glycerol Solution	516561	Sigma Aldrich
Pluronic F-127 20% Solution	P3000MP	Life Technologies
Potassium Fluoride	1630	Th. Geyer
PowerLoad Concentrate 100x	P10020	Life Technologies
Q5® High-Fidelity DNA Polymerase	M0491L	New England Biolabs
Quick-Load® Purple 1 kb Plus DNA Ladder	N0550G	New England Biolabs
Roti-Safe GelStain	3865.1	Carl Roth
Sodium Chloride (NaCl)	3957.1	Carl Roth
T4 Ligase	M0202S	New England Biolabs
Thapsigargin	BML-PE180-0001	Enzo Life Sciences
Tris, pure	5429.3	Carl Roth
Water, Bioscience grade, Nuclease free	T143.5	Th. Geyer
X-Rhod-1, AM, cell permeant	X14210	Life Technologies
β-Mercaptoethanol	A11080100	Th. Geyer

Table 2: List of Plasmids

Plasmid number	Name	Bacterial resistance	Eukaryotic resistance
TB#001	pCAG-hOPN5-eYFP Neomycin	Ampicillin	G418/Neomycin
TB#005	pCAG-hOPN5-eYFP-Puromycin	Ampicillin	Puromycin
TB#007	pCAG-hOPN5(T164A)-eYFP Neomycin	Ampicillin	G418/Neomycin
TB#009	ClaI-hOPN5(T164A)-PfmI	Ampicillin	None
TB#019	hOPN5(F114S) plus addons	Kanamycin	None
TB#020	pCAG-hOPN5(F114S)-eYFP Neomycin	Ampicillin	G418/Neomycin
TB#021	hOPN5(I203D) plus addons	Kanamycin	None
TB#022	pCAG-hOPN5(I203D)-eYFP Neomycin	Ampicillin	G418/Neomycin
TB#023	hOPN5(S218C) plus addons	Kanamycin	None
TB#024	pCAG-hOPN5(S218C)-eYFP Neomycin	Ampicillin	G418/Neomycin
TB#025	hOPN5(F217L) plus addons	Kanamycin	None
TB#026	pCAG-hOPN5(F217L)-eYFP Neomycin	Ampicillin	G418/Neomycin
TB#027	hOPN5(F217I) plus addons	Kanamycin	None
TB#028	pCAG-hOPN5(F217I)-eYFP Neomycin	Ampicillin	G418/Neomycin
TB#029	hOPN5(F217V) plus addons	Kanamycin	None
TB#030	pCAG-hOPN5(F217V)-eYFP Neomycin	Ampicillin	G418/Neomycin
TB#031	hOPN5(Y301H) plus addons	Kanamycin	None
TB#032	pCAG-hOPN5(Y301H)-eYFP Neomycin	Ampicillin	G418/Neomycin
TB#033	hOPN5(Y174F) plus addons	Kanamycin	None
TB#034	pCAG-hOPN5(Y174F)-eYFP Neomycin	Ampicillin	G418/Neomycin
TB#035	hOPN5(Y268F) plus addons	Kanamycin	None
TB#036	pCAG-hOPN5(Y268F)-eYFP Neomycin	Ampicillin	G418/Neomycin
TB#037	hOPN5 plus addons #1278	Kanamycin	None
TB#072	pCAG-hOPN5-eYFP Bsr	Ampicillin	Blasticidin
TB#073	pCAG-hOPN5-eCFP Neo	Ampicillin	G418/Neomycin
TB#074	pCAG-hOPN5-mCherry Neo	Ampicillin	G418/Neomycin
TB#075	AAV_ITR-CAG-hOPN5-eYFP-WPRE-polyA-ITR	Ampicillin	None
TB#076	pCAG-TRPC6-mCherry Bsr	Ampicillin	Blasticidin

TB#119	pCMV-hM2-CFP Neo #1298	Ampicillin	G418/Neomycin
TB#120	CAGhOPN5d4IRESeGFP	Ampicillin	G418/Neomycin
TB#121	G_{i1}-CASE	Ampicillin	G418/Neomycin
TB#122	G_{i2}-CASE	Ampicillin	G418/Neomycin
TB#123	G_{i3}-CASE	Ampicillin	G418/Neomycin
TB#124	G_{o1}-CASE	Ampicillin	G418/Neomycin
TB#125	G_s(short)-CASE	Ampicillin	G418/Neomycin
TB#126	G_q-CASE	Ampicillin	G418/Neomycin
TB#127	G_{15}-CASE	Ampicillin	G418/Neomycin
TB#128	G_{13}-CASE	Ampicillin	G418/Neomycin
TB#129	pCAG-mOPN4-IRES-GFP #1239	Ampicillin	G418/Neomycin
TB#130	pCAG-hM2-mCherry Bsr	Ampicillin	G418/Neomycin
TB#131	pCAG-hOPN5-mCherry Bsr	Ampicillin	G418/Neomycin
TB#132	22ABHLMP_cOPN5_mScarlet-I_GeneArt	Kanamycin	None
TB#133	pCAG-cOPN5(WT)-eYFP Neo	Ampicillin	G418/Neomycin
TB#134	pCAG-cOPN5(WT)-eYFP Bsr	Ampicillin	Blasticidin
TB#135	pCAG-cOPN5(WT)-mScarlet-I Bsr	Ampicillin	Blasticidin
TB#138	pCAG-hOPN5(WT)-mScarlet-I Bsr	Ampicillin	Blasticidin

Table 3: List of Primers

Oligo number	Oligo name	Sequence	Length
TB_001	hOPN5-F114S-FP	atgggctggaagcttctttggctgtggaagcc	32
TB_002	hOPN5-F114S-RP	ccataccagcggcagccg	18
TB_003	hOPN5-Y174F-FP	tctgggggacttcgtacctgagc	23
TB_004	hOPN5-Y174F-RP	cctaccaagggcatggtg	18
TB_005	hOPN5-I203D-FP	catcctgaacgacctcttcttctgcctc	28
TB_006	hOPN5-F217L-FP	tgtgatcgtgctgtcctacgtaaagatc	28
TB_007	hOPN5-I203D-RP	aaaacctggccccctacc	18
TB_008	hOPN5-F217L/I/V-RP	gccgttgggagcaagagg	18
TB_009	hOPN5-F217I-FP	tgtgatcgtgatctcctacgtaaagatc	28
TB_010	hOPN5-F217V-FP	tgtgatcgtggtgtcctacgtaaagatc	28
TB_011	hOPN5-Y268F-FP	ctggattcctttcgcagtggtgtc	24
TB_012	hOPN5-Y268F-RP	gcaatcaggaatccagcac	19
TB_013	hOPN5-S218C-FP	gatcgtgttctgctacgtaaagatcattg	29

TB_014	hOPN5-S218C-RP	acagccgttgggagcaag	18
TB_015	hOPN5-Y301H-FP	tgcagcgatgcacaatcccatca	23
TB_016	hOPN5-Y301H-RP	gattttgcaagtagggttgg	20
TB_022	CAG-Promoter-Seq/GenTyp-FP	ggctctagagcctctgctaacc	22
TB_023	hOPN5-GenTyp-RP	tgcaagtagggttggcaccac	21
TB_027	TRPC6-FP-SalI	acgcgtcgacctcgagctcgatatcgccaccatgagccagagc	43
TB_028	TRPC6-RP-NotI	aaaagcggccgcgggcggtaccgttctgcggct	33
TB_031	mCherry-FP-NotI	aaaagcggccgcgtcagccaccatggtgagcaagggcgaggag	43
TB_032	mCherry-RP-AgeI	taaccggtcaatttcattacttgtacagctcgtc	34
TB_033	TRPC6-Seq-2-FP	cctcatgattacttctgcaag	21
TB_034	TRPC6-Seq-3-FP	gcagcatcattcattgcaag	20
TB_035	TRPC6-Seq-4-FP	gcaagacatctcaagtctcc	20
TB_036	hOPN5-Seq-2-FP	gcgatgttgatttgtgctgg	20
TB_085	M2_XhoI_FP	catactcgaggccaccatgaagacgatcatcgc	33
TB_086	M2_NotI_RP	aagaatgcggccgcccttgtagcgcctatgttc	33
TB_099	mCherry_SeqRP	atgaactccttgatgatggc	20
TB_130	I-NEB-cOPN5-eYFP-FP	gaattgcccttgctgccaccatgagcggcatggccagc	38
TB_131	I-NEB-cOPN5-eYFP-RP	accatggtggcggccgcggccacttccagctgtgttccagac	42
TB_132	V-NEB-cOPN5-eYFP-FP	gccgcggccgccaccatg	18
TB_133	V-NEB-cOPN5-eYFP-RP	ggtggcagcaagggcaattccacc	24
TB_143	mOPN4-XhoI-FP	ccgctcgagggaattgcccttgctgccaccatggactctccttcaggac	49
TB_144	mOPN4-NotI-RP	ggtggcggccgcggcggccagatgtctgagagtcac	36

Table 4: List of Restriction Endonucleases

Restriction endonuclease	Article no.	Company
BamHI	ER0051	ThermoFischer
BcuI (SpeI)	ER1251	ThermoFischer
BglII	ER0082	ThermoFischer
BshTI (AgeI)	ER1461	ThermoFischer

Cfr9I (XmaI)	ER0171	ThermoFischer
DpnI	ER1701	ThermoFischer
Eco32I (EcoRV)	ER0303	ThermoFischer
Eco52I (EagI)	ER0332	ThermoFischer
EcoRI	ER0271	ThermoFischer
HindIII	ER0503	ThermoFischer
KpnI	ER0521	ThermoFischer
NcoI	ER0572	ThermoFischer
NheI	ER0972	ThermoFischer
NotI	ER0592	ThermoFischer
PacI	ER2201	ThermoFischer
PaeI (SphI)	ER0601	ThermoFischer
PagI (BspHI)	ER1281	ThermoFischer
PdmI (XmnI)	ER1531	ThermoFischer
PstI	ER0612	ThermoFischer
SacI	ER1132	ThermoFischer
SalI	ER0642	ThermoFischer
ScaI	ER0431	ThermoFischer
SmaI	ER0663	ThermoFischer
SspI	ER0771	ThermoFischer
XhoI	ER0692	ThermoFischer

Table 5: List of Kits

Kit name	**Article no.**	**Company**
DC Protein Assay	5000111	Bio-Rad
GFP Elisa Kit	AKR-121	Cell Biolabs
IP-One-G_q HTRF kit	62IPAPEB	Cisbio
KLD Enzyme Mix	M0554S	New England Biolabs
Monarch DNA Gel Extraction Kit	T1020L	New England Biolabs
NEBuilder HiFi DNA Assembly Cloning Kit	E5520 S	New England Biolabs
NucleoBond Xtra Midi	740.410.100	Macherey-Nagel
NucleoBond Xtra Midi Plus	740412.50	Macherey-Nagel
NucleoSpin Plasmid Mini	740588.250 /11699382	Macherey-Nagel
NucleoSpin® Gel and PCR Clean-up	740.609.250	Macherey-Nagel

PCR Mycoplasma-Test kit	A3744,0020	PANReac AppliChem
Quick Ligation Kit	M2200S	New England Biolabs

Table 6: List of Buffers

Tyrode solution

Components	Concentration (mM)
$CaCl_2$	1.8
Glucose	10
HEPES	10
KCl	5.4
$MgCl_2$	2
NaCl	140

TRPC6 assay external bath solution

Components	Concentration (mM)
$CaCl_2$	2
CsCl	5
Glucose	10
HEPES	10
$MgCl_2$	1
NaCl	140

TRPC6 assay internal solution

Components	Concentration (mM)
BAPTA	10
$CaCl_2$	5
CsCl	120
GTP	0.2
HEPES	10
$MgCl_2$	1
NaCl	9.4

10x TAE buffer

Components	Concentration (mM)
Acetic acid	20
EDTA	1
Tris	40

Membrane lysis buffer

Components	Concentration (mM)
DDM	2% (w/v)
NaCl	150
Protease inhibitor tablet	1 per 50 mL
Tris, 99% pure	50

Table 7: List of Bacterial cells

Cells	Article no.	Company
10-beta Competent *E.coli*	C3019H	New England Biolabs
Turbo Electrocompetent *E.coli*	C2986K	New England Biolabs
XL10-Gold Ultracompetent Cells	200315	Agilent

Table 8: List of mammalian Cell lines

Cell line	Antibiotic resistance
Ad HEK293	-
HEK293 G_i KO hOPN5 (WT) eYFP	Neomycin
HEK293 $G_{q/11}$ KO hOPN5 (WT) eYFP	Neomycin
HEK293 hOPN5 (F114S) eYFP	Neomycin
HEK293 hOPN5 (F217I) eYFP	Neomycin
HEK293 hOPN5 (F217L) eYFP	Neomycin
HEK293 hOPN5 (F217V) eYFP	Neomycin
HEK293 hOPN5 (S218C) eYFP	Neomycin

HEK293 hOPN5 (T164A) eYFP	Neomycin
HEK293 hOPN5 (WT) eYFP	Neomycin
HEK293 hOPN5 (WT) eYFP, GIRK1/2	Neomycin,Puromycin, and Blasticidin
HEK293 hOPN5 (WT) eYFP, TRPC6 mCherry	Neomycin and Blasticidin
HEK293 hOPN5 (WT) mCherry	Blasticidin
HEK293 hOPN5 (WT) mCherry, G_q-CASE	Blasticidin and Neomycin
HEK293 hOPN5 (Y174F) eYFP	Neomycin
HEK293 hOPN5 (Y268F) eYFP	Neomycin
HEK293 hOPN5 (Y301H) eYFP	Neomycin
HEK293 M2-mCherry, G_{i1}-CASE	Blasticidin and Neomycin

Table 9: List of Consumables

Consumables	Article No.	Company
0.2 mL flat cap tubes	72.737.002	Sarstedt
0.5 mL flat cap tubes	72.699	Sarstedt
1.5.mL flat cap tubes	72.690.001	Sarstedt
10 cm cell culture dishes	83.3902.300	Sarstedt
13 mL tubes for bacterial culture	62.515.006	Sarstedt
2 mL flat cap tubes	72.691	Sarstedt
22 mm glass coverslips	BB02200220	Epredid
384-well cell culture plates	784075	Sigma Aldrich
6-well cell culture plates	83.3920	Sarstedt
96-well cell culture plates	83.3924.005	Sarstedt
Black 96-well plates	165305	ThermoFischer
CyroPure tubes	72.379.002	Sarstedt
Half 96-well cell culture plates	675090	Greiner
Hemocytometer	717810	Neubauer
Patch clamp pipettes	GB150TF-10	Science-Products
Pipette tips 10 µL	70.1130	Sarstedt
Pipette tips 1000 µL	70.3050.020	Sarstedt
Pipette tips 200 µL	70.3030.020	Sarstedt
T25 cell culture flasks	83.3910.002	Sarstedt
T75 cell culture flasks	658170	Greiner

Aluminium 1 m AlCuMgPb	EN AW-2007	Bikar Metalle

Table 10: List of Devices

Devices	Article no.	Company
380x ET Bandpass filter 25 mm	F49-380	AHF Analysetechnik
549/15 ET Bandpass filter 25 mm	F49-500	AHF Analysetechnik
Bioclav - Moist heat sterilization Autoclave	3.021 031/93303	Schütt Labortechnik
BNC connector, straight, 2x socket	UG 914 U	Reichelt Elektronik
Bright field light source	TH4-200	Olympus
Centrifuge 5415 R	5426 0016252	Eppendorf AG
CFP Ultra Bandpass Filterset	F46-807	AHF Analysetechnik
CLARIOStar	430-0759	BMG Labtech
Eletrcoporator 2510	4307 001852	Eppendorf AG
Fibre Patch cable	M28L01	Thorlabs
GeneFlash UV transilluminator	SYGE/1511	Syngene
GFL Shaking Incubator 3031	10079814E	GFL Gesellschaft für Labortechnik
HEKA Patch-clamp amplifier EPC10	591265	HEKA
HERAsafe KS 12 EN 12469:2000 Class II Biological Safety Cabinets	40602693	Thermo Electron Corporation,
Inverted microscope	IX73P1F	Olympus
Inverted microscope	IX53P1F	Olympus
Microwave TYP	NN-E201W	Panasonic
Mini-Centrifuge Sprout plus	4666426	Th.Geyer
Minitron	10945	Infors HT
Multiskan Skyhigh Spectrophotometer	1550-800319B	ThermoScientific
Olympus-U-FF Filter module for BX3/IX3	F91-917	AHF
Omicron LED hub	2170504	Omicron-Laserage Laserproduckte
Optoscan monochromator	7932	Cairn Research
OptoSource illuminator	7933	Cairn Research
Power Supply unit EV200 Series		Peqlab
Power Supply Unit for one K-Cube or T-Cube	KPS101	Thorlabs
Scotsman AF 80 AS 230/50/1 Ice machine	DD 9526 12 T	Scotsman Europe - Frimont SPA
Silver wire 380 µm	AG-15W	Science Products
Transferpette S, variabel 0.1-2.5 µL	9280141/705869	Th. Geyer
Vortex Mixer VX-200	6292017	Th. Geyer

Memmert Water bath	LC21.0220	Memmert
X-cite Xylis	XT720L	AHF

Table 11: List of Softwares and online tools

Software	Version.	Company
Benchling	2023	Benchling Incorporation
BioRender	2023	BioRender
Cell Profiler	4.2.5	Broad Institute
FiJji: Fiji Is Just ImageJ	1.54c	National Institues of Health
GraphPad Prism 9	9.5.1 (733)	GraphPad
Olympus cellSens Dimesnion	4.2	Evident
Origin 2019: Data Analysis and Graphing Software	2019 (9.30)	OriginLab Corporation
Patchmaster	2 x92	HEKA
SnapGene Viewer	7.0.1	SnapGene Dotmatics

2.2. Methods

2.2.1 Molecular Biology Techniques

2.2.1.1 Generation of plasmids

All the plasmids were generated by a restriction site based cloning strategy. The codon-optimized gene sequences used in this thesis were ordered from GeneArt Gene synthesis (Thermo Fisher Scientific, USA). The cloning scheme was planned, taking advantage of the SnapGene Viewer software and Benchling online software. To generate the desired plasmid of choice, the DNA fragment of interest was generated either by PCR or by digestion from another plasmid with suitable restriction endonuclease sites. The vector backbone and insert fragments were digested with chosen restriction endonucleases to produce compatible overhangs for ligation. The appropriate DNA fragments were extracted and purified after performing gel electrophoresis, and the resulting fragments were ligated and transformed into *E. coli* for plasmid amplification. The correct insertion of the desired fragment was confirmed by diagnostic restriction digestion and Sanger sequencing. In the following subchapters, each of the steps followed for plasmid generation is explained in detail.

2.2.1.2. Quantification of plasmid DNA and storage

The concentration of the plasmid DNA was determined spectrophotometrically using a NanoDropTM 2000 spectrophotometer (Thermo Fisher Scientific Inc., USA). The spectrophotometer uses the absorbance of light through the samples to quantify the concentration of DNA. Quantification of DNA was performed at 260 nm, at its maximal absorbance. The DNA concentration was determined according to Beer-Lambert's law. In addition, the DNA samples were measured at 280 nm, at which the proteins have the maximal absorbance. A nucleic acid to protein ratio of A260/A280 is normally used as an indicator of the purity of DNA samples. The DNA samples were stored at 4 °C for further use and at -20 °C for long-term storage.

2.2.1.3. Plasmid DNA isolation from bacterial cultures

Plasmids are amplified in bacteria and can be purified by alkaline cell lysis. Plasmid DNA is separated from chromosomal DNA by taking advantage of the differential denaturation by the lysis buffer consisting of the detergent sodium dodecyl sulphate (SDS) and sodium hydroxide (NaOH). SDS breaks open the phospholipid bilayer, whereas NaOH denatures the proteins. It is followed by a series of steps, after which the plasmids are isolated and purified. In this project, I used two different protocols depending on the envisioned plasmid amount and

purity.

2.2.1.3.1. Small scale plasmid purification (Mini-Prep)

The small-scale plasmid DNA isolation was performed using the NucleoSpin Plasmid Mini-Prep kit from Macherey-Nagel (Germany) by strictly adhering to the manufacturer's instructions. For the plasmid extraction, a single isolated bacterial colony with the desired plasmid was inoculated in 5 mL of LB with appropriate antibiotics. The culture was grown for 8 - 12 h at 37 °C at 240 rpm using an INOVA incubator, and 4 mL were taken for plasmid isolation. The plasmids were always eluted with 50 µL of pre-warmed (60 °C) nuclease-free water. DNA concentration of the plasmids was determined, and the plasmids were stored at 4 °C for further use.

2.2.1.3.2. Large scale plasmid purification (Midi-Prep)

The large-scale plasmid DNA isolation was performed using the NucleoBond Xtra Midi kit for transfection-grade plasmid from Macherey-Nagel (Germany). A starter culture was inoculated from a single bacterial colony or 100 µL of the preserved Mini-Prep bacterial culture in 5 mL of LB with appropriate antibiotics. It was grown for 8 h at 37 °C at 240 rpm. Then, the starter culture was used to inoculate 120 mL of LB with appropriate antibiotics and was grown for 14 - 16 hrs at 37 °C at 180 rpm using an INOVA incubator. The plasmid extraction was performed by strictly adhering to the manufacturer's instructions, including the recommended instructions, to obtain better DNA yields. The resulting plasmid DNA pellet was dissolved in 200 µL of pre-warmed (60 °C) nuclease-free water. The plasmid DNA concentration was measured, and the plasmid DNA was diluted to a final concentration of 1 µg/µL for easeful future use.

2.2.1.4. Restriction digestion of plasmids

The restriction endonucleases used belong to the type II site-specific deoxyribonucleases, which recognize specific palindromic sequences and cut the DNA, creating either blunt ends, 5' or 3' overhangs (cohesive overhangs). All the restriction endonucleases were bought from Thermo Fisher Scientific Baltics UAB (Lithuania). To prepare DNA fragments for ligation, 15 µg of the chosen plasmid DNA was used in a reaction mixture containing a total volume of 40 µL. The desired combination of restriction endonucleases was chosen for the restriction digestion, and the appropriate restriction buffer was picked with the help of the online tool Thermo double cutter. The reaction mixture was incubated for 3 - 4 h to ensure complete digestion of the plasmid DNA before the restriction endonucleases were denatured by incubating the sample mixtures at 65 °C for 10 min. The samples were directly used or frozen at -20 °C. Restriction digestion was also used as a diagnostic tool to verify plasmids obtained after a cloning experiment.

Since the nucleotide sequence and size of the plasmids are known, digested fragments on the gel can verify whether it is the desired plasmid. Restriction enzymes were chosen to produce single, double, and triple fragments. In the case of the diagnostic restriction digestion, a final volume of 20 µL with a final plasmid DNA concentration of 50 ng/µL was preferred. The manufacturer's instruction was followed to set up the restriction digestion reaction mixture.

2.2.1.5. Polymerase chain reaction and site-directed Mutagenesis

The polymerase chain reaction (PCR) was employed to amplify desired DNA fragments using specific pairs of self-designed primers produced by biomers.net GmbH (Germany). Here, the thermostable DNA polymerase Q5 high-fidelity polymerase (New England Biolabs GmbH, Germany) was used to amplify the DNA fragments of interest. The amplification proceeds with DNA denaturation at 95 °C followed by Q5 polymerase binding to a single-stranded DNA template. It catalyzes the linking of phosphodiester bonds between nucleotides as dictated by the template strand sequence during the elongation phase. The main components of a PCR reaction are the DNA template, short DNA oligonucleotides (primers) that flank the DNA fragments of interest, all four deoxyribonucleotide triphosphates as substrates for the synthesis of the new DNA strand, DMSO to aid in hybridization step to lower the annealing temperature of the primers, buffer with essential metal ions and salt for the proper functioning of the polymerase.

The protocol included an initial denaturation step at 98 °C for 3 min, a three-step cycle for 30 times, which included a denaturation step at 98 °C for 30 s, an annealing or hybridization step for 30 s whose temperature was calculated based on the primers used for the PCR and an elongation step at 72 °C for a time duration depending on the length of the amplified product (30 s/kb) and a final elongation step at 72 °C for 10 min. Finally, the samples were cooled to 4 °C for an infinite time until the samples were removed from the PCR cycler. The annealing temperature was determined by the T_m °C calculation tool (https://tmcalculator.neb.com). The PCRs were performed in the ARKTIK Thermal Cycler (Thermo Fischer Scientific Oy, Finland). Subsequently, after the PCR, a DpnI digest was performed to remove the template DNA of bacterial origin since DpnI targets only the methylated template DNA and does not affect the amplified PCR product. 10 units of DpnI restriction endonuclease (Thermo Fischer Scientific Baltics UAB, Lithuania) were added directly into the PCR mixture and incubated at 37 °C for 1 h. The digested PCR mixture was purified with the Monarch PCR & DNA CleanUp Kit (New England Biolabs GmbH, Germany) according to the manufacturer's instructions. Finally, the DNA concentration was determined and stored at -20 °C or directly taken for further use.

Site-directed mutagenesis (SDM) was performed in order to mutate a single amino acid in the protein of interest. Back-to-back PCR amplification strategy was employed to amplify

the whole plasmid containing the gene of interest with specific primer pairs comprising the modified nucleotides to include the mutation in the desired position. The primers needed for the PCR were self-designed. The forward primer is designed with modified nucleotides for amino acid substitution in the middle while preserving at least 10 nucleotides complementary to the 3' end, whereas the reverse primer is entirely complementary to the 3' to 5' strand of template DNA. It is designed such that the 5´ ends of the two primers align back to back. Finally, after a successful PCR, a mutated gene is created as a result of nucleotide-exchanged primers. The above described PCR protocol consisted of increasing elongation times appropriately to ensure that the whole plasmid was amplified. The amplified PCR product is then subjected to Kinase, Ligase, and DpnI (KLD) treatment to phosphorylate the 5' end, to ligate the 5' end to the 3' and remove the bacterial origin methylated template DNA, respectively. 1 µL of the KLD enzyme mixture was added to 3 µL of the PCR product with the KLD buffer and made up to a final volume of 10 µL with nuclease-free water. The mixture was incubated at 25° C for 10 min and directly used for further steps.

2.2.1.6. DNA ligation

T4 DNA ligase (Thermo Fisher Scientific Baltics, Lithuania) was used to ligate the end nucleotides between the plasmid backbone and insert fragments by the formation of a phosphodiester bond between the free hydroxy group at the 3'-end and the 5'-phosphate group of the other nucleotide. A molar ratio of 1:5 (vector DNA to insert DNA) was used to prepare the ligation reaction mixtures (total volume of 20 µL). The ligations were performed at 16 °C overnight in a PCR cycler.

2.2.1.7. Transformation of competent Bacteria

Bacterial competent cells are specially treated bacterial cells that can readily take up foreign DNA in their vicinity. The quality of the competent cell preparation is crucial for amplifying plasmids.

2.2.1.7.1. Production of competent cells

A single colony of the desired *E. coli* strain or 10 µL of the stock cell suspension was inoculated in 5 mL of LB medium without antibiotics overnight at 37 °C, 250 rpm. The next day, a starter culture was prepared with 100 mL of LB medium in a 250 mL conical flask. LB medium was inoculated with 500 µL of overnight culture and grown at 37 °C, 180 rpm until OD_{600} of 0.4 - 0.5, which required approximately 3.5 h - 4 h. The bacterial culture was centrifuged at 2000 rpm with slow deceleration for 15 min at 4 °C. The pellet was resuspended in the residual drops of LB on ice after discarding the supernatant. 10 mL of TSB buffer was added to the cell suspension, mixed gently, and incubated on ice for 10 min. 100 µL aliquots were made in 1.5 mL microfuge tubes. The aliquoted cell suspensions were snap-frozen with liquid nitrogen and stored at -80 °C.

2.2.1.7.2. Bacterial transformation using heat shock (42 °C)

Heat shock transformation is performed in a divalent cation-rich environment to counteract the electrostatic repulsion between the plasmid DNA and lipid bilayer of the cellular membrane. Heat shock-competent *E. coli* cells were thawed on ice for at least 15 min. 50 µL of the cells were used for a single transformation procedure. The cells were incubated for at least 15 min with 20 µL of ligation product, 5 µL of the PCR product, or 100 ng of plasmid DNA on ice. Heat shock was performed at 42 °C for 45 s, followed by 2 min on ice. 450 µL of fresh SOC media was added to the cells to start the recovery phase, and cells were incubated at 37 °C on a shaker (250 rpm) for an hour. The cells were centrifuged for 1 min at 11,000 rpm. The cell pellet was re-suspended in 100 µL of the supernatant, and the remaining supernatant was discarded. In the end, cells were plated on the pre-warmed LB plates with appropriate antibiotics with a disinfected metal rod. The LB plate was incubated overnight at 37 °C.

2.2.1.7.3. Preparation of Electrocompetent bacteria

A single colony of the desired E. coli strain or 25 µL of the stock cell suspension was inoculated in 50 mL of LB medium without antibiotics in a 100 mL conical flask overnight at 37 C, 180 rpm shaking. The next day, 5 mL of the overnight culture was inoculated in 500 mL of LB medium and grown at 37 °C, 180 rpm, until OD_{600} of 0.6. The bacterial culture was cooled down quickly on an ice bath. It was left on ice for 30 min with intermittent shaking every 10 min and transferred to the pre-cooled centrifuge bottles. Bacteria were pelleted down by centrifuging at 8000 rpm for 20 min and resuspended carefully with 500 mL of sterile ice-cold water under sterile conditions. The resuspended bacterial cells were centrifuged again at 8000 rpm for 20

min. The washing procedure was repeated twice. Then, the bacterial pellet was resuspended in 50 mL of sterile ice-cold water, followed by 450 mL of ice-cold 10% glycerol solution, and centrifuged at 8000 rpm for 20 min. The pellet was resuspended in 30 mL of ice- cold 10% glycerol solution, and the whole volume was transferred to the pre-cooled centrifuge tube and centrifuged again at 8000 rpm for 20 min. The resulting bacterial pellet was resuspended in approximately 4 mL of ice-cold 10% glycerol solution. Finally, 100 µL of the resulting bacterial cell suspension were aliquoted in 1.5mL microfuge tubes and snap-frozen in liquid nitrogen. The electrocompetent cell aliquots were stored at -80 °C.

2.2.1.7.4. Bacterial transformation using Electroporation

Electroporation is the process of using a pulse of high-voltage electricity to create pores in the cell membranes for a short duration (< 6 ms), during which the plasmids can enter the bacteria. This transformation process is often used for transforming large ligated plasmids as their transformation efficiency hugely decreases with the increasing size of the plasmids. The ligation mixture products were cleaned with a Monarch Gel Extraction Kit (New England Biolabs, USA). The ligation product was eluted in 10 µL of pre-warmed (60 °C) nuclease-free water. The electrocompetent *E. coli* cells were removed from the -80°C freezer and thawed on ice. 10 µl of purified ligation product was added to 50 µL of cells, and the mixture was carefully transferred to the electroporation cuvette (1 mm, VWR, USA) without creating bubbles, as this may interfere with the success of the transformation. The cell mixture was pulsed at 2.1 kV. 1 mL of SOC (at RT) was immediately added, and the tubes were incubated on a shaker (250 rpm, 37 °C) for an hour. The bacterial culture was centrifuged at 11,000 rpm for 1 min. 900 µL of the supernatant was discarded, and the pellet was resuspended in the remaining supernatant. The bacterial suspension was added to a pre-warmed (37 °C) Agar plate with appropriate antibiotics and was spread evenly across the plate. The plates were incubated overnight at 37 °C.

2.2.1.8. Sanger sequencing of plasmid DNA

Sanger sequencing utilizes a single DNA primer, a DNA polymerase, deoxynucleotide triphosphates (dNTPs), and modified di-deoxynucleotide triphosphates (ddNTPs) producing DNA fragments with random incorporation of chain-terminating dideoxynucleotides during DNA amplification followed by capillary electrophoresis and its subsequent automated read out to yield chromatograms of the sequenced DNA. All the generated plasmids were verified for sequence fidelity using the Sanger sequencing facility from

Microsynth Seqlab GmbH (Germany). Microfuge tubes containing 12 µL of plasmid sample with at least 20 ng/µL of the desired primer (4 pmol/µL) were prepared for each sequencing reaction as suggested by the guidelines provided by the sequencing facility.

2.2.2. Cell culture

2.2.2.1. Culturing of cell lines and culture conditions

Human embryonic Kidney 293 (HEK293) cells are immortalized human embryonic kidney cells commonly used as a model cell line to overexpress proteins of interest and investigate their function. HEK293 (AD293, ATCC, USA) and HEK293 cells with knock out (KO) of $G_{q/11}$ or G_i proteins (generated by Schrage *et al.*, 2015; Hisano *et al.*, 2019) were cultured using Dulbecco's Modified Eagle's Medium (DMEM, Thermo Fisher Scientific) containing 4.5 g/L D-Glucose supplemented with 10% Fetal calf serum (FCS, PAN-Biotech, Germany), 0.1 mmol/L nonessential amino acids (Thermo Fisher Scientific, USA), 100 U/mL penicillin, 100 mg/mL streptomycin (Thermo Fisher Scientific, USA) in T25 flasks (Sarstedt, Germany). The cells were passaged when they reached a confluency of 80% to 90% using Trypsin (PAN-Biotech, Germany) at a dilution of 1:20 ratio. The usage of trypsin was limited to a brief duration of 3 - 5 min at 37 °C and subsequently antagonized by FCS containing DMEM to minimize the impact of the trypsin on cell viability. The cells were grown in a sterile incubator at 37 °C with 5% CO_2. Mycoplasma contamination was excluded every six months using the PCR Mycoplasma Test Kit (AppliChem GmbH, Germany) by strictly adhering to the manufacturer's instructions.

2.2.2.2. Transfection of Plasmid DNA to create transgenic HEK cell lines

The lipid-based transfection reagents Lipofectamine 3000 (Thermo Fisher Scientific, USA) and FuGeneHD (Promega, USA) were used to transfect HEK293 cells with the desired plasmids in antibiotic-free media on 6-well plates (Sarstedt, Germany). Plates were seeded with 50,000 cells/well in 2 mL of DMEM, as described before. The manufacturer's protocol was adapted accordingly to obtain good transfection efficiencies. The transfection mixture was prepared with DMEM without 10% FCS supplementation and afterward added to the desired wells. Cells were incubated overnight, and after approximately 18-24 h, fresh DMEM medium was used to exchange the old medium from the 6-well plate.

2.2.2.3. Antibiotic selection and maintenance of transgenic cell lines

Antibiotic selection pressure allows to select cells that express the resistance genes to obtain a stable polyclonal transgenic cell line. We used the antibiotics G418, Blasticidin, or Puromycin depending on the antibiotic resistance genes the plasmids contain. The specific concentration of antibiotics used was determined by a dose-response curve for antibiotic selection of HEK293 cells to determine the lowest possible concentration of the antibiotic needed to kill non-transfected control cells completely. Transgenic cells were selected with 900 µg/mL of G418, 10 µg/mL of Blasticidin, or 5 µg/mL of Puromycin maintained after two weeks of selection with 600 µg/mL of G418, 5 µg/mL of Blasticidin or 3 µg/mL of Puromycin to ensure that the cells retain the plasmid and subsequently express the protein of interest.

2.2.2.4. Generation of Monoclonal cell populations by Limiting Dilution

To further increase the expression rate of the proteins of interest, we generated monoclonal cells arising from one cell, a so called single clonal origin. A similar expression profile is vital for certain experimental conditions to reduce variability. Monoclonal cell lines were generated from polyclonal transgenic cell lines by seeding at a limited dilution of 4 cells/mL cell density with 100 µL into each well of a 96-well plate (Sarstedt) with appropriate antibiotics. The culture medium was replaced weekly with the appropriate antibiotics to aid the selection pressure and provide fresh nutrients. Approximately after two weeks, the wells were checked for monoclonal transgenic cells with fluorescence signals under the Olympus IX53 microscope (Olympus, Japan) equipped with an eYFP AT filter set (AHF, Analysentechnik, Germany). Six clones were picked from the 96-well plate by trypsinization, subsequently seeded on a 6-well plate, and further propagated in T25 flasks. All cell lines generated were maintained with antibiotic selection pressure using appropriate antibiotics and with concentrations as described in the maintenance of transgenic cell lines.

2.2.2.5. Cryopreservation of cell lines

Polyclonal, monoclonal transgenic and wild-type HEK293 cells were frozen as fast as possible after generation to save the status with a high expression rate, to have backups, and to send them to collaboration partners. The freezing medium consisted of 80% FCS and 20 % DMSO. One million cells were pipetted into one CryoPure 2 mL cryopreservation tube (Sarstedt, Germany) in 500µL DMEM and then mixed with equal amounts of the freezing medium and directly transferred to a -80° C freezer storage unit in Styrofoam boxes (Sarstedt,

Germany) for slow cool down and after at least 18 h, shifted into liquid nitrogen tanks for long-term storage. To use a cryopreserved cell line, the retrieved cell suspension from the liquid nitrogen tank was quickly thawed by adding 2 mL of pre-warmed DMEM (37 °C). The resulting cell suspension was centrifuged to remove any traces of the freezing medium. After discarding the supernatant, the cells were resuspended in fresh DMEM and transferred into a T25 flask, and appropriate antibiotics were added.

2.3. Analytical methods

2.3.1. IP_1 assay

IP_1 molecules are the direct degradation product of IP_3 produced downstream of the activation of the G_q signaling cascade. The IP_1 concentrations in the different HEK293 cell lines were measured using the homogeneous time-resolved fluorescence competitive immunoassay IP-One-G_q HTRF kit (Cisbio, US). The assay was adapted based on the manufacturer's instructions to obtain better output efficiencies. 10,000 cells of desired monoclonal HEK293 cells were plated on a half area CELLSTAR® 96-well plate (Greiner Bio-One, Germany) coated with 10 µg/mL fibronectin (Sigma-Aldrich, Germany) and grown overnight under normal culturing conditions. Prior to the start of the experiment, 50 µL of DMEM supplemented with 2 µM all-trans-retinal (ATR, Sigma-Aldrich, Germany) was added to the wells after removing the old medium. The experiments were performed in complete darkness. The 50 µL culture medium was aspirated and replaced with 14 µL of fresh medium with ATR, and to this 14 µL of Stim Buffer was added. The Stim Buffer contains LiCl causing IP_1 to accumulate upon receptor activation by preventing degradation. Then, UV light illumination with (50 µW/mm^2, 1 s, every 5 min for 30 min) was performed through an inverted fluorescence microscope Olympus IX83 equipped with an RTC MT20 lamp, a 4x UPLSAPO objective (0.16 NA) and a DAPI Filter (387/11 Excitation and AT415 dichroic mirror, AHF Analysetechnik, Germany) controlled by the CellSens® Dimensions software (Olympus, Japan) to a set of wells. To another set of wells, 1 µM of the pan G_q blocker FR90035945 was added 10 min before the experiment to block the G_q signaling and stimulated with UV light. Another group of wells was treated with 300 µM of the muscarinic agonist Carbamoylcholine chloride (CCh, Sigma-Aldrich, Germany) as a positive control for G_q signaling. Cell lysis was performed after 30 min of the experimental duration with 12 µL of the lysis buffer from the kit for 10 min. 14 µL of the cell lysate was added to 6 µL of the detection buffer containing d2-labeled IP_1 and monoclonal anti-IP_1 Tb^{2+} cryptate in a 384 well Polystyrene microplate (Greiner Bio-One). IP_1 levels were measured in the cell lysate using the CLARIOstar® microplate plate reader (BMG Labtech, Germany). The IP_1 concentrations of the lysate samples were calculated by correlation of the 665/620 nm ratio with a previously determined IP_1 standard curve performed as described by the manufacturer's instructions.

2.3.2. Ca^{2+} imaging

Ca^{2+} imaging is a microscopy-based technique that utilizes the fluorescent calcium indicators that increase in fluorescence upon binding to Ca^{2+} ions, thereby aiding in the quantification of the dynamic changes of Ca^{2+} in the cells or organs of interest. I used the cell-permeant red-shifted Xanthene based rhodamine like Ca^{2+} fluorescent indicator X-Rhod-1, AM (580/602 nm) for the monometric measurement of [Ca^{2+}] ions. The Acetoxy methyl (AM) group renders it to be an uncharged dye that can efficiently permeate cell membrane. Once inside the cell, the AM groups are cleaved by nonspecific esterases, resulting in a charged dye that is trapped within the cytosol. Ca^{2+} imaging was performed on all of the different transgenic HEK293 WT as well as the $G_{q/11}$ and G_i KO cell lines. Cells were grown on 22 × 22 mm glass plates pre-coated with 10 µg/mL fibronectin. Cells were loaded with 1.5 µM X-Rhod-1 AM, 1x PowerLoad™ Concentrate (Thermo Fisher Scientific) and supplemented with 2 µM ATR in 500 µL of Tyrode solution containing in mM: 1.8 $CaCl_2$, 140 NaCl, 5.4 KCl, 2 $MgCl_2$, 10 Glucose, 10 HEPES; pH adjusted to 7.4 using NaOH (all substances from Sigma-Aldrich) for 20 min at room temperature along with a subsequent de-esterification step for 20 min at 37 °C. All experiments were performed at 35° C with constant perfusion of Tyrode solution to the cells on an inverted IX73 microscope (Olympus, Japan) equipped with a 20x objective (LUCPLFLN 20XPH/0.45).

LEDHub (Omicron, Germany) was used for light illumination which was equipped with a UV-LED (385 nm) consisting of a 10% neutral density filter, and a green light LED (500– 600 nm) with a 549/15 nm bandpass filter (AHF Analysetechnik, Germany). The light of the LED Hub was coupled to the IX73 microscope via a 2 mm light guide (NA 0.5) and a dual port coupler (Cairn Research, UK) and directed onto the objective using HC BS 561 nm beamsplitter. Emission of X-Rhod-1, AM was collected through a 709/167 nm bandpass filter (AHF Analysetechnik, Germany), recorded using a PCO edge 4.2 camera (PCO AG, Germany) in tandem with µManager software (Version 2.0 gamma) or an Andor Zyla sCMOS camera (Andor, Oxford instruments, UK) in tandem with Andor Solis™ software (Andor Oxford instruments, UK). PowerLab 8/35 system and the LabChart 8.1.16 software (AD Instruments, Australia) was used for synchronizing the timing of LEDs and the camera. The amplitude of the Ca^{2+} transients was determined as the highest values from the baseline and was used for analysis. Desensitization and the recovery from desensitization of light-induced Ca^{2+} transients were investigated by paired UV pulses (1 mW/mm^2) with 1, 3, and 10 s pulse duration with interpulse interval in the range from 150,180, 240, 300 to 400 s. Recorded images were analyzed with both ImageJ 1.52p and CellProfiler 4.2.1 (open-source software, US). For the analysis of desensitization and recovery time, the maximum amplitude of the second Ca^{2+} transient was normalized to the first one.

Wavelength sensitivity for activation was investigated with the same setup used for determining the light sensitivity in tandem with monochromatic light pulses generated by the OptoScan Monochromator (Cairn Research, UK). The light guides for X-Rhod-1, AM imaging light, and the monochromatic light were directed onto the microscope via the dual port coupler with the aid of Beamsplitter HC 555 (AHF Analysentechnik, Germany) to use both light sources simultaneously. The amplitude of the Ca^{2+} transients were analyzed as described above, and the Ca^{2+} increase was normalized using the highest amplitude obtained in each of the individual experiments. The specific wavelength was determined by plotting the normalized Ca^{2+} increase versus the wavelength (nm) with the aid of the Govardovskii equation (Govardovskii et al., 2000).

2.3.3. Electrophysiological measurements: Patch clamp

Transgenic HEK293 cells expressing the respective channels and hOPN5 were plated at a low density (40,000 cells/well) on fibronectin-coated (10 µg/mL) coverslips. The culture medium was supplemented with 2 µM ATR and appropriate antibiotics. All electrophysiological recordings were performed within two days after seeding at room temperature in the whole cell configuration with an EPC 10 amplifier (HEKA, Germany) with a 10 kHz sampling rate on an Olympus IX73 microscope, 20x objective (LUCPLFLN 20XPH/0.45). Patch pipettes made of borosilicate glass (Science Products, Germany) had resistances of 2.5 to 3.5 MΩ. The external solution comprised (in mM) 140 NaCl, 5 CsCl, 2 $CaCl_2$, 1 MgCl2, 10 HEPES, 10 Glucose; pH adjusted to 7.4 using NaOH and the internal solution 9.4 NaCl, 120 CsCl, 1 $MgCl_2$ 10 HEPES, 10 BAPTA, 0.2 GTP; pH adjusted to 7.2 using CsOH. Cells were voltage clamped at −40 mV, and current-voltage relations were obtained by triangular voltage ramps from −100 mV to +60 mV for every 5 s. Current density values were measured for each cell at -60 to +60 mV. Illumination with UV light (385 nm, 1 mW/mm^2) for 2 s was performed for the cells, and 1 µM of OAG was applied as a positive control to activate the TRPC6 channels.

2.3.4. G-CASE - BRET assays

Bioluminescence resonance energy transfer (BRET) is a technique to monitor protein-protein interactions. It involves the use of a bioluminescent donor, and a fluorescent acceptor wherein the energy transfer occurs upon bioluminescence from the donor to the acceptor. This technique is based on Förster resonance energy transfer (FRET) but avoids the inherent problems associated with it, such as photobleaching, autofluorescence and non-specific signals. The BRET effect appears, if the distance between the bioluminescent donor

and acceptor fluorophores is in close proximity and does not exceed a radius of ~50 Å.

BRET measurements were performed based on the protocol adapted from Schihada, Shekhani and Schulte, 2021 to detect the dissociation of the G protein heterotrimer G_{α} from $G_{\beta\gamma}$ subunits. This assay uses G protein-based tri-cistronic activity sensors (G-CASE) plasmids Nluc luciferase was coupled to the G_{α} subunit and acted as the bioluminescent donor, which shows luminescence upon addition of the substrate Furimazine and cpVenus coupled to G_{γ} subunit was used as acceptor. The Nluc emission was measured using a 450/40 nm monochromator setting with a gain of 3600, and the cpVenus emission was measured using a 535/30 nm monochromator setting with a gain of 4000 with an integration time of 0.3 s in both measurements. 50,000 HEK293 cells expressing desired proteins were seeded at least 16 h prior to the experiment. The cells were washed with HBSS prior to the start of the experiment and incubated with a 1:1000 dilution of furimazine stock (Promega, USA). A dose-response curve was done with ATP for G_q-CASE and with CCh for G_i-CASE expressing cells, and a final concentration of 3 mM ATP was used for the experiments. All the measurements were done at 37 °C with a CLARIOstar plate reader (BMG, Germany). The ratio of the cpVenus values to that of the Nluc bioluminescence provided the BRET ratio, and it was normalized to the first six basal values.

2.4. Protein biochemistry

2.4.1. HEK293 cells lysis and membrane protein extraction

HEK293 cells were centrifuged at 1000 rpm for 5 min and then washed with the Tris wash buffer to remove contaminants or debris. DDM (n-dodecyl β-D-maltoside) is a mild non-ionic detergent to solubilize and extract membrane proteins. Tris-based membrane extraction buffer contained in mM: Tris 50, NaCl 150, 2% DDM, and with protease inhibitors. After washing, cells were resuspended in the extraction buffer. 500 µL of extraction buffer was used for HEK293 cells from a 10 cm culture plate to achieve the desired detergent concentration and sample-to-buffer ratio. The cell mixture was incubated at 4 °C for 30 min on a vertically rotating platform. After incubation, the mixture was centrifuged at 13,300 rpm for 10 min at 4 °C to separate the soluble fraction (containing the solubilized membrane proteins) from the insoluble fraction (containing the membrane debris). The supernatant was transferred to a clean 1.5 mL microfuge tube. The extracted membrane proteins were directly used for downstream assays, and the rest of the samples were stored at -20 °C.

2.4.2. ELISA

The enzyme-linked immunosorbent assay (ELISA) allows quantitative

detection of an analyte (antigen) in a liquid sample. The sandwich ELISA method was used here which consists of both capture and detection antibodies specific for the antigen to be detected, and the antigen gets sandwiched between them. This method has the highest sensitivity among all other ELISA methods. For the experiments, anti-GFP precoated 96-well plates were used. A 1 µg/µL stock of membrane protein lysate was prepared for all the samples, and 10 ng/µL and 1 ng/µL were used for ELISA. 100 µL of membrane lysate sample was added to the anti-GFP antibody coated plate, and all the samples were assayed in duplicate. The manufacturer's protocol was strictly adhered. Finally, the absorbance of each well used was measured in a spectrophotometer at 450 nm as the primary wavelength. The quantity of fluorescent protein present in the samples was calculated based on the standard curve that was done in parallel to the samples.

3 Results

The main goal of the thesis was to characterize in detail the physical and functional properties of wild-type (WT) hOPN5 as well as to prove its selective and repetitive activation of the G_q signaling cascade in HEK293 cells. The other important goal was to develop new hOPN5 mutants with enhanced properties for optogenetic stimulation.

3.1. Generation of HEK293 cells with heterologous expression of hOPN5 (WT)

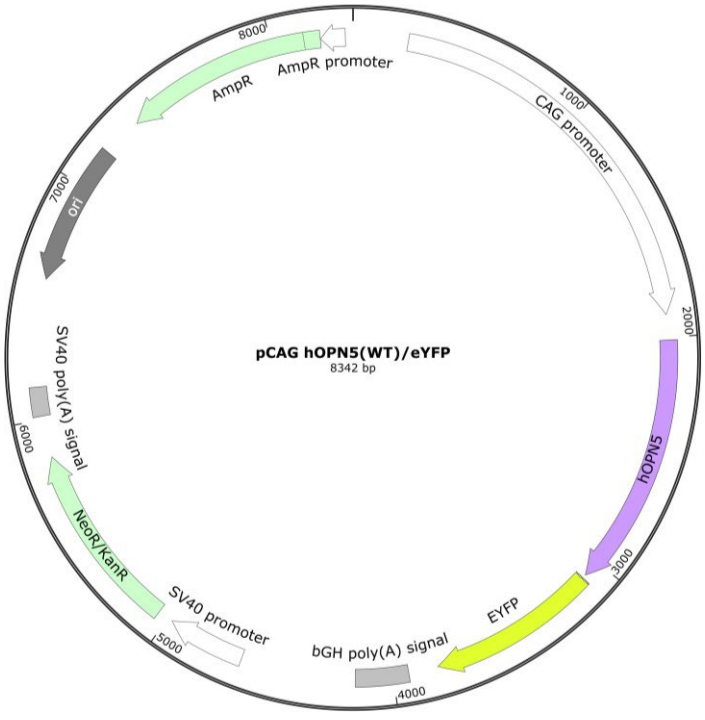

Figure 12: Schematic representation of the hOPN5 (WT)/eYFP plasmid.
Gene cassette leading to hOPN5 (WT)/eYFP expression along with antibiotic resistance cassette conferring resistance to G418 in mammalian heterologous expression systems.

To characterize the signaling cascade downstream of hOPN5 (WT), I used a stable HEK293 cell line expressing hOPN5 (WT) generated within the working group of Philipp Sasse (University of Bonn). The expression of the heterologous protein was maintained with Geneticin (G418) antibiotic pressure. The G418 resistance was conferred by the Neomycin resistance gene encoding aminoglycoside 3'-phosphotransferase. The expression cassette in the plasmid consisted of a codon-optimized hOPN5 (WT) with a C-terminal fusion of enhanced yellow fluorescent protein (eYFP) under the control of the chicken β-actin promoter with a chimeric β-globin intron sequence (CAG) (Figure 12). The transgenic HEK293 cells had an

appreciable membrane localization of hOPN5 (WT), clearly seen by the eYFP fluorescence (Figure 13). The hOPN5 (WT) cell line displayed an average of 60% eYFP positive cells. An expression strength analysis using ELISA showed that for every ng of total protein from the cell lysate, ~80 pg of the hOPN5 (WT) fusion protein was present.

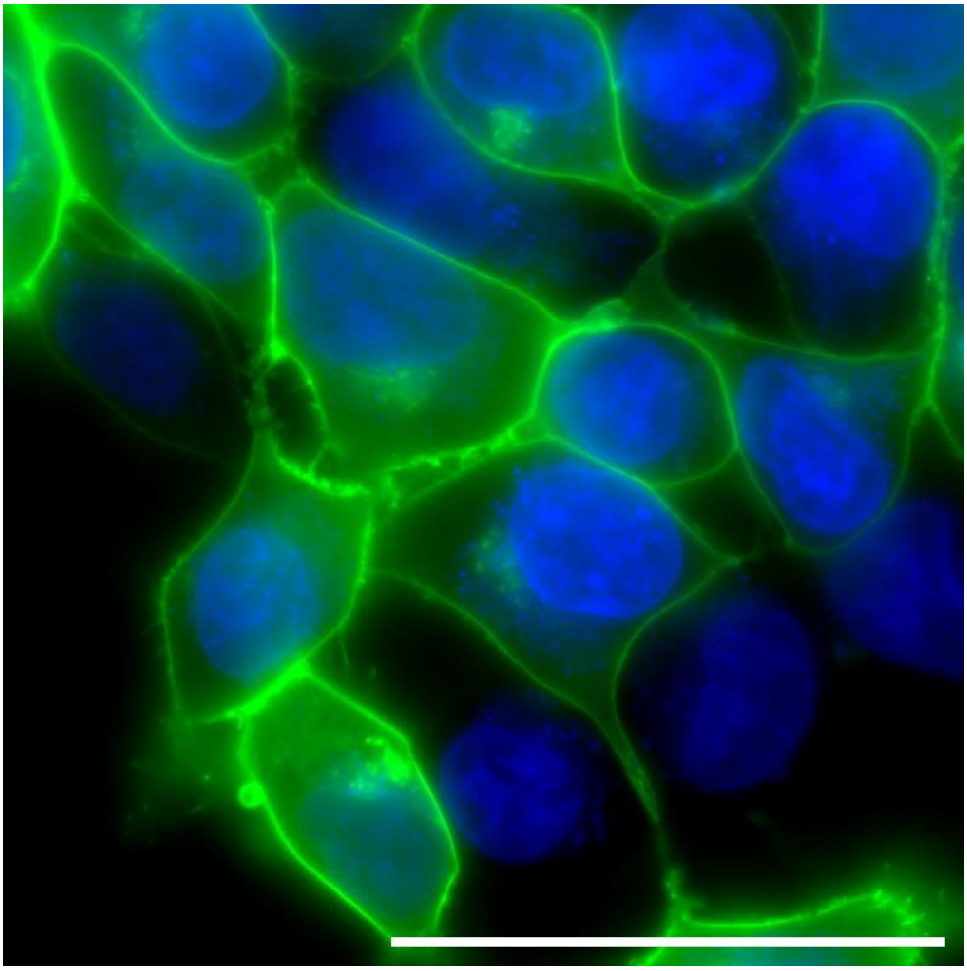

Figure 13: Representative image of transgenic HEK293 cells expressing hOPN5 (WT)/eYFP.
Expression of hOPN5 (WT) in fusion with eYFP (green) and the nuclei stained with DAPI (blue), bar = 50 µm.

3.1.1. UV light induced IP_3 accumulation in hOPN5(WT) HEK293 cells

To prove the activation of the G_q signaling cascade by hOPN5 upon UV light illumination, experiments were designed to address each step of the G_q signaling cascade sequentially.

The activated membrane-bound $G_{\alpha q}$ subunit stimulates the nearby PLC-β, which lyses the PIP_2 into cytosolic IP_3 and membrane-bound DAG. The activation of the G_q

signaling cascade was determined by measuring inositol monophosphate (IP_1) levels triggered by UV light or agonist-mediated activation of the G_q signaling cascade. IP_1 is the stable degradation product of IP_3, which was prevented from further degradation by adding LiCl (50 µM) during the assay. UV light illumination (385 nm, 50 µW/mm^2, 1 s every 5 min for 30 min) elevated the IP_1 levels in transgenic hOPN5 (WT) HEK293 cells but not in control HEK293 cells.

This increase in IP_1 levels was entirely abolished by pre-incubating the cells with the G_q specific blocker FR90035945 (Schrage et al., 2015) before the UV light illumination. Elevated levels of IP_1 were observed both in control HEK293 cells as well as hOPN5 (WT) HEK293 cells after pharmacological stimulation of the Muscarinergic acetylcholine receptor 3 (M3) by carbachol (CCh). The basal levels of IP_1 in both cell lines were not altered, excluding the dark activity of hOPN5 (WT) (Figure 14). Also, the over-expression of hOPN5 (WT) still preserved the CCh-mediated IP_1 increase, showing that the ectopic overexpression did not induce any adverse effects on the native G_q signaling.

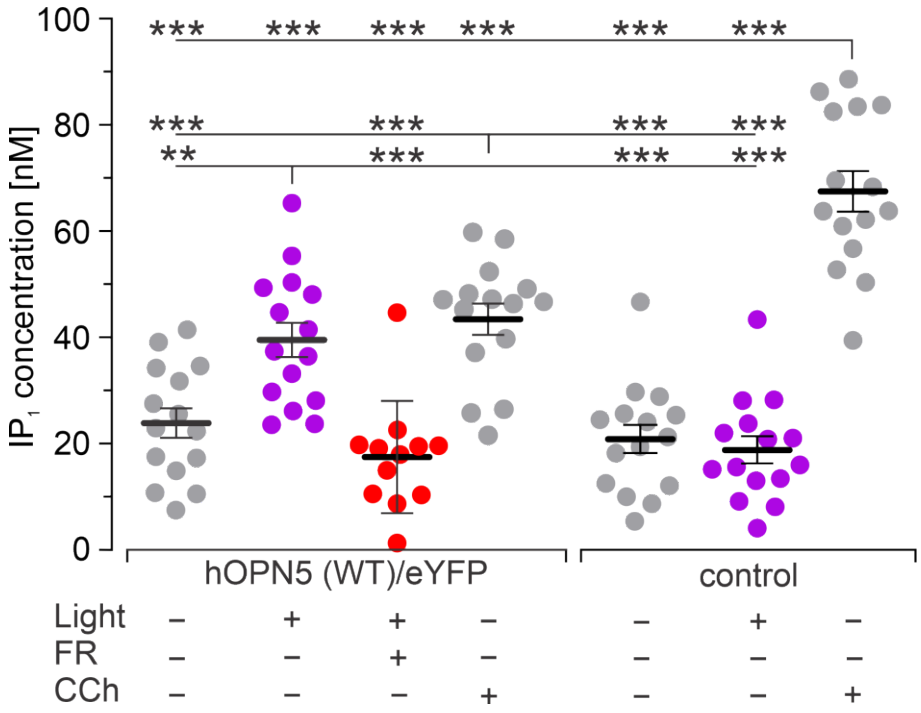

Figure 14: IP_1 accumulation in hOPN5 (WT) HEK293 cells after UV light illumination.
IP_1 levels in hOPN5 (WT)/eYFP and control HEK293 cells without any stimulation (gray) and after UV light stimulation (50 µW/mm^2, 1 s every 5 min for 30 min), without (violet) or with G_q protein specific blocker FR900359 (1 µM, red) and after CCh application (300 µM, 30 min, gray). Each dot represents the outcome from one well of a 96-well plate. Statistical analysis was performed with one-way ANOVA and Tukey's multiple comparisons post-test (p(control vs. control light): 0.99; p(control vs. hOPN5): 0.99; p(control vs. hOPN5 FR): 0.99; p(control light vs. hOPN5): 0.89; p(control light vs. hOPN5 FR): 0.99; p(hOPN5 vs. hOPN5 FR): 0.79; p(hOPN5 CCh vs. hOPN5 light): 0.97). IP_1 concentrations [nM] are represented as mean ± SEM. *p < 0.05, **p < 0.01, ***p < 0.001, ****p < 0.0001.

3.1.2. Light induced Ca^{2+} transients in HEK293 cells expressing hOPN5 (WT)

The enzymatic activity of PLC-β on PIP_2 produces cytosolic IP_3 molecules, which activate the IP_3 receptors in the ER and release Ca^{2+} into the cytosol, which can be monitored by Ca^{2+} imaging. I used this approach to prove the activation of the G_q signaling cascade and compare the efficiencies of Ca^{2+} increase by G_q protein activation, triggered either by agonist-activated or light-activated G_q protein coupled receptors.

3.1.2.1. UV light vs. pharmacological stimulation induced Ca^{2+} transients

To quantify the G_q protein activation upon UV light illumination in detail, I performed Ca^{2+} imaging with X-Rhod-1, AM (a red-shifted monometric Ca^{2+} indicator). The reason for using X-Rhod-1 was to avoid any interference with the activation or deactivation of hOPN5 by the Ca^{2+} dye excitation light (542 - 556 nm, 50 ms excitation, every 5 s, 0.2 mW/mm^2). Transgenic HEK293 cells expressing hOPN5 (WT) consistently produced Ca^{2+} transients upon UV light illumination (385 nm, 1 mW/mm^2, 100 ms), but no Ca^{2+} transients were observed in control HEK293 cells. UV light-induced Ca^{2+} transients were compared to pharmacological stimulation with CCh (2 mM), which activates the endogenously expressed G_q coupled M3 receptors or with ATP (1.5 mM) acting on endogenous P2Y receptors. This comparison suggested that the UV light consistently induced Ca^{2+} transients, similar to ATP-mediated Ca^{2+} transients and slightly more potent than CCh-induced Ca^{2+} transients. More importantly, the pharmacologically induced Ca^{2+} transients were not different in their maximal transients in hOPN5 (WT) HEK293 cells and control group HEK293 cells proving that ectopic overexpression of hOPN5 (WT) did not affect the endogenous G_q protein signaling. This is a vital information for its potential in future translational research (Figure 15).

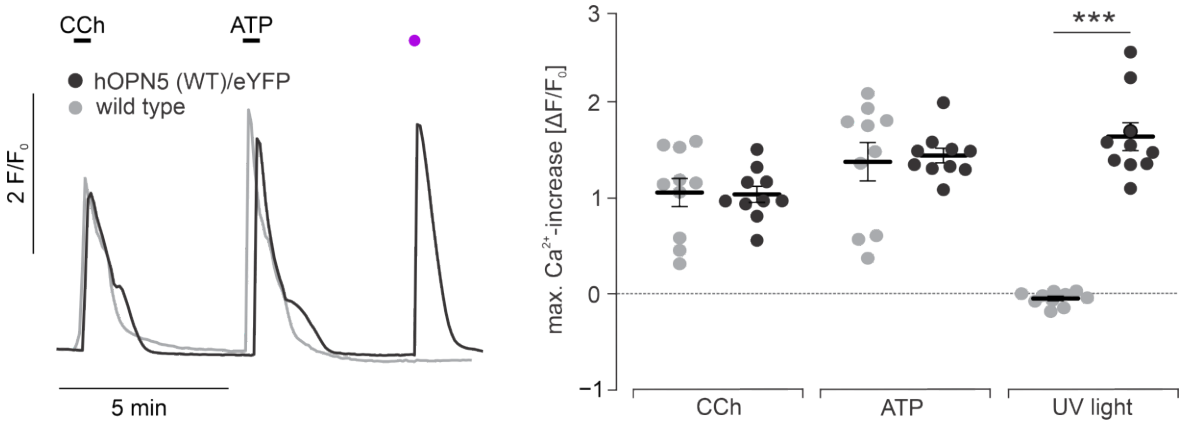

Figure 15: Ca^{2+} transients in HEK293 cells induced by UV light vs. pharmacological stimulation.
Representative traces of Ca^{2+} transients (left) induced by UV light (violet, 1 mW/mm^2, 1 s), CCh (2 mM) and, ATP (1.5 mM) in transgenic hOPN5(WT) (black) and control (gray) HEK293 cells. Comparison of the maximal amplitudes of Ca^{2+} transients in both cell lines (right, n = 10, each dot represents the average of one region of interest of ≥ 100 cells). Statistical analysis was performed with a two-way ANOVA test along with Sidak's multiple comparison post-test to determine the difference between hOPN5 (WT) HEK293 cells and control HEK293 cells (p(CCh) and p(ATP) = 0.99). Maximal Ca^{2+} increase values are presented as mean values ± SEM. ***p < 0.001.

3.1.2.2. Determination of light sensitivity by Ca^{2+} imaging

Determining the light sensitivity is essential to characterize the optogenetic protein for later use in experiments. I used Ca^{2+} imaging with increasing light intensities of UV light pulses and the resulting amplitude of the Ca^{2+} transients to quantify light sensitivity. UV light pulses (385 nm, 100 ms) increasing in light intensity from 0.1 µW/mm^2 to 300 µW/mm^2 were used for the stimulation protocol. Even very low light intensities of 1 µW/mm^2 already induced Ca^{2+} transients. The maximal amplitude of the Ca^{2+} transients was plotted against its corresponding log of light intensities, which produced a sigmoidal dependence very similar to the canonical dose-response curve used in pharmacology (Figure 16. a). The effective half maximal light intensity (eLi50) was 3.37 ± 0.1 µW/mm^2 (n = 15, Figure 16. b), and the maximal height of Ca^{2+} transients was 2.1 ± 0.1 $\Delta F/F_0$ (n = 15, Figure 16. c). To eliminate any possible functional strain on the hOPN5 (WT) by the fusion of eYFP, an additional transgenic hOPN5 (WT) HEK293 cell line with cytosolic GFP expression was generated. This was achieved by introducing an internal ribosome entry sequence (IRES) between the hOPN5 (WT) and the GFP gene sequences in the expression cassette of the plasmid. During Ca^{2+} imaging, the cells which expressed hOPN5 (WT) and GFP as separate moieties displayed an increase in the light-induced Ca^{2+} transient amplitude 2.29 $\Delta F/F_0$ (n = 15, Figure 16. c), but they showed an almost identical eLi50 of 3.21 ± 0.1 µW/mm^2 (n = 15, Figure 16. b) compared to the hOPN5(WT) fused to the eYFP cell line (Figure 16. b). This comparison proves that there is no hindrance to the function of hOPN5 (WT) with the use of the eYFP protein tag.

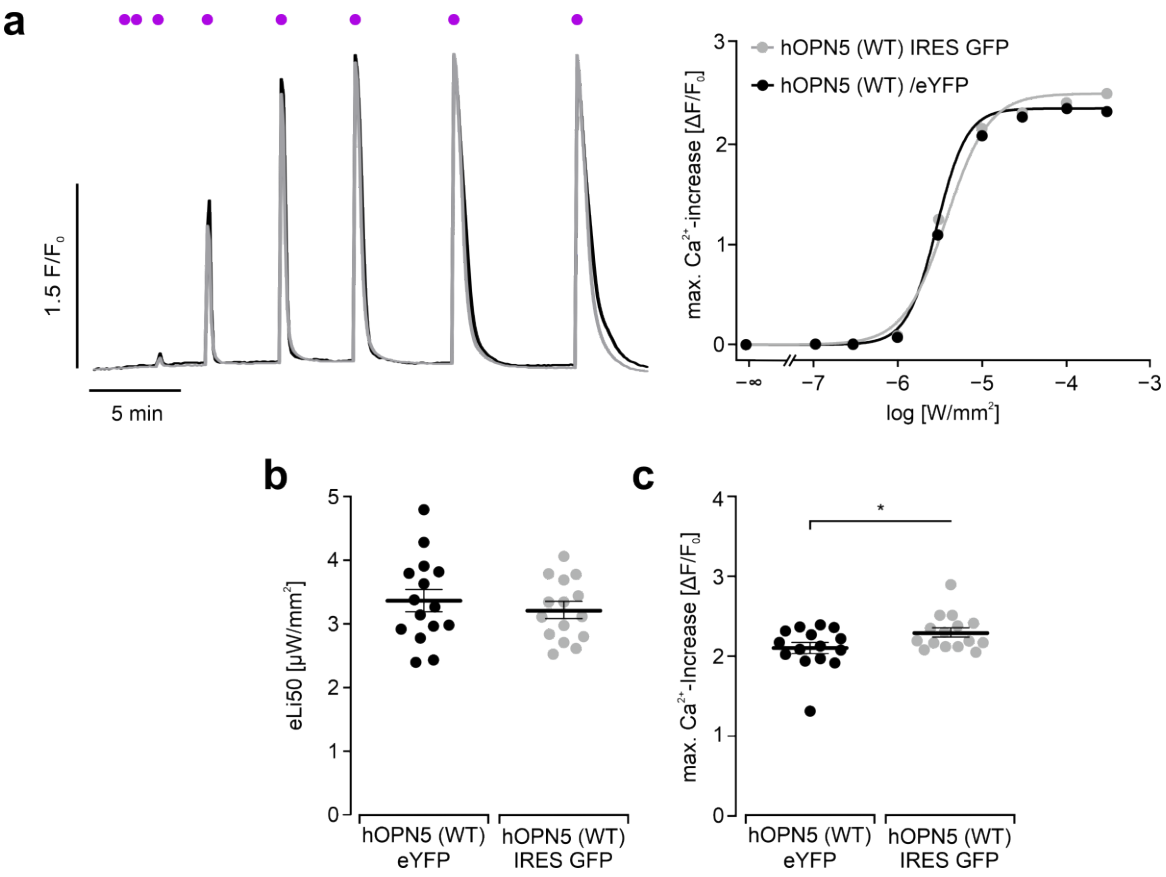

Figure 16: Determination of light sensitivity of hOPN5 (WT) in HEK293 cells.
a. Representative traces of Ca^{2+} transients of hOPN5 (WT)/eYFP (black) and hOPN5(WT) IRES GFP (gray) HEK293 transgenic cell lines after 100 ms long UV light pulses with increasing light intensities (violet dots from left: 0.1, 0.3, 1, 3, 10, 30, 100, and 300 µW/mm^2, light intensities are indicated in logarithmic scale,). Corresponding dose-response curves to analyze the half-maximal effective light intensity (eLi50, right) were plotted using the maximal amplitudes of Ca^{2+} transients (right). **b.** Comparison of the eLi50 ($p = 0.47$) as well as **c.** the maximal amplitudes of Ca^{2+} transients ($p = 0.042$) in both transgenic HEK293 cell lines (unpaired, two-sided Student's t-test), each dot represents the average of one coverslip with ≥ 100 cells. eLi50 and maximum Ca^{2+} increase data points are presented as mean values ± SEM. *$p < 0.05$.

3.1.2.3. Wavelength specificity

The other important factor to be assessed is the wavelength specificity for hOPN5 (WT). In previous work in the lab of Philipp Sasse, different levels of spectral responses were observed for hOPN5 (WT) during Ca^{2+} imaging upon illumination with varying wavelengths of light ranging from 370 to 550 nm (30 ms, 15 nm bandwidth). The amplitudes of Ca^{2+} transients were used to calculate the percentage of maximum Ca^{2+} response for each wavelength, and the specific activation wavelength was determined using the Govardovskii equation. The maximal activation wavelength was determined to be 406 ± 2.4 nm (N = 11, Figure 17) in these experiments with relatively high light energy (30 ms, ~1 mW/mm^2). As hOPN5 (WT) is

suggested to be a bi-stable opsin (Kojima et al., 2011), the most appropriate wavelength for deactivation was determined by using a second light pulse of longer wavelengths (400 to 550 nm, 300 ms, >1 mW/mm^2) applied immediately (~4 ms delay) after a supramaximal stimulation with 390 nm (1.2 mW/mm^2, 30 ms). The second light pulse led to the inhibition of the Ca^{2+} transients, and the inhibition effect was determined to be maximal at 511 ± 1.7 nm (N = 10, Figure 16).

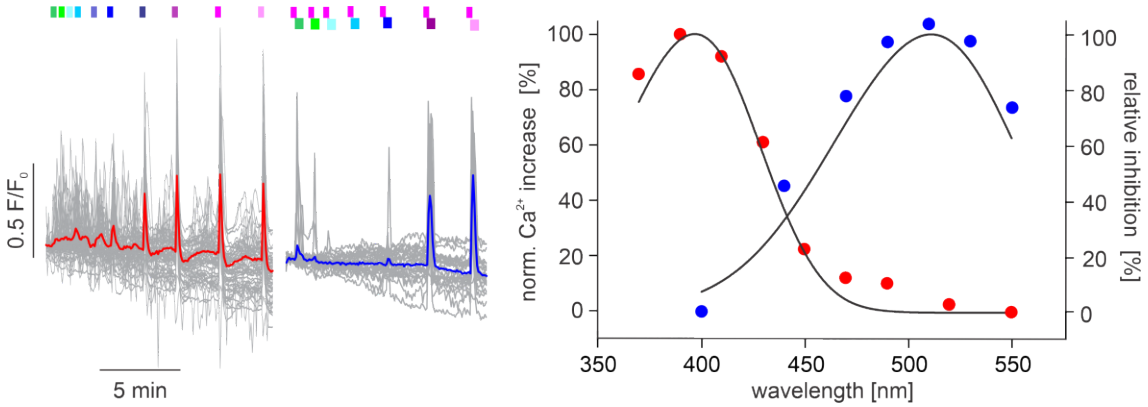

Figure 17: Determination of the wavelength specificity of hOPN5 (WT).
Representative traces of Ca^{2+} transients (left, 55 and 26 individual cells in gray, average in red and blue) obtained in transgenic hOPN5 (WT) HEK293 cells induced by light pulses with different wavelengths (red, 30 ms, from left in nm: 550, 530, 510, 490, 470, 450, 430, 410, 390, 370). Ca^{2+} transients (blue) after activating with UV light (390 nm, 1.2 mW/mm^2, 30 ms) followed by a ~4 ms gap with different wavelengths for deactivation (300 ms, from left in nm: 550, 530, 510, 490, 470, 440, 400, >1 mW/mm^2). Analysis of wavelength specificity (right) for activation (red, percentage of maximal Ca^{2+} response) and deactivation (blue, calculated as % of relative inhibition) fitted using the Govardovskii equation (black, R^2 = 0.98 and 0.93). Experiments were performed by Prof. Tobias Brügmann.

3.1.2.4. Desensitization and subsequent recovery of hOPN5 (WT) mediated Ca^{2+} increase

The repetitive stimulation of an optogenetic GPCR is a highly desired characteristic for its experimental and translational potential and a clear advantage compared to perfusion with drugs. For efficient repetitive stimulation, the optogenetic protein should show the fewest possible desensitization. Therefore, the desensitization of hOPN5 (WT) was functionally determined using Ca^{2+} imaging in transgenic hOPN5 (WT) HEK293 cells. Paired UV light pulses of 1, 3, and 10 s duration were used, and the second pulse started at least 150 s after the first UV light pulse (Figure 18. a). Desensitization was only observed for the longer light pulses. For light pulses ≥3 s, there is a clear indication of desensitization with ~30% in the case of 3 s long pulse and ~43 % in the case of 10 s long pulses (Figure 18. b, c).

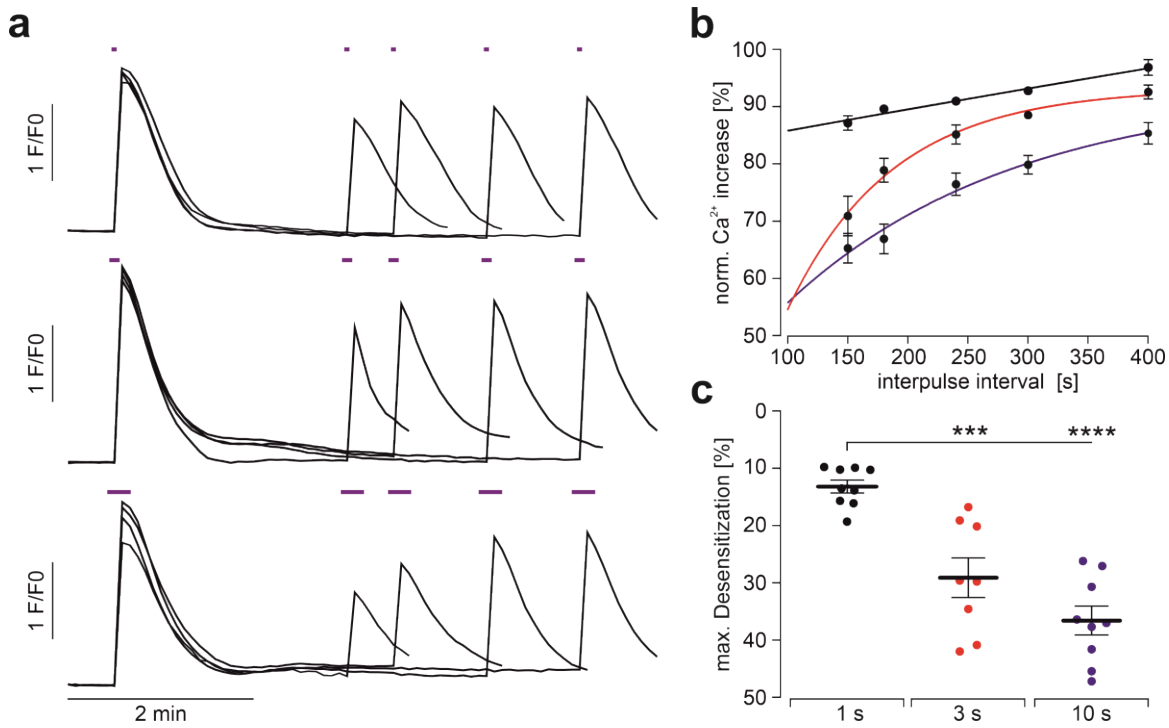

Figure 18: Desensitization and subsequent recovery of light-induced Ca^{2+} transients. **a.** Representative Ca^{2+} transient traces induced by paired pulses of 1, 3, and 10 s long UV light (violet bars, 1 mW/mm^2) with increasing interpulse intervals (150, 180, 240, 300 s). **b.** Average normalized Ca^{2+} transient amplitudes in order of the increasing interpulse intervals with their respective one-phase decay fits (1 s: black fit, n = 9; 3 s: red fit, n = 8; 10 s: blue fit, n= 9). **c.** Statistical analysis of the effect of pulse duration on the maximal desensitization was performed with an ordinary one-way ANOVA with Tukey's multiple comparison post-test (p(1 vs. 3 s) < 0.001; p(1 vs. 10 s) < 0.0001; p(3 vs. 10 s) = 0.11). Each dot represents the mean of one coverslip with ≥ 100 cells. All Ca^{2+} increase and maximum desensitization values are presented as mean ±SEM.

3.1.3. UV light induced TRPC6 activation by hOPN5 (WT)

DAG is produced after the lysis of PIP_2 by PLC-β, the main effector protein of $G_{\alpha q}$ proteins. DAG binds to the TRPC6 channels in close vicinity and activates the channels, leading to the influx of Ca^{2+} ions into the cytosol. I performed patch clamp experiments with HEK293 cells expressing TRPC6 channels and hOPN5 (WT) to prove the activation of TRPC6 channels by the DAG produced as a result of the G_q signaling cascade activation by hOPN5 (WT) upon light stimulation. UV light illumination (385 nm, 1 µW/mm^2, 4 s) induced an apparent increase in the current density (Figure 19. a) with a characteristic TRPC6 specific 'S' trace, having a flattening at 0 to +40 mV curve close to the reversal potential and the increase in both inward and outward current at more negative (≥ -20 mV) and more positive (≥ 40 mV) membrane potentials (Dietrich et al., 2005a; Dryer and Kim, 2018). This was also seen as a relative change in the inward current by ~5 times and the outward current by ~8 times compared to the HEK293 cells not illuminated with UV light quantified at -60 mV and +60 mV, respectively (Figure 19. b, c).

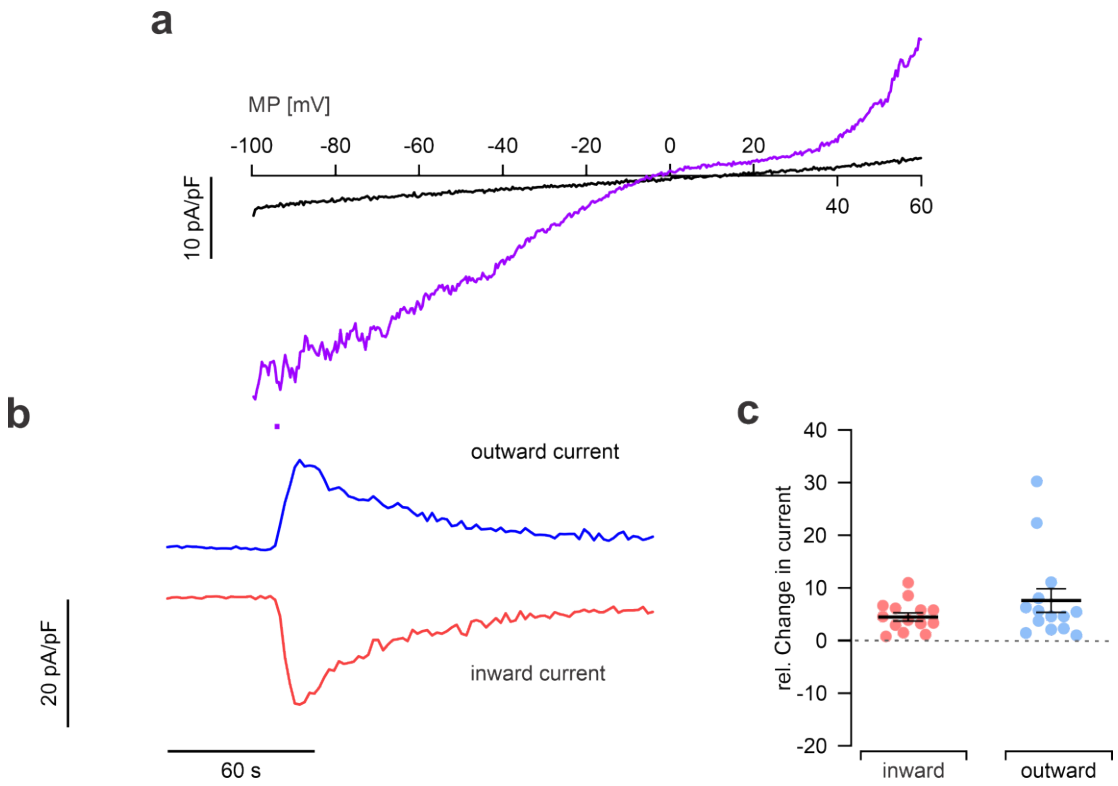

Figure 19: hOPN5 (WT) mediated TRPC6 channel activation by DAG.
a. Representative current traces during voltage ramps (outward currents in the positive direction and inward current in the negative direction) of hOPN5/TRPC6 HEK293 cells before (black) and after UV light stimulation (385 nm, 1 mW/mm^2, 4 s, violet). **b.** The time course of inward current (red) and outward current (blue) at -60 and +60 mV, 4 s UV light indicated by the violet bar. **c.** Relative change in inward and outward current at -60 and +60 mV in individual cells (dots) after activation of TRPC6 channels by UV light in hOPN5 (WT) HEK293 cells.

3.2. Investigating the possible promiscuity of hOPN5 (WT)

3.2.1. Light mediated activation of hOPN5 does not reduce cAMP levels

To investigate the reported activation of $G_{\alpha i}$ proteins by hOPN5 (Sugiyama et al., 2014), Berivan Mansurogulu from the University of Bonn measured cAMP levels after adenylyl cyclase activation with forskolin (FSK) and additional UV light illumination in hOPN5 (WT) HEK293 cells or CCh mediated Muscarinergic acetylcholine receptor 2 (M2) activation in M2 HEK293 cells with the GloSensor luminescence assay. There was no apparent light-mediated decay of cAMP levels in hOPN5 (WT) HEK293 cells despite using supramaximal intensities of UV light (500 ms, 110 µW/mm^2), as determined from Ca^{2+} imaging experiments.

An apparent reduction in cAMP levels was observed in experiments with M2 expressing HEK293 cells after CCh (100 µM) stimulation (Figure 20).

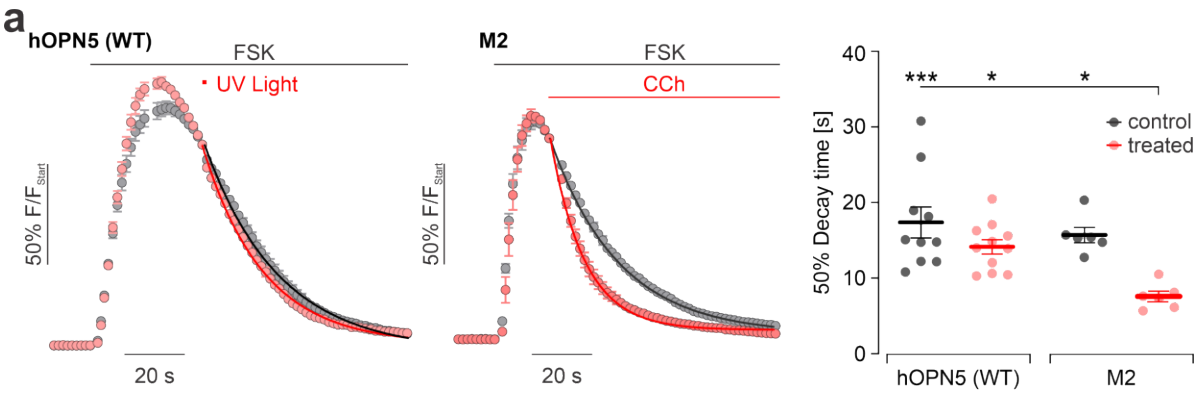

Figure 20: cAMP GloSensor luminescence-based assay with transgenic HEK293 cells expressing hOPN5 (WT) and M2.
Time courses of cAMP levels (average of ≥ 6 individual wells of hOPN5(WT) and M2 expressing HEK293 cells, respectively) measured by GloSensor luminescence after Forskolin addition (10 µM, FSK) normalized to the time point of UV light illumination (500 ms, 110 µW/mm^2) or CCh (100 µM) application. Statistical analysis of 50% decay time analyzed by an exponential fit of each well individually (each dot represents one well) with ordinary one-way ANOVA with Tukey's multiple comparison test (p(hOPN5 control vs. hOPN5 light): 0.32; p(hOPN5 control vs. M2 control): 0.87; p(M2 control vs. M2 CCh): 0.012; p(hOPN5 light vs. M2 CCh): 0.024). Experiments were performed by Berivan Mansurogulu.

3.2.2. hOPN5 needs G_q proteins to produce Ca^{2+} transients

The next step was to perform Ca^{2+} imaging experiments in hOPN5 (WT) expressing HEK293 cells with genetic ablation of either $G_{q/11\alpha}$ or $G_{i\alpha}$ genes. These experiments investigated the requirement of $G_{q/11\alpha}$ proteins in inducing Ca^{2+} transients of hOPN5 (WT). In $G_{q/11}$ KO cells, UV light-mediated Ca^{2+} transients were entirely abolished, whereas ATP (1.5 mM) still evoked minimal Ca^{2+} increases (Figure 21. a). Additionally, UV light-induced Ca^{2+} transients in G_i KO cells were even more pronounced compared to hOPN5 (WT) HEK293 cells with intact endogenous G_α proteins. The proper functioning of endoplasmic Ca^{2+} storage and release was checked in all three cell lines by blocking the Sarco/endoplasmic reticulum Ca^{2+} ATPase (SERCA) pump with cyclopiazonic acid (CPA), which elevated cytosolic Ca^{2+} levels gradually (Figure 21. a, b). These experiments prove that the $G_{q\alpha}$ proteins are essential to produce Ca^{2+} transients upon light activation of hOPN5 (WT) but not $G_{i\alpha}$ proteins. This result further proves that hOPN5 (WT) activates the G_q signaling cascade.

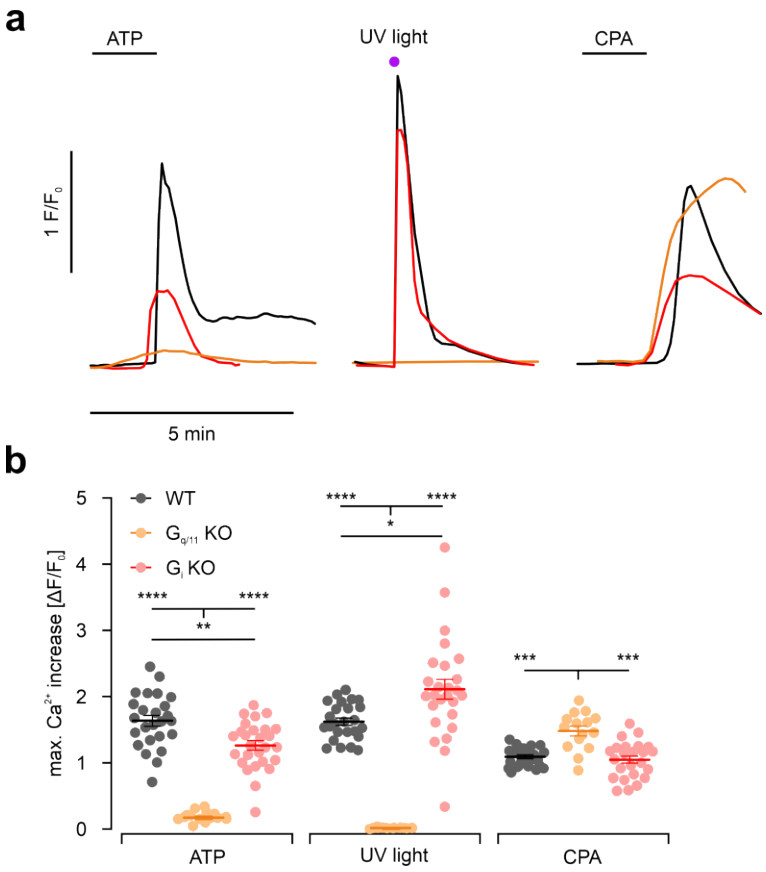

Figure 21: Ca^{2+} transients in G_i or $G_{q/11}$ HEK293 cells compared to control HEK293 cells. **a.** Representative traces of Ca^{2+} transients and **b.** aggregated data of the maximal amplitude induced by ATP (1.5 mM), UV light (1 mW/mm², 1 s), and cyclopiazonic acid (CPA, 50 µM), respectively, in HEK293 WT cells (black), HEK293 G_i KO cells (red) and HEK293 $G_{q/11}$ KO cells (orange), all expressing hOPN5(WT). Statistical analysis was performed with a two-way ANOVA repeated measurements test. p values were obtained from Tukey's multiple comparison test performed for the different stimulants used (N = 15 for $G_{q/11}$ KO cells, N = 26 for G_i KO cells, and N = 25 for HEK293 WT cells; p = 0.76 for HEK293 WT versus G_i KO cells in CPA treatment). Maximum Ca^{2+} increase values are represented as mean ± SEM. *p < 0.05, **p < 0.01, ***p < 0.001, ****p < 0.0001

3.2.2. hOPN5 (WT) inhibits GIRK channels

Patch clamp experiments were performed to record G protein-coupled inwardly rectifying potassium (GIRK) channel currents to exclude the promiscuous UV light-mediated activation of G_i signaling by hOPN5 (WT). GIRK channel assay is ideally suited to determine the promiscuity of a certain GPCR to activate either G_i or G_q proteins or both. Activation of G_i proteins will increase GIRK currents, whereas G_q signaling will inhibit the constitutive conductance of K^+ via PIP_2 depletion and also by the phosphorylation of the GIRK 1/2 subunits by PKCs, both processes triggered by the activation of G_q signaling cascade. PIP_2 is a requisite for stabilizing the GIRK channels in the cell membrane (Breitwieser, 2005).

HEK293 cells that overexpress GIRK channels 1/2 and hOPN5 (WT) were used for the electrophysiology recordings performed by Daniela Malan (University of Bonn). The UV light activation inhibited GIRK channels (Figure 22. a) in HEK293 cells expressing hOPN5(WT) and GIRK1/2 channels but not in control HEK293 cells expressing only GIRK1/2 channels (Figure 22. b). No significant differences were observed in the UV light-induced GIRK inhibition even after incubating the cells with the specific G_i protein blocker Pertussis toxin (PTX). In clear contrast, the G_q specific blocker, FR900359 clearly abolished the inhibitory effect of hOPN5 (WT) (Figure 22. c). Promiscuous activation of G_i proteins, if present should have been seen after the G_q blocker application as this would have led to an increase in the GIRK currents. Thus, in HEK293 cells, hOPN5 (WT) is specific for G_q proteins, and activation of G_i proteins can be excluded.

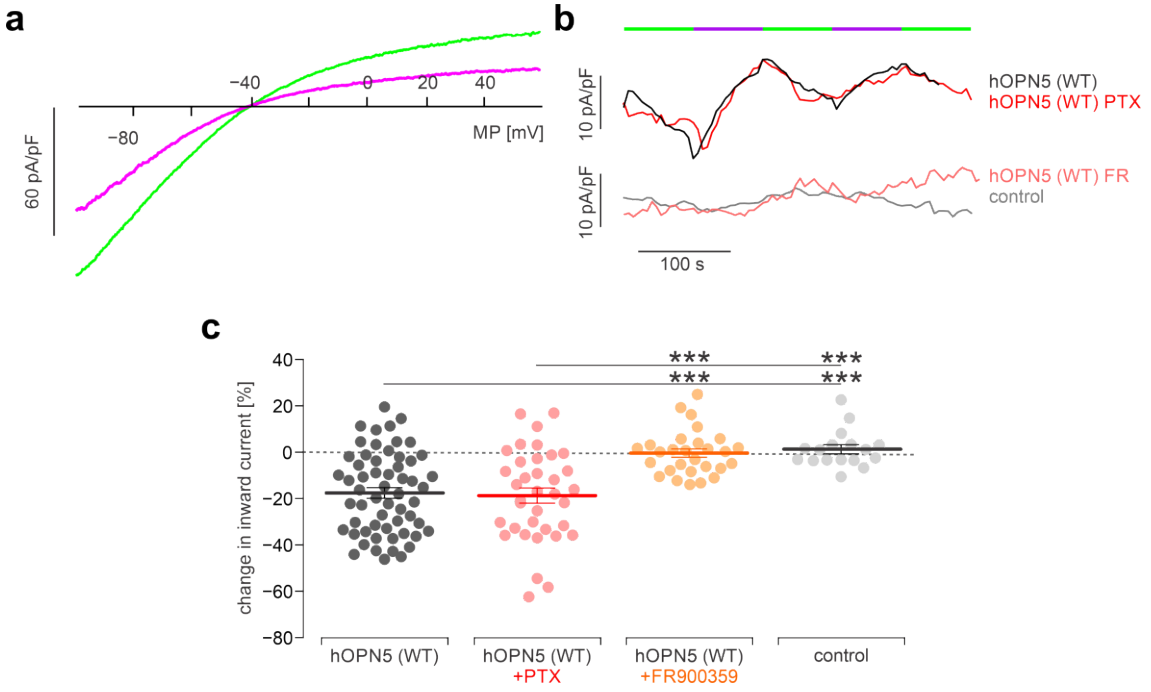

Figure 22: hOPN5 (WT) mediated GIRK channel inhibition via the activation of the G_q signaling cascade.
a. Representative current-voltage ramps (outward currents in the positive direction) of hOPN5(WT)/GIRK HEK293 cells during UV (385 nm, 1 mW/mm^2, 75 s, violet) and green (500–600 nm, 14 mW/mm^2, 75 s, green) light illumination, respectively. **b.** Time course of inward currents (in the negative direction) at −80 mV during UV (violet bars) and green light illumination (green bars). **c.** Change in inward current at −80 mV induced by UV light illumination (each dot represents one individual cell) in control WT and hOPN5(WT) cells both expressing GIRK1/2 channels HEK293 cells without and with PTX or FR900359 treatment. Statistical analysis was performed with a non-parametric ANOVA test with Tukey's multiple comparison posttest. p(hOPN5(WT) vs. hOPN5(WT) PTX) = 0.99; p(hOPN5(WT) FR vs. control WT) = 0.99. Change in the inward current [%] is represented as mean ± SEM. ***p < 0.001. Experiments were performed by Daniela Malan.

Finally, it can be concluded that hOPN5 (WT) is a highly light-sensitive optogenetic GPCR with selective G_q protein activation, which is crucial for its translational potential and for its use in furthering the understanding of the G_q signaling in both physiological and pathophysiological processes.

3.3. Development of new hOPN5 mutants with enhanced optogenetic properties

The secondary objective of this thesis was to engineer enhanced hOPN5 variants to control the G_q signaling cascade. In particular, the maximal activation and deactivation wavelengths of hOPN5 should be separated far apart from each other to utilize their bistable nature better. Also, to obtain a red-shifted hOPN5 mutant so as to reduce UV toxicity in translational applications and to improve retinal retention of hOPN5 by targeting the appropriate amino acids along with improving activation and deactivation kinetics of hOPN5. A couple of strategies were employed that include multiple sequence alignments of relevant opsin proteins and bovine or squid rhodopsin structure-based models along with molecular dynamics simulations to identify amino acids that affect the electronic resting state of retinal in the binding pocket of OPN5. I explored the amino acid mutations F114S, T164A, Y174F, I203D, F217I/L/V, S218C, Y268F and Y301H in hOPN5 in HEK293. I introduced these mutations in the hOPN5 (WT) gene by site-directed mutagenesis using specific primers with the desired nucleotide changes (Figure 23). Due to the size constraint of the mammalian expression plasmid (8.3 kb) for the site-directed mutagenesis, I used a smaller plasmid (3.4 kb) containing the hOPN5 gene provided by the working group of Philipp Sasse (University of Bonn). The generated plasmids were confirmed by Sanger sequencing to ensure the incorporation of the desired nucleotide changes in the mutant hOPN5 gene. hOPN5 (T164A) mutant gene sequence was procured from GeneArt (Thermofisher). All the mutant hOPN5 genes were cloned into the mammalian expression plasmid, previously used (see above) using SacI/NotI restriction endonucleases and amplified in NEB Turbo *E. coli* cells. All the newly constructed mammalian expression plasmids were again sequenced to ensure the presence of the desired gene sequence without any non-specific mutations (Figure 24).

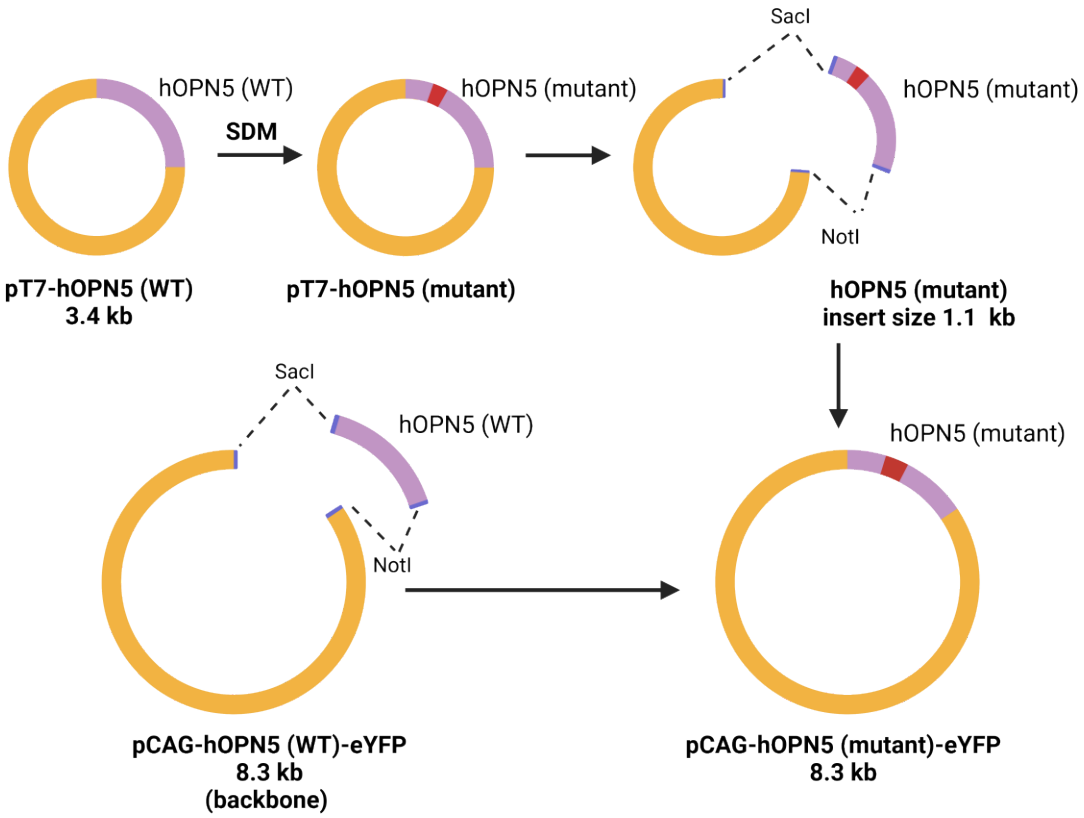

Figure 23: Schematic representation of the strategy to generate expression plasmids containing the mutant hOPN5 genes.
hOPN5 (WT) gene containing plasmid (3.4 kb) was used for site-directed mutagenesis with specific primers and was amplified by PCR. After the generation of the mutated hOPN5 gene containing plasmid, the hOPN5 (mutant) gene was digested with SacI/NotI restriction endonucleases and ligated with the mammalian expression plasmid which was also previously digested with the same restriction endonucleases. The plasmids were amplified in NEB Turbo *E. coli* and were used for the transfection in HEK293 cells.

Wild-type chicken OPN5 (cOPN5 (WT)) was recently reported on its G_q protein coupling capabilities (Dai et al., 2022). So, to benefit from understanding its structural and functional features and to attribute those specific interesting mutations to hOPN5 (WT), I also generated a mammalian expression plasmid with cOPN5 (WT) gene from the ordered plasmid containing its gene sequence (GeneArt, Thermofisher). The same cloning strategy using SacI/NotI restriction endonucleases was used to construct the cOPN5 (WT) mammalian expression plasmid.

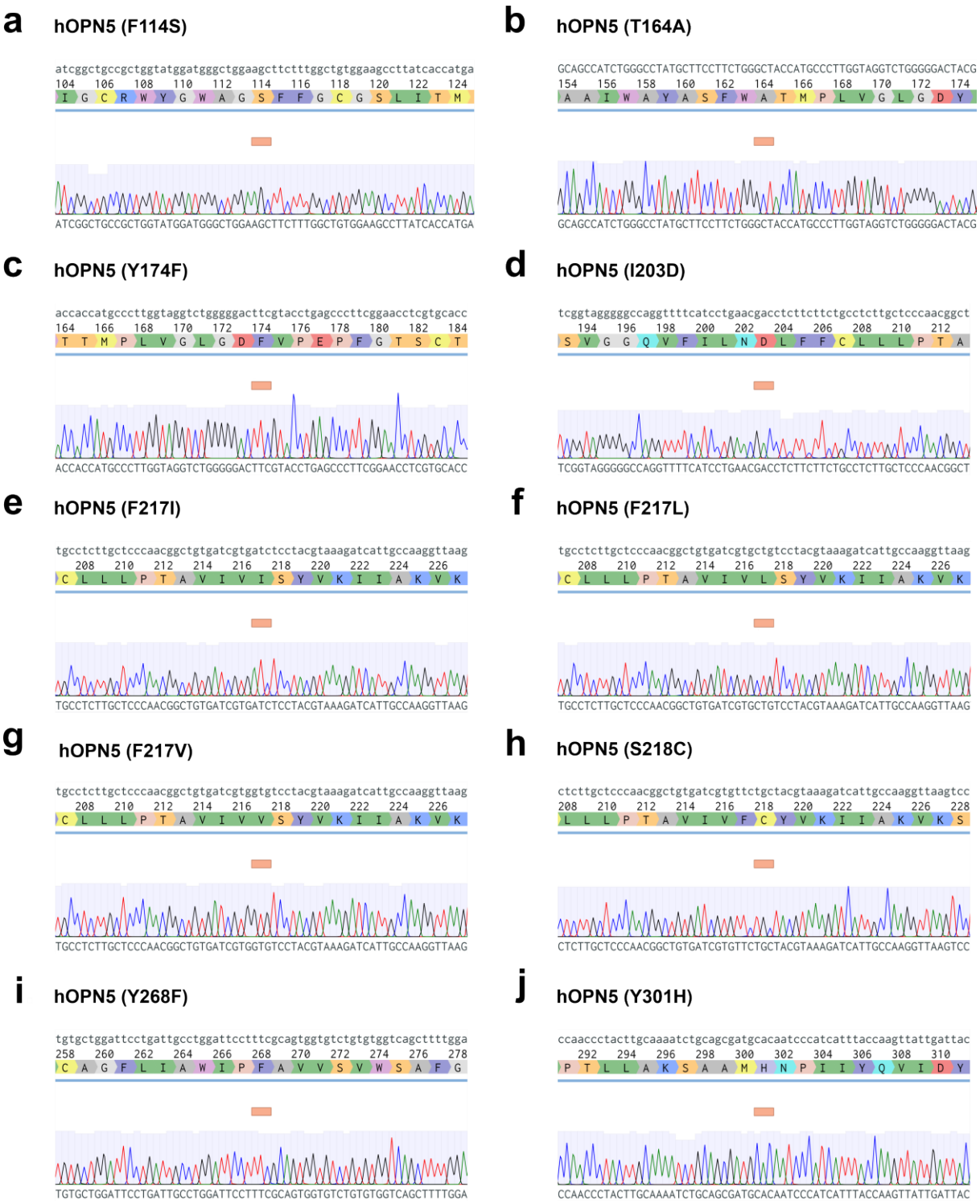

Figure 24: Sanger sequencing results of all plasmids with the desired mutation.
a - j. The chromatogram traces of the sequenced plasmids from Sanger sequencing aligned with the *in silico* generated plasmid nucleotide sequences of the mutant hOPN5 plasmids.

3.3.1 Expression rate and expression strength of the different hOPN5 mutants

HEK293 cell lines expressing different OPN5s were created by lipid-based transfection with each of the newly constructed OPN5 plasmids. The ectopic expression of the different OPN5 variants was stably maintained with G418 antibiotic pressure. All the new HEK293 cell lines displayed appreciable membrane-localized OPN5/eYFP fluorescence except the hOPN5 (I203D) mutant, which did not yield any eYFP fluorescence corresponding to the failed expression of the mutant (Figure 25). Thus, the hOPN5 (I203D) mutant was not analyzed further. The percentage of eYFP positive cells and the expression strength differed greatly among the different cell lines.

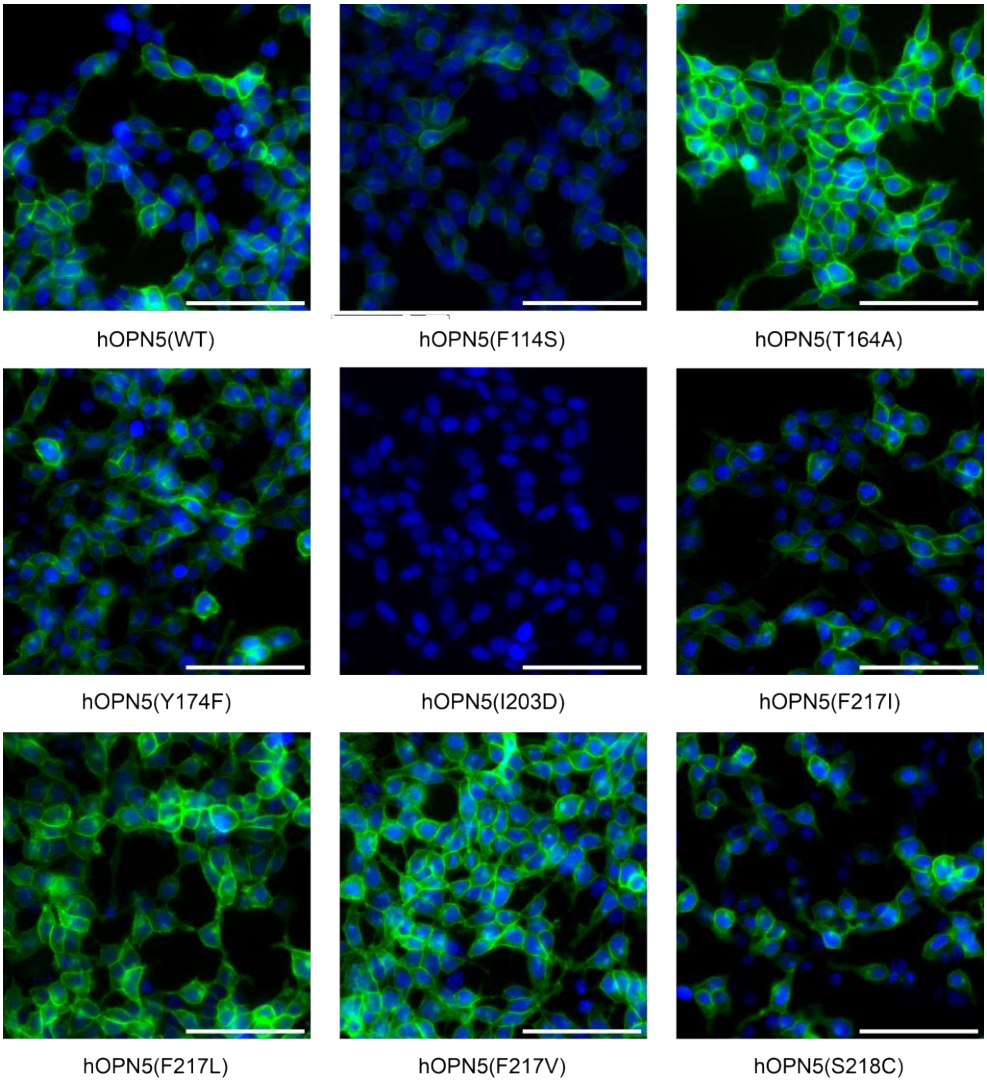

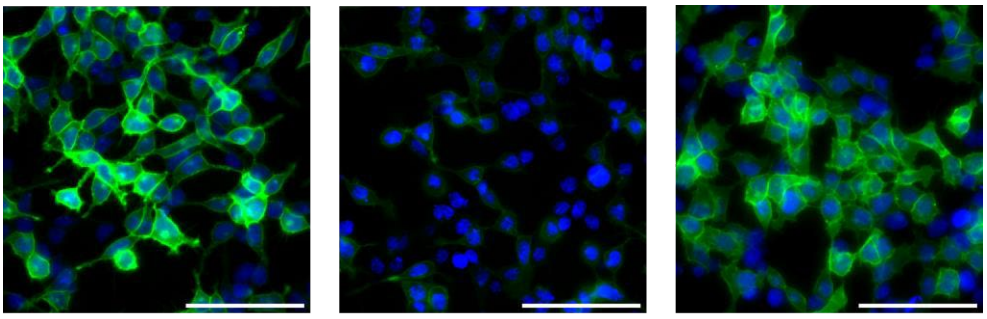

Figure 25: Representative images of the different OPN5 variants expressing cell lines.
Transgenic HEK293 cells expressing different variants of OPN5 proteins in fusion with eYFP (green) and nuclei stained with DAPI (blue), bar = 100 µm.

For detailed quantification, I calculated the expression rate of the different OPN5 variants in HEK293 cells as a percentage of the eYFP positive cells to the total number of cells in a region of interest (Figure 26). hOPN5 (T164A) and hOPN5 (F217V) cell lines displayed the highest expression rate (≥ 95%). hOPN5 (F217I), hOPN5 (F217L), hOPN5 (S218C), cOPN5 (WT) cell lines had similar expression rate of ~ 75 % which were still significantly higher compared to hOPN5 (WT). hOPN5 (WT), hOPN5 (F114S), hOPN5 (Y268F) and hOPN5 (Y301H) cell lines had a similar expression rate of ~ 60%. hOPN5 (F114S) had a similar expression rate to hOPN5 (WT) but with a small significant increase (Figure 26).

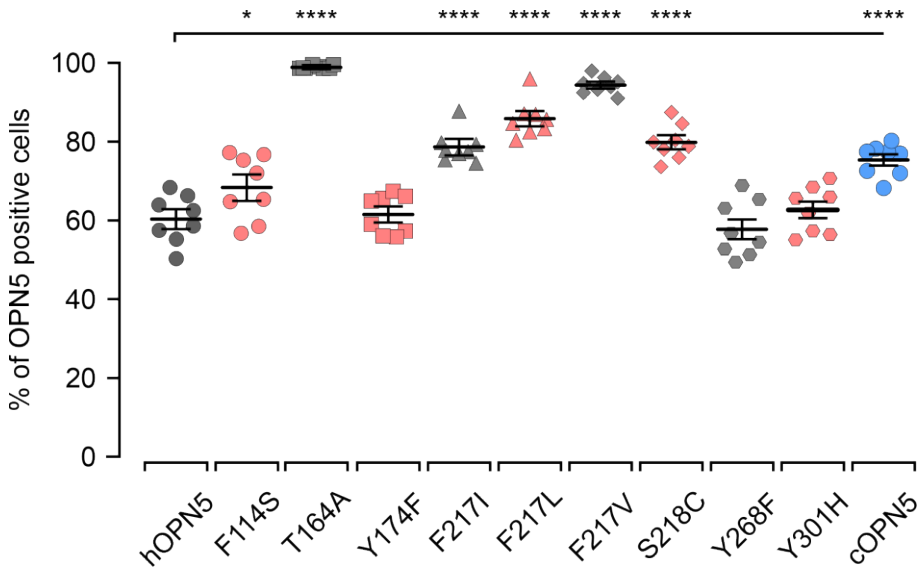

Figure 26: Percentage of OPN5 positive cells in stable HEK293 cell lines.
The percentage of different OPN5/eYFP positive cells with respect to the total number of cells (each dot represents one region of interest containing ≥ 200 cells, n = 8). Statistical analysis was performed with one-way ANOVA and Dunnett's multiple comparisons post-test for each OPN5 cell line compared to the hOPN5 (WT) cell line. The percentage of OPN5 positive cells is represented as mean ± SEM. All non-significant p values are > 0.91. *p < 0.05, ****p < 0.0001.

To determine the expression strength, I measured the expressed eYFP as pg per ng of total protein from the cell lysates by ELISA. The measurement of eYFP can be used as a direct measure of the expression strength of OPN5 due to their expression as a single fusion protein. The eYFP amount was quantified from the standard curve with the known concentration of GFP, as eYFP is a mutated variant of GFP (Rekas et al., 2002). The hOPN5 (WT) displayed an expression strength of ~80 pg of eYFP fusion protein per ng of the total protein. As expected from the previous expression rate studies (Figure 26), the hOPN5 (T164A) mutant had the highest expression strength, which was 3.5 times more (~280 pg) eYFP fusion protein compared to hOPN5 (WT), followed by hOPN5 (S218C) mutant which was 2 times more (~172 pg) eYFP fusion protein compared to hOPN5 (WT). hOPN5 (F217V) and hOPN5 (F217I) expressed almost 1.5 times more than hOPN5 (WT). cOPN5 (WT) expressed slightly higher levels (~90 pg) of eYFP fusion protein per ng of the total protein compared to hOPN5 (WT). hOPN5 (Y174F), hOPN5 (Y268F) and hOPN5 (F217I) had expression strengths slightly lower than hOPN5 (WT). hOPN5 (F114S) and hOPN5 (Y301H) mutants had the least expression strength even though eYFP positive cells were above 60% (Figure 26), both mutant cell lines expressed one-third of the eYFP fusion protein amount of hOPN5 (WT) (Figure. 26).

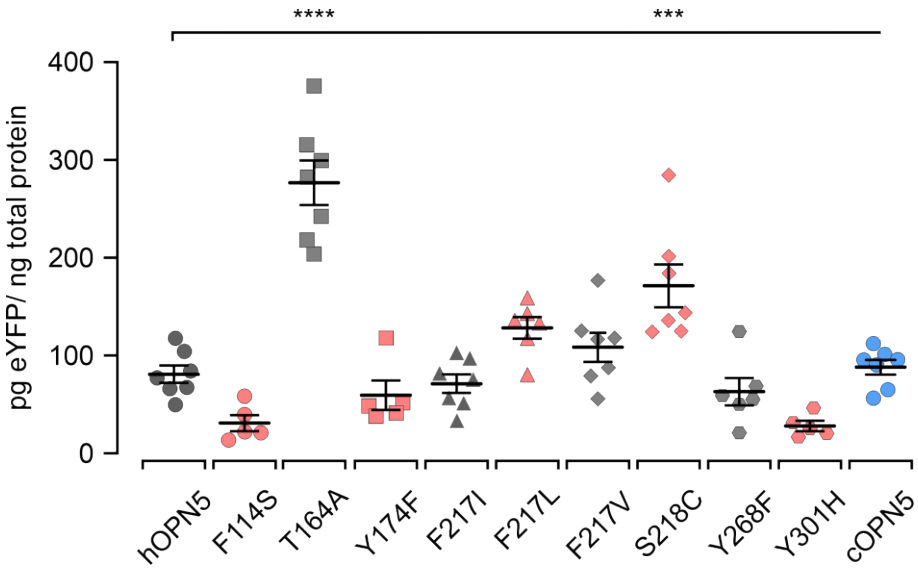

Figure 27: Expression strength of the OPN5 variants in the respective stable cell lines. Analyzed by ELISA. Statistical analysis was performed with one-way ANOVA and Dunnett's multiple comparisons post-test of each OPN5 cell line compared to that of the hOPN5 (WT) cell line. Expression strength values are represented as mean ± SEM. All non-significant p values are > 0.1.

3.3.2 Light sensitivity of the different mutant OPN5 proteins

The light sensitivity for the HEK293 cell lines expressing different OPN5 proteins was determined using the Ca^{2+} imaging with X-Rhod-1, AM using UV light pulses (385

nm, 100 ms). Increasing light intensity pulses from 0.1 µW/mm^2 to 600 µW/mm^2 were used for most of the mutant hOPN5 cell lines and cOPN5 (WT) cell lines, while light intensities from 1 µW/mm^2 to 3 mW/mm^2 were used for hOPN5 (F114S) and hOPN5 (Y301H) cell lines as these cells were less light sensitive. The Ca^{2+} imaging was also performed on hOPN5 (WT) HEK293 cells with the new stimulation protocol to compare with the other newly generated HEK293 cells. The maximal amplitude of the Ca^{2+} transients from these different OPN5 cell lines was plotted against their light intensities to calculate the eLi50, previously described in the characterization of hOPN5 (WT) cell lines. The new analysis of hOPN5 (WT) cells had an average eLi50 of 4.03 ± 0.3 (n = 21) which is slightly higher than in previous eLi50 experiments (Figure 16). This can be explained by the use of a different camera with less quantum efficiency compared to the camera used before and by using a newly adapted, completely automated data analysis method using Cell profiler software.

The cOPN5 (WT) cell line displayed the highest light sensitivity with an average eLi50 of 2.06 ± 0.1 µW/mm^2 (n = 16). The light sensitivity of mutants hOPN5 (T164A) 3.23 ± 0.2 µW/mm^2 (n = 12), hOPN5 (F217L) 4.21 ± 0.4 µW/mm^2 (n =15), hOPN5 (F217V) 4.77 ±0.3 µW/mm^2 (n = 15), hOPN5 (F217I) 5.36 ± 0.5 µW/mm^2 (n = 10) and hOPN5 (S218C) 6.27 ± 0.6 (n = 17) were not statistically different compared to hOPN5 (WT). hOPN5 (Y174F) 7.33 ± 0.4 µW/mm^2 (n = 14), hOPN5 (Y268F) 13.56 ± 0.9 µW/mm^2 (n = 14) were slightly less light sensitive than hOPN5 (WT). However, the eLi50 of hOPN5 (F114S) was of 80.83 ± 5.67 µW/mm^2 (n =15) and hOPN5 (Y301H) was of 161. 5 ± 11.3 µW/mm^2 (n = 14), these mutants displayed very low light sensitivity (Figure 29. a). Next, I also analyzed the maximum amplitudes for all different OPN5 cell lines. Compared to hOPN5 (WT) (1.6 $\Delta F/F_0$), the mutants hOPN5 (T164A), hOPN5 (F217I), hOPN5 (F217L), and hOPN5 (S218C) had similar efficiencies to induce Ca^{2+} transients and were not significantly different in the maximum Ca^{2+} amplitudes. The mutants hOPN5 (Y174F) had 1.4 $\Delta F/F_0$, and hOPN5 (F217V) had 1.3 $\Delta F/F_0$, respectively, which was slightly less efficient in inducing Ca^{2+} transients. The mutants hOPN5 (Y268F) had 0.9 $\Delta F/F_0$, hOPN5 (F144S) had 0.8 $\Delta F/F_0$, and hOPN5 (Y301H) had 0.4 $\Delta F/F_0$ and displayed thus less efficiency to produce Ca^{2+} transients. The cOPN5 (WT) had 1.1 $\Delta F/F_0$ even though the eLi50 was the best among all other OPN5 (Figure. 28 and 29).

The changes in the light sensitivities and maximal Ca^{2+} amplitudes can be attributed to the changes induced by amino acid substitution in the three-dimensional structure of the protein, leading to strained protein folding issues as well as the electrostatic changes in the retinal chromophore environment causing spectral changes. The other factors that must be considered while assessing of the hOPN5 mutant proteins are their expression rate and the expression strength in their respective cell lines.

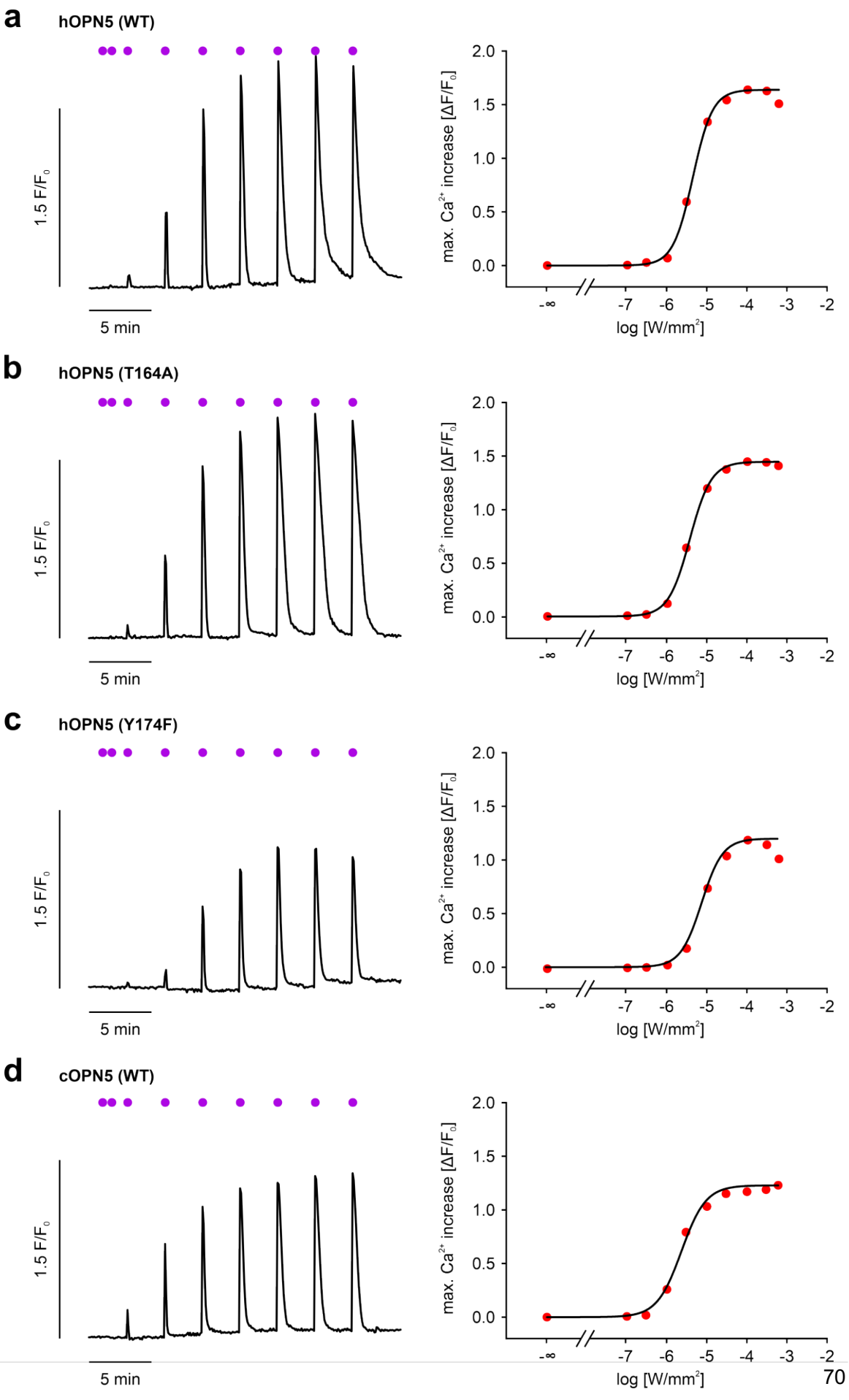
a
hOPN5 (WT)
1.5 F/F0
5 min
max. Ca2+ increase [ΔF/F0]
2.0
1.5
1.0
0.5
0.0
-∞
-7
-6
-5
-4
-3
-2
log [W/mm2]
b
hOPN5 (T164A)
1.5 F/F0
5 min
max. Ca2+ increase [ΔF/F0]
log [W/mm2]
c
hOPN5 (Y174F)
1.5 F/F0
5 min
max. Ca2+ increase [ΔF/F0]
log [W/mm2]
d
cOPN5 (WT)
1.5 F/F0
5 min
max. Ca2+ increase [ΔF/F0]
log [W/mm2]

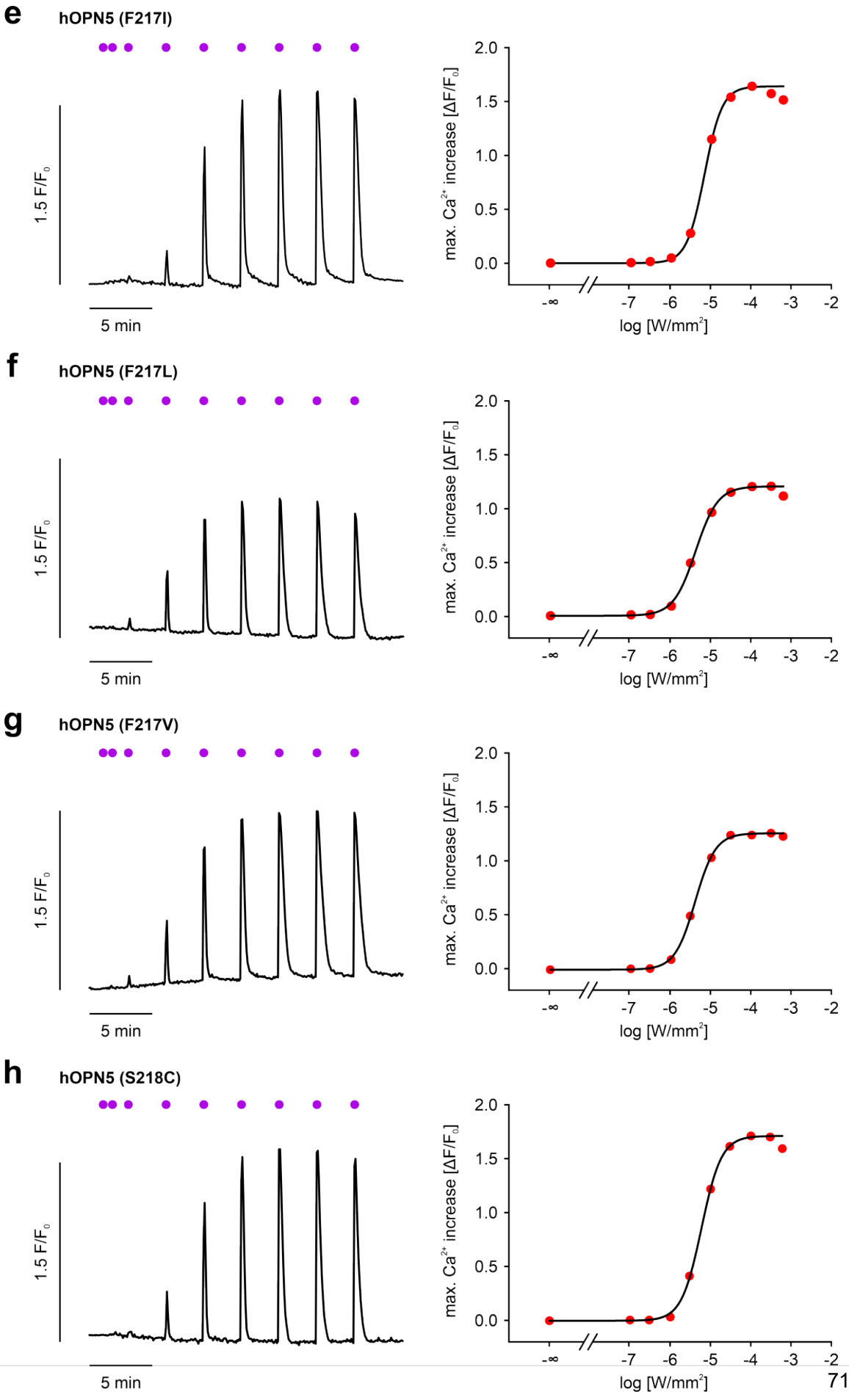
e
hOPN5 (F217I)
1.5 F/F0
5 min
max. Ca2+ increase [ΔF/F0]
2.0
1.5
1.0
0.5
0.0
-∞
-7
-6
-5
-4
-3
-2
log [W/mm2]
f
hOPN5 (F217L)
1.5 F/F0
5 min
max. Ca2+ increase [ΔF/F0]
log [W/mm2]
g
hOPN5 (F217V)
1.5 F/F0
5 min
max. Ca2+ increase [ΔF/F0]
log [W/mm2]
h
hOPN5 (S218C)
1.5 F/F0
5 min
max. Ca2+ increase [ΔF/F0]
log [W/mm2]

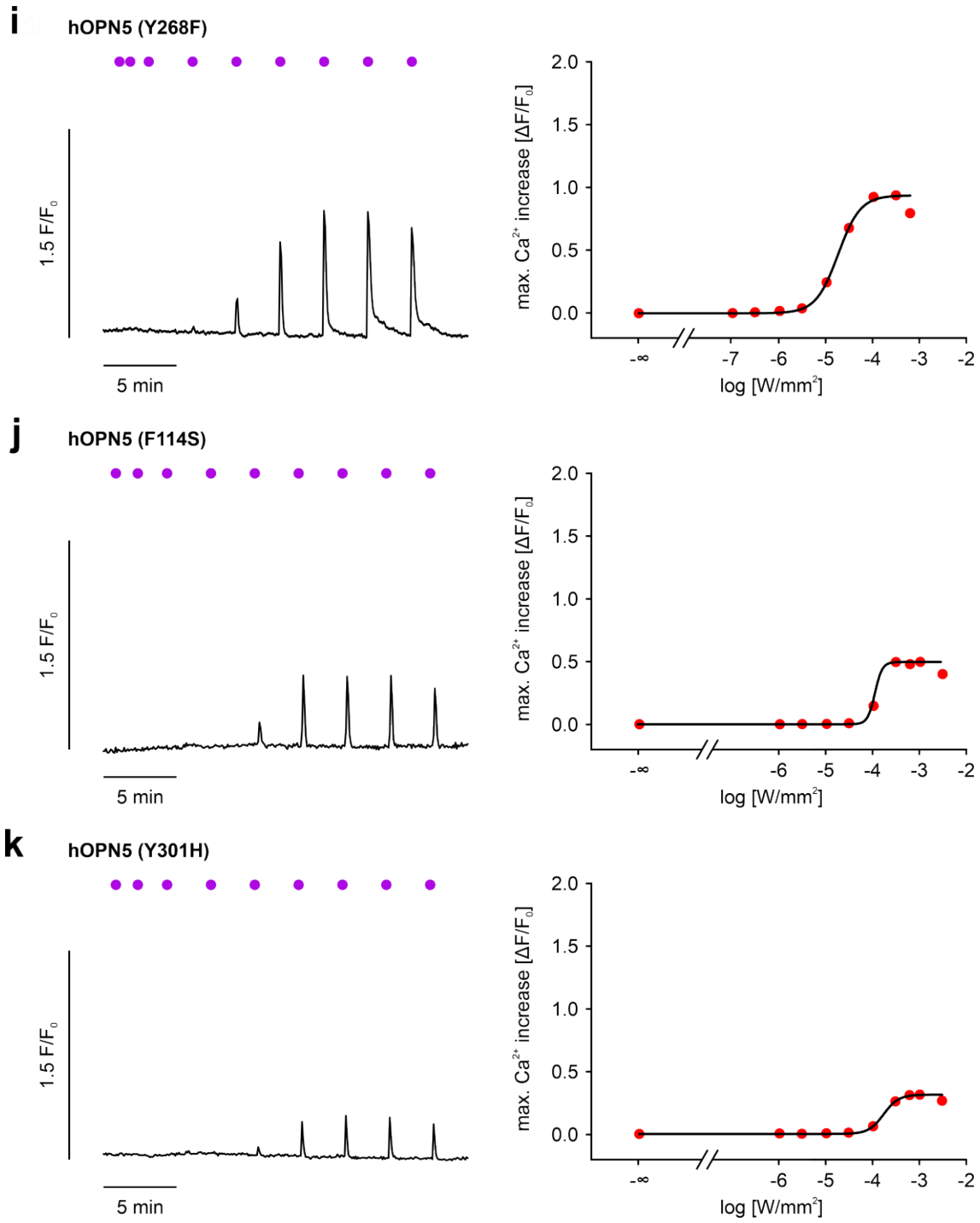

Figure 28: Representative traces of Ca^{2+} transients of all different OPN5 variant HEK293 cell lines for the determination of light sensitivity.

Ca^{2+} transients (left, an average of ≥ 200 cells in black) after 100 ms long UV (385 nm) light pulses with increasing light intensity (violet dots from left: 0.1, 0.3, 1, 3, 10, 30, 100, and 300 µW/mm² for **a, b, c, d, e, f, g, h,** and **i**. 1, 3, 10, 30, 100, 300, 600, 1000, and 3000 µW/mm² for **j, k**) and determination of eLi50 on the right with a hill fit (right, black, red dots correspond to the highest Ca^{2+} amplitude for each of the light intensities).

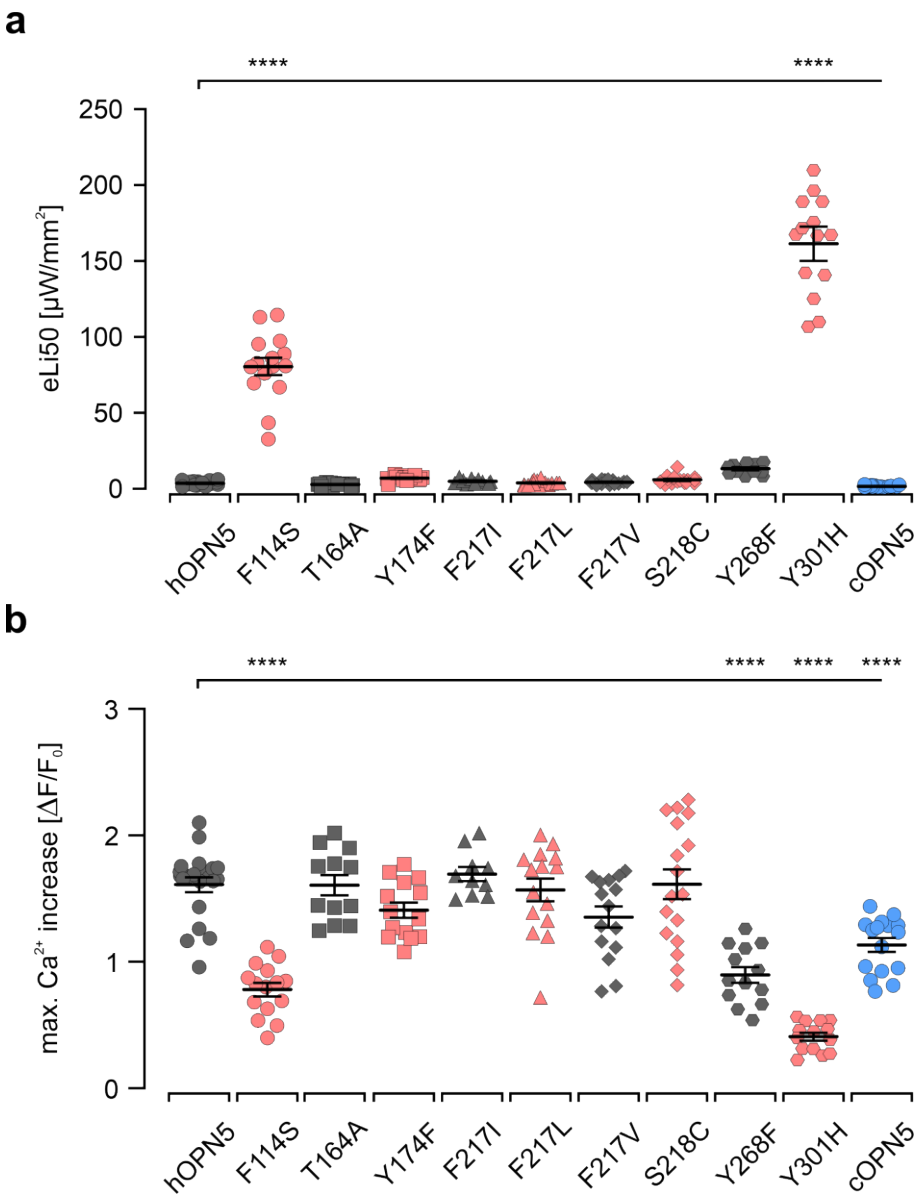

Figure 29: Statistical comparison of eLi50 values and maximal Ca^{2+} transient amplitudes of the different OPN5 variants cell lines.

a, Aggregated data of the determined eLi50 values for all different OPN5 variants. Statistical analysis was performed with one-way ANOVA and Šídák's multiple comparisons post-test for the eLi50 values of each mutant, comparing it to the eLi50 of hOPN5 (WT). All non-significant p values are > 0.45. **b,** Aggregated data of the maximal Ca^{2+} transient amplitudes of each of the different OPN5 variants. Statistical analysis was performed with one-way ANOVA and Šídák's multiple comparisons post-test for the maximum effect of each mutant compared to that of the hOPN5 (WT). One symbol represents the average of one coverslip with ≥ 200 cells. Both eLi50 and maximum Ca^{2+} increase values are represented as mean ± SEM. All non-significant p values are >0.09. ****p < 0.0001.

3.3.3 Wavelength specificity of the different mutant OPN5 proteins

The determination of the specific activation wavelength of the different OPN5 variants was performed using Ca^{2+} imaging. The new setup with the CAIRN monochromator (U.K.) has the advantage that the light intensity can be adapted for each wavelength, and thus the different wavelengths can be used even at very low light intensities. In addition, I adapted the light intensity used for each OPN5 variant in my experiments to 80% percent of the maximal effective light intensity (eLi80) of the respective OPN5 variant. eLi80 was calculated from the hill fit analyzed to determine the light sensitivity (Figure 29). The eLi80 value (in $\mu W/mm^2$) was determined to be for cOPN5 (WT) as 4.66 ± 0.3 (n = 16), hOPN5 (WT) 7.98 ± 0.6 (n = 21), hOPN5 (T164A) 6.41 ± 0.6 (n = 12). hOPN5 (F217L) 8.08 ± 0.8 (n =15), hOPN5 (F217V) 9.38 ± 0.6 (n = 15), hOPN5 (F217I) 10.5 ± 0.9 (n = 10), hOPN5 (S218C) 12.82 ± 1.5 (n = 17), hOPN5 (Y174F) 15.93 ± 0.9 (n = 14), hOPN5 (Y268F) 28.27 ± 2.1 (n = 14), hOPN5 (F114S) 133.8 ± 7.4 (n = 15) and hOPN5 (Y301H) 279.2 ± 17.7 (n = 14) (Figure 30).

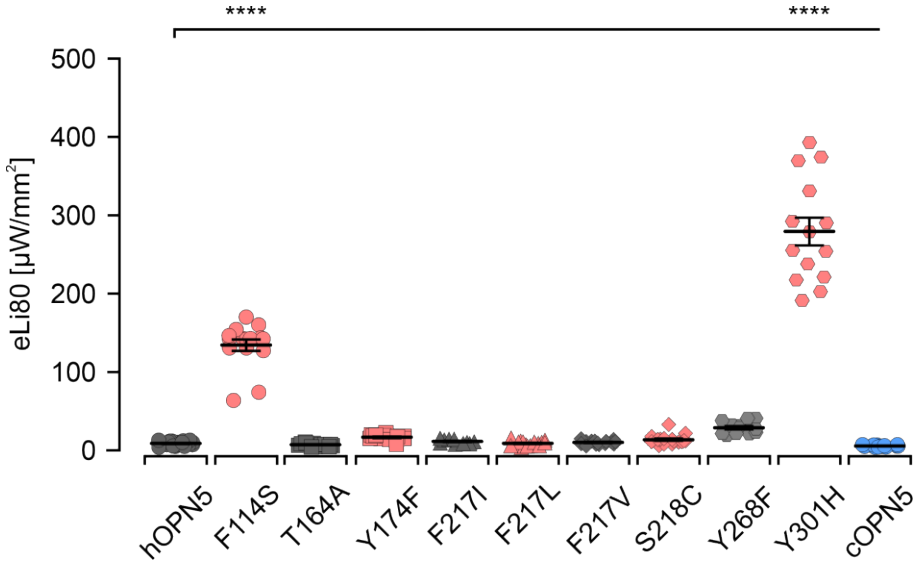

Figure 30: eLi80 of all the different OPN5 variants.
Aggregated data of the eLi80 values for all different OPN5 variants. Statistical analysis was performed with one-way ANOVA and Šídák's multiple comparisons post-test for the eLi80 values of each mutant compared to the eLi80 of hOPN5 (WT). One symbol represents the average of one coverslip with ≥ 200 cells. All eLi80 values are represented as mean ± SEM. All non-significant p values are > 0.08.

The light stimulation protocol was designed with different wavelength pulses from 370 nm to 530 nm. A predetermined light intensity for all wavelengths of 10 $\mu W/mm^2$ and light pulse duration of 30 ms was used for cOPN5 (WT), hOPN5 (WT), hOPN5 mutants T164A, F217L, F217V, F217I, S218C, and Y174F adapted from their eLi80 values. Since the hOPN5

mutants Y268F, F114S, and Y301H had low light sensitivities, and the stimulation protocol was closely adapted from the eLi80 values of those mutants. The maximal Ca^{2+} transient amplitudes for each wavelength were used to calculate the normalized maximal Ca^{2+} increase, and the specific activation wavelength was calculated using Govardovskii's equation (Govardovskii et al., 2000). The most efficient activation wavelength for hOPN5 (WT) was 387.8 ± 0.80 nm (n = 13), for hOPN5 T164A 388 ± 1.21 nm (n = 18), Y174F 380.8 ± 0.52 nm (n = 10), F217I 381.4 ± 1.60 nm (n = 12), F217L 385.5 ± 1.04 nm (n = 16), F217V 386.1 ± 1.23 nm (n = 10), S218C 383.2 ± 1.70 nm (n = 15), and for cOPN5 (WT) 406.3 ± 2.51 nm (n = 10). For hOPN5 mutants which had low light sensitivities, the specific activation wavelength was for F114S 392.8 ± 2.81 nm (n = 6), Y268F 385.9 ± 0.95 nm (n = 10) and for Y301H 389 ± 1.8 (n = 11). All the hOPN5 mutants had a very similar activation wavelength compared to that of the hOPN5 (WT), while the mutants Y174F and F217I had an average of 5 nm left shift towards the direction of UV light. The cOPN5 (WT) on the other hand, had a right shift of almost 20 nm from the hOPN5 (WT) towards the blue region. This change could also be attributed to its increased light sensitivity, and further experiments with lower light intensities should be performed to assess the maximal wavelength (Figure 30).

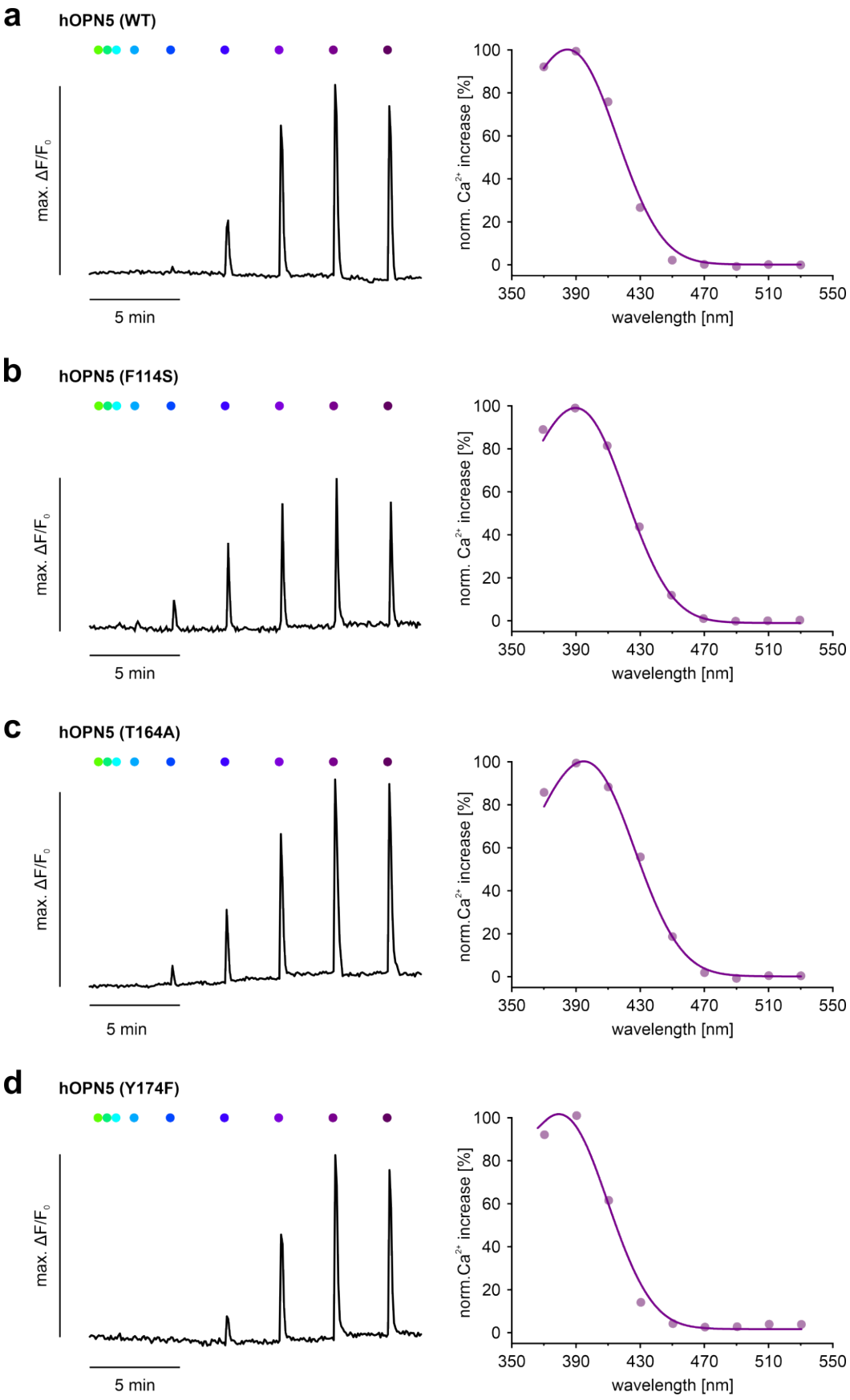
a
hOPN5 (WT)
max. ΔF/F0
5 min
norm. Ca2+ increase [%]
wavelength [nm]
b
hOPN5 (F114S)
max. ΔF/F0
5 min
norm. Ca2+ increase [%]
wavelength [nm]
c
hOPN5 (T164A)
max. ΔF/F0
5 min
norm.Ca2+ increase [%]
wavelength [nm]
d
hOPN5 (Y174F)
max. ΔF/F0
5 min
norm.Ca2+ increase [%]
wavelength [nm]

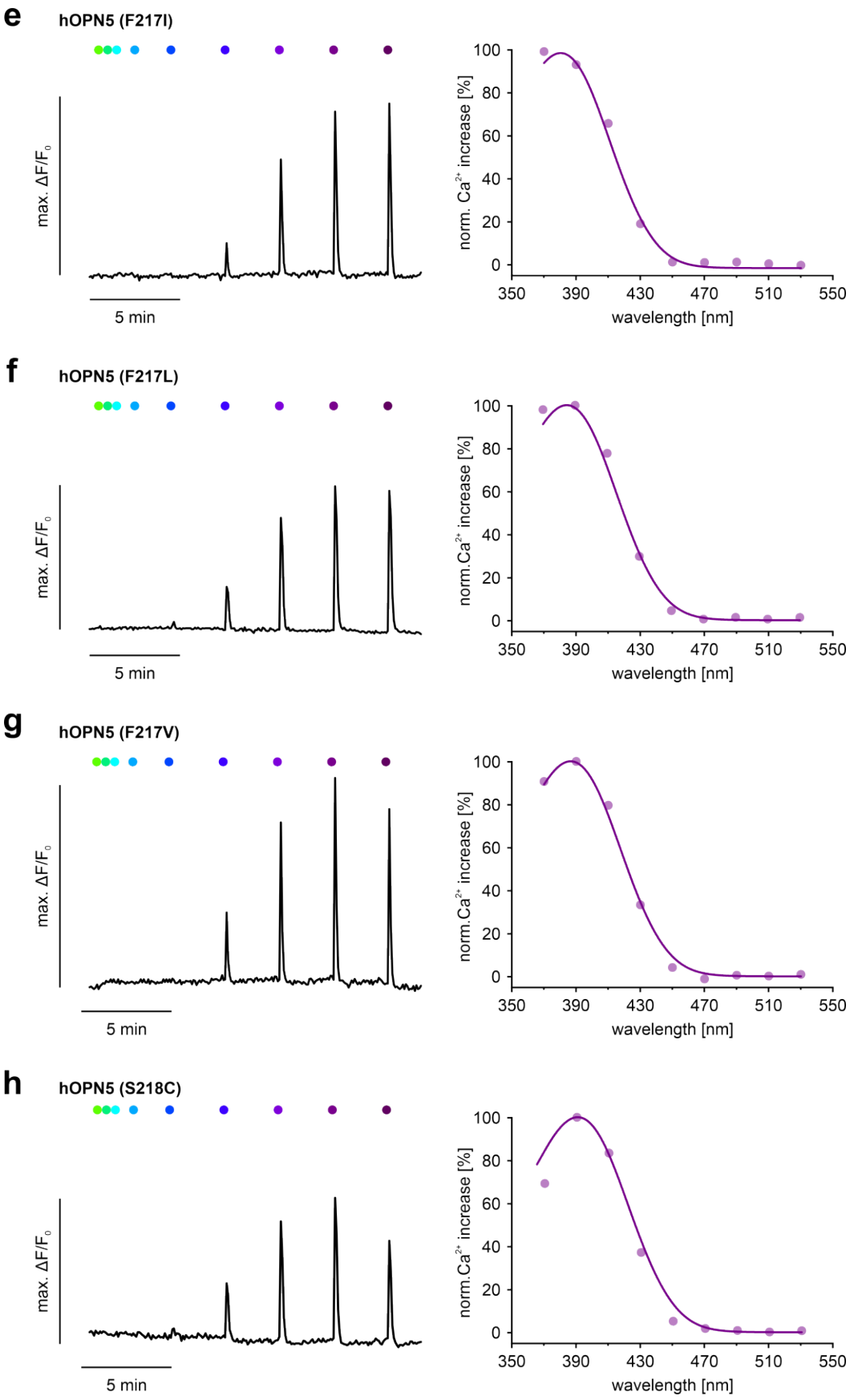
e
hOPN5 (F217I)
max. ΔF/F0
5 min
norm. Ca2+ increase [%]
wavelength [nm]
f
hOPN5 (F217L)
max. ΔF/F0
5 min
norm.Ca2+ increase [%]
wavelength [nm]
g
hOPN5 (F217V)
max. ΔF/F0
5 min
norm.Ca2+ increase [%]
wavelength [nm]
h
hOPN5 (S218C)
max. ΔF/F0
5 min
norm.Ca2+ increase [%]
wavelength [nm]

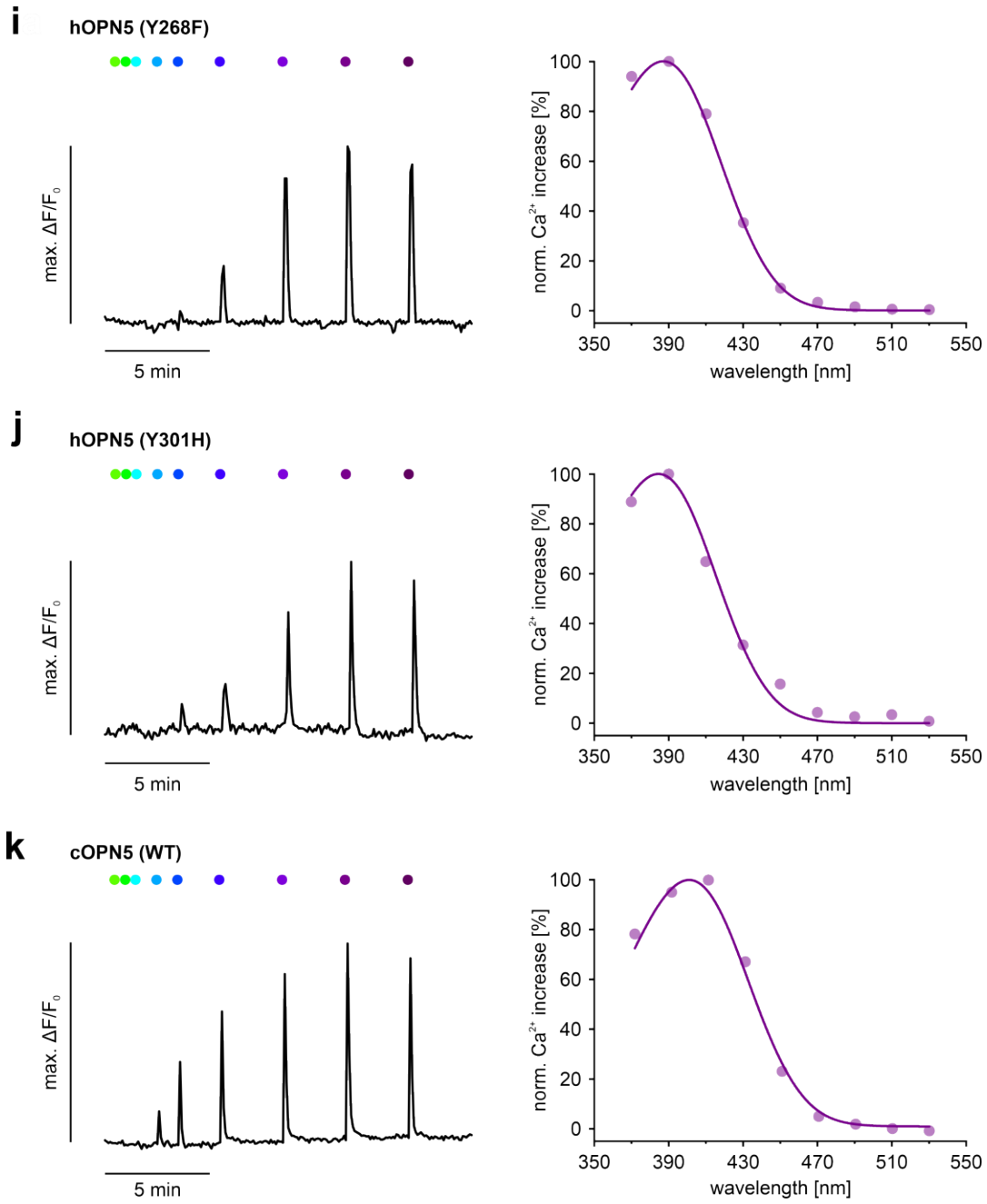

Figure 31: Representative traces of Ca^{2+} transients of different HEK293 cell lines for the determination of wavelength specificity.

Ca^{2+} transients (left, average of ≥ 200 cells in black) after different wavelength pulses from left to right in nm: 530, 510, 490, 470, 450, 430, 410, 390, 370 (30 ms long, 10 µW/mm²) for **a., c., d., e., f., g., h.,** and **k.** The same stimulation protocol was used with a modified pulse and light intensity duration for **b.** (30 ms long, 30 µW/mm²), **i.** (300 ms long, 30 µW/mm²), and **j.** (1000 ms long, 30 µW/mm²). Corresponding analysis of maximal activation wavelength (right, red, calculated as % Ca^{2+} increase) fitted by Govardovskii equation (purple, $R^2 \geq 0.98$).

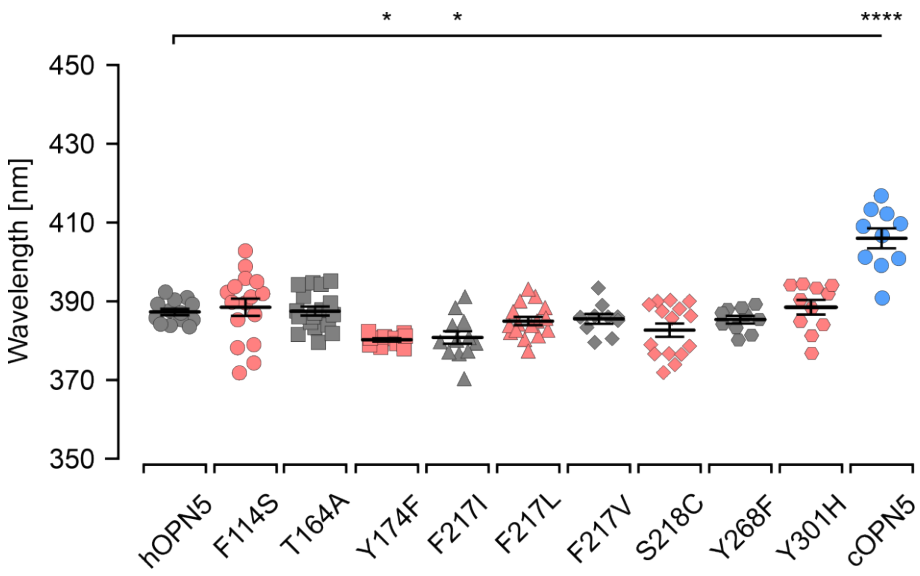

Figure 32: Averages of the most efficient activation wavelength of different OPN5 proteins.
Most efficient wavelength for activation of different OPN5 variants. Statistical analysis was performed with one-way ANOVA and Tukey's multiple comparisons post-test for the activation wavelength of each OPN5 protein compared to that of hOPN5 (WT). Maximal activation wavelength values are represented as mean ± SEM. All non-significant p values are > 0.2.

3.3.4 Determination of retinal retention in hOPN5 (WT), hOPN5 (T164A) and cOPN5 (WT) HEK293 cells

The retinal retention is one of the important properties that influence the effectiveness of rhodopsins in a heterologous expression system. The visual rhodopsins in the native rod or cone cells rely on constant replenishment of 11-cis retinal from photoisomerases and retinoid processing machinery in the retinal pigment epithelium cells (Yang et al., 2021). So, the opsins are subjected to bleaching after a single illumination and cannot function unless 11-cis retinal is replenished. However, the heterologously expressed rhodopsins require a supply of retinal to function in non-native environments so as not to get bleached. The availability of retinal is henceforth critical as the apoprotein without retinal is biochemically unstable and more prone to degradation (Tichy et al., 2019). Therefore, it is important to assess the retinal retention capacity of any rhodopsin to ascertain its future use as an ideal optogenetic tool. The standard protocol used for Ca^{2+} imaging involves supplementing HEK293 cells with 2 µM ATR during the Ca^{2+} indicator loading phase. The three HEK293 cell lines expressing hOPN5 (WT), hOPN5 (T164A), and cOPN5 (WT) were chosen for the retinal retention studies due to their very high light sensitivity and effectiveness in triggering Ca2+ transients upon UV light illumination. First, I performed Ca^{2+} imaging experiments without ATR supplementation during Ca^{2+} dye loading. This did not alter the eLi50 values as well as the maximal Ca^{2+}

transient amplitude values. Further, I used Panserin 401, a serum and ATR-free culture medium (pan-Biotech, Germany) to starve the cells of retinol (Vitamin A). It was previously claimed by Brueggemann & Sullivan, 2002 that HEK293 cells possess a functional retinoid processing machinery and convert the retinol (Vitamin A) from the fetal bovine serum used for the culturing of the HEK293 cells. The three different cell lines were starved for up to 8 days with Panserin 401 medium exchange every 2 days. The hOPN5 (WT) cell line displayed an apparent drop in the light sensitivity starting from the second day of starvation from ~4 $\mu W/mm^2$ (n = 20) to ~35 $\mu W/mm^2$ (n = 10), which dropped further to ~100 $\mu W/mm^2$ (n = 6) on the eighth day of starvation (Figure 33.a left). The maximal Ca^{2+} increase level also dropped from ~1.5 $\Delta F/F_0$ (n = 20) to ~0.8 $\Delta F/F_0$ (n = 10) after the second day and further declined to ~0.5 $\Delta F/F_0$ (n = 6) on the eighth day (Figure 33.a right). In the case of the hOPN5 (T164A) mutant cell line, there was a significant change in the light sensitivity only after the fourth day of starvation from ~3.2 $\mu W/mm^2$ (n = 14) to ~14 $\mu W/mm^2$ (n = 8) and to ~107 $\mu W/mm^2$ (n = 7) on the eighth day (Figure 33.b left). The maximal Ca^{2+} increase level dropped significantly from the first day of starvation from ~1.6 $\Delta F/F_0$ (n = 12) to ~1.3 $\Delta F/F_0$ and further declined to 0.7 $\Delta F/F_0$ (n = 7) on the eighth day of starvation (Figure 33.b right). In the cOPN5 (WT) cell line, the light sensitivity dropped on the second day of starvation from ~2 $\mu W/mm^2$ (n = 16) to ~13 $\mu W/mm^2$ (n = 12) and continued to decline to ~90 $\mu W/mm^2$ (n = 6), but the maximal Ca^{2+} increase stayed similar with a significant decline observed only on the eighth day of starvation. The maximal Ca^{2+} increase was ~1.1 $\Delta F/F_0$ observed until the second day of starvation and was ~0.9 $\Delta F/F_0$ till the sixth day and decreased to ~0.6 $\Delta F/F_0$ on the eighth day of starvation (Figure 33). The eLi50 and the maximal Ca^{2+} increase of all three different OPN5 variants were compared with each other (Figure 33). cOPN5 (WT) was effective enough to produce a maximal Ca^{2+} increase even after six days of starvation, and the light sensitivity was also the best among the three OPN5s even during the specific days of starvation. In comparison, the next best was hOPN5 (T164A), which had higher light sensitivity and was more effective in producing Ca^{2+} transients compared to hOPN5 (WT) under similar starvation durations. This already provides the vital information that the T164A amino acid substitution improves retinal retention.

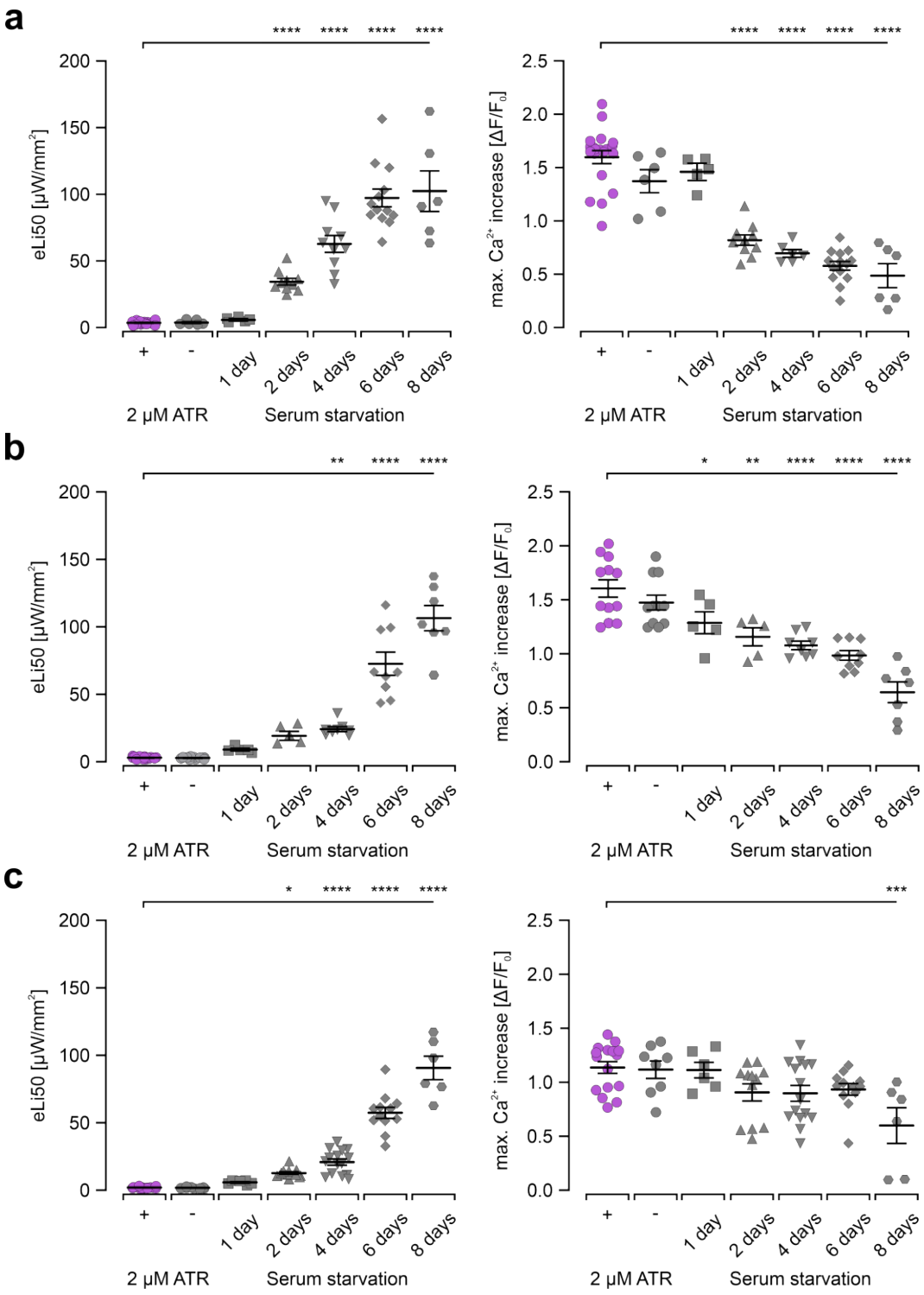

Figure 33: Analysis of retinal retention after serum starvation.

Aggregated data of the determined eLi50 values (left) for **a.** hOPN5 (WT), **b.** hOPN5 (T164A) and **c.** cOPN5 (WT) cell lines after different starvation durations calculated using dose-response curve hill fit. Aggregated maximal Ca^{2+} increase (right) for the corresponding experiments to the left. Statistical analysis was performed with one-way ANOVA and Šídák's multiple comparisons post-test for the eLi50 values compared to the HEK293 cells supplemented with 2 µM ATR expressing the same OPN5 variant. One symbol represents the average of one coverslip with ≥ 200 cells. eLi50 and maximal Ca^{2+} increase values are represented as mean ± SEM. All non-significant p values are > 0.11.

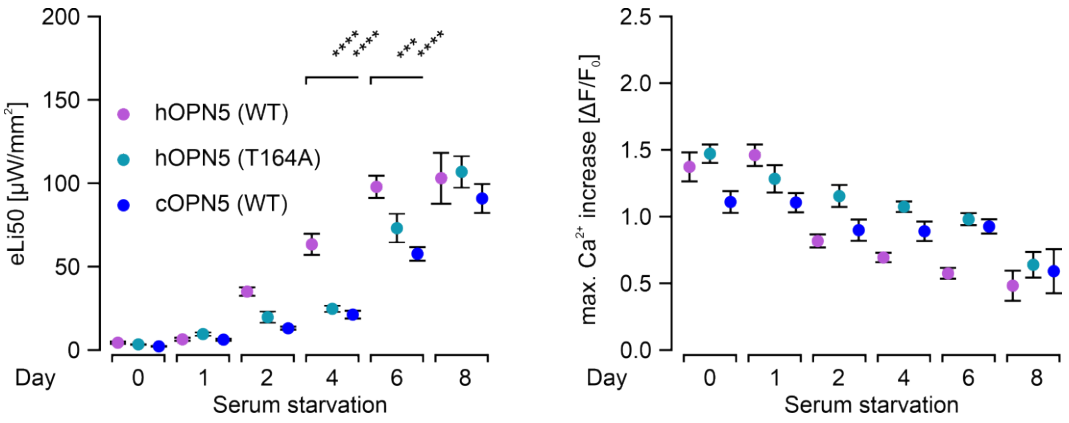

Figure 34: Comparison of eLi50 and maximal Ca^{2+} increase of three different OPN5 variants in stable HEK293 cell lines after serum starvation.
Mean ± SEM values for the determined eLi50 values (left) and maximal Ca^{2+} increase (right) of hOPN5 (WT), hOPN5 (T164A), and cOPN5 (WT) cell lines (in purple, cyan, and blue) after different starvation durations. Statistical analysis was performed with two-way ANOVA and Tukey's multiple comparisons test comparing hOPN5 (WT) values to the others for every starvation condition. All non-significant p values are > 0.1.

3.3.5 Establishment of G-CASE assay to exclude the promiscuity of the different OPN5 variants to other G_α proteins

The BRET-based G protein tri-cistronic activity sensors (G-CASE) assay is based on the GPCR-mediated G_α and $G_{\beta\gamma}$ dissociation. Each G-CASE plasmid contains one distinct G_α subunit with a fusion of the donor NanoLuciferase (Nluc), a distinct G_β without any modification, and a distinct G_γ with an N-terminal fusion of the acceptor circularly permuted Venus fluorescent protein (Schihada et al., 2021). Activation of the GPCR will lead to the dissociation of the G protein heterotrimer from the GPCR as well as the G_α and $G_{\beta\gamma}$ subunits from each other. Therefore, without the activation of the GPCR, there is a pronounced BRET signal as the $G_{\alpha\beta\gamma}$ heterotrimer is intact, while the BRET signal will decline upon activation of the GPCR.

HEK293 cell line expressing the G_q-CASE and hOPN5 (WT) was generated, and experiments with ATP stimulated the endogenous G_q coupled P2Y receptors, which displayed an apparent decrease in the BRET values as expected. The decrease was more profound as the ATP concentration increased from 0.3 to 30 mM (Figure 35. a). Also, another HEK293 cell line expressing the G_{i1}-CASE and M2 receptor was generated. CCh was used to stimulate the G_i-coupled M2 receptor, yielding a concentration-dependent BRET signal decrease (Figure 35. b). These experiments were done as a 'proof of concept' and I will use them to establish a protocol with light stimulation of OPN5 variants to prove the coupling of G_q proteins. Further, to explore the binding of OPN5 variants to other G_α proteins as well. Currently, the light stimulation protocol and the experimental setup are under preparation for use with the

cell lines of different OPN5 variants along with different G-CASEs specific for each G protein heterotrimer group.

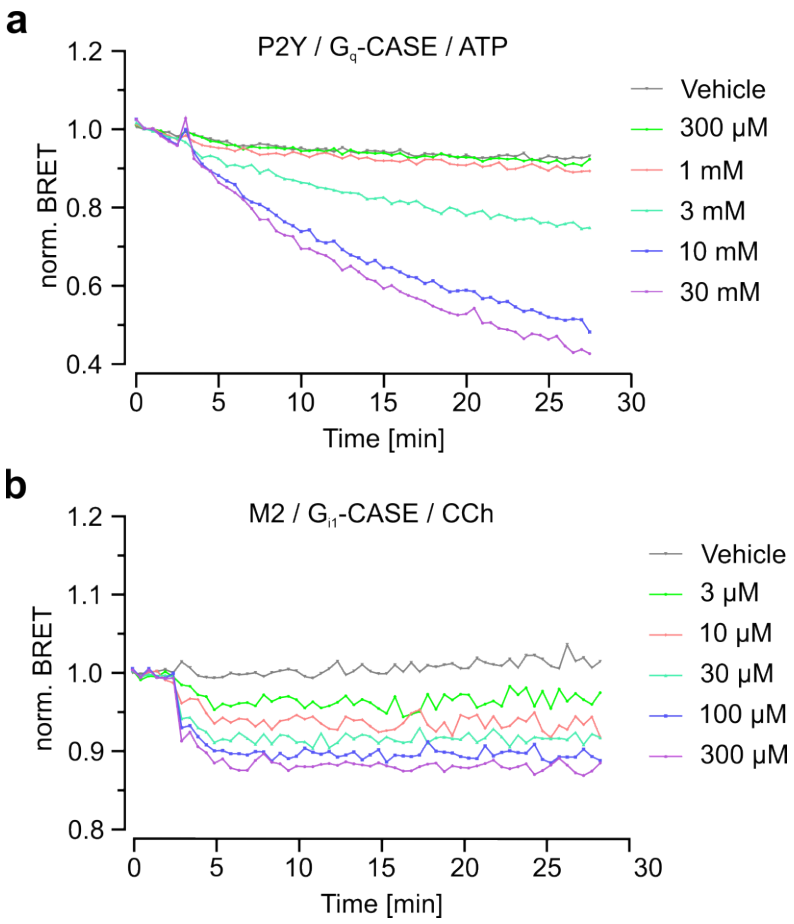

Figure 35: G-CASE assay to exclude promiscuous coupling to other G_α proteins.
a. Time courses of the normalized BRET values of G_q-CASE after adding increasing concentrations of ATP (in mM: 0.3, 1, 3, 10, 30) to stimulate endogenously expressed P2Y receptors. **b.** Normalized BRET values of G_{i1}-CASE after the addition of increasing CCh concentrations (in µM: 3, 10, 30, 100, and 300) for stimulation of over-expressed (M2) receptors. Each data point represents the mean ± SEM of ≥ 3 independent experiments.

4 Discussion

The role of G_q signaling is pivotal in many cellular processes but is also involved in the pathogenesis of many diseases, including cancer, autoimmunity, cardiac hypertrophy, and heart failure. The current knowledge regarding G_q signaling provides fundamental information on their functioning and regulation. However, the dynamics and encoding of extracellular signal reception into intracellular processing are not understood yet, including the differences between pulsatile or tonic activation and the subsequent transfer of the signals between different effector proteins. Also, the timescale at which a physiological process becomes pathophysiological remains elusive. Conventional strategies like overexpression or knockout models with chemical stimulation provided vital information, but they had their limitations with undesired side effects using global agonists, which led to non-specific activation of similar GPCRs elsewhere. To address this issue, G_q protein-specific DREADDs were engineered, which were receptive only to their synthetic agonists, and with genetic manipulation cell-specific expression with suitable promoters was also achieved. However, there remained the problem of administering DREADD agonists *in vivo*, which included less availability to induce a response due to diffusion and limited temporal precision. A technique that bypasses chemical agonist-mediated activation of GPCRs along with high spatiotemporal resolution was desired. Optogenetics uses light-sensitive proteins that modulate biochemical events in a targeted manner with high spatiotemporal precision. The light-sensitive proteins can further be expressed in a cell-specific manner using suitable promoters and have been used profoundly in Neuroscience (Rost et al., 2022; Yizhar et al., 2011). The existence of light-sensitive GPCRs has come into focus, and the possibility for them to address the shortcomings of other methods is currently being explored. Light-sensitive GPCRs allow researchers to mimic certain physiological signaling, such as the pulsatile or tonic release of neurotransmitters or hormones, with high temporal and spatial precision. In recent years, light-sensitive GPCRs that couple specifically with high efficiency to a particular signaling cascade were discovered. JellyOp protein specifically activates the G_s signaling cascade (Koyanagi et al., 2008; Makowka et al., 2019), UVLamP protein specifically couples to the G_i signaling cascade (Eickelbeck et al., 2019; Koyanagi et al., 2004) and OPN4 protein activates the G_q signaling cascade. However, recent reports on the OPN4 lead to ambiguity, as it has been shown to activate both G_i and G_q proteins in specific cell

types (Bailes and Lucas, 2013). Therefore, the need to find a light-sensitive GPCR to specifically couple to the G_q signaling cascade and to prove its selectivity to G_q signaling formed the main objective of this research work.

4.1 hOPN5 (WT) for selective optogenetic control of G_q signaling

In the first part of the thesis, the use of hOPN5 as a highly efficient tool to control the G_q signaling cascade in the heterologous expression system HEK293 was demonstrated. The characterization of the hOPN5 (WT) was performed with a sequential and detailed analysis of the G_q signaling cascade with respect to each second messenger produced upon activation (Figure 36).

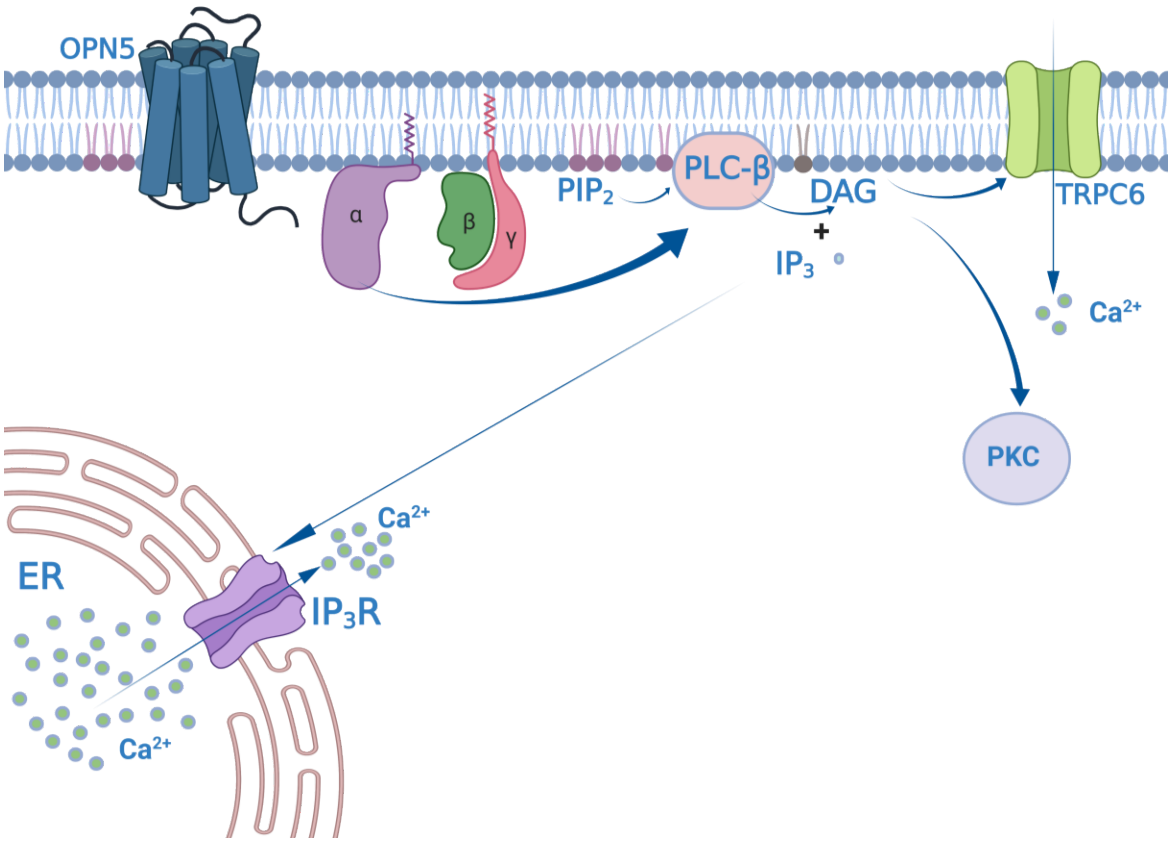

Figure 36: Schematic representation of the G_q signaling cascade.
Stimulation of the G_q protein coupled receptor induces the dissociation of the G-protein heterotrimer complex from the GPCR, and subsequently, the $G_{q\alpha}$ subunit activates PLC-β, which lyses PIP_2 to produce IP_3 and DAG. IP_3 binds to IP_3 receptors in the ER/SR to release Ca^{2+} ions into the cytosol. DAG

activates TRPC channels, increasing the cytosolic Ca^{2+} concentration and activating PKC, phosphorylating the downstream proteins. Generated using BioRender.com

4.1.1. hOPN5 mediated regulation of G_q specific second messengers

The second messengers are produced in response to a stimulus delivered by a first messenger (external stimuli). Subsequently, the second messenger transmits the information to the intracellular side, that generates the cell's response to the stimulus. The G_q signaling cascade does not have a single second messenger but three second messengers (IP_3, DAG, and Ca^{2+}) that are produced and have distinct roles in the G_q signaling cascade.

Firstly, I focused on the second messenger IP_3, and an increase in IP_3 levels corresponds to the activation of the G_q signaling cascade (Rhee, 2001). Hence, upon hOPN5 (WT) stimulation an increase in IP_3 levels was hypothesized to support the claim of hOPN5 (WT) coupling to $G_{q\alpha}$ proteins. The IP_1 assay (Figure 14) provides proof of an increase in the IP_1 levels observed only in hOPN5 (WT) cells upon UV light illumination, and this effect was abolished by the G_q specific blocker FR90035945 (Schrage et al., 2015). The hOPN5 (WT) dark activity was excluded based on the basal IP_1 levels in the control group and hOPN5 (WT) HEK293 cells. Also, the ectopic over-expression did not seem to cause any undesirable reaction with the G_q signaling supported by the CCh stimulation of endogenously expressed M3 receptor stimulation to increase IP_1 levels (Figure 14). The results of the IP_1 assay provided the first hint that hOPN5 can activate G_q proteins.

An increase in cytosolic Ca^{2+} is one of the prominent processes that occur upon G_q signaling cascade activation. Ca^{2+} increase occurs by activating the IP_3 receptors by IP_3 molecules, and these receptors are localized in the ER/SR, which release stored Ca^{2+} into the cytosol. The other way by which Ca^{2+} increase happens is by the activation of TRP channels like TRPC3/6/7 by DAG, the other second messenger produced during the lysis of PIP_2 by PLC-β in the G_q signaling cascade (Dietrich et al., 2003; Rhee, 2001). I performed Ca^{2+} imaging experiments with X-Rhod-1 to further support the claim of the G_q protein coupling of hOPN5 (WT). UV light stimulation of hOPN5 triggered Ca^{2+} release, which was compared to the pharmacological stimulation of endogenously expressed M3 receptor with CCh or P2Y receptor with ATP, both of which are strictly G_q specific in HEK293 cells (Figure 15). The hOPN5-mediated Ca^{2+} release efficiency was similar to the P2Y-mediated Ca^{2+} release.

Furthermore, the light sensitivity was functionally determined with the Ca^{2+} imaging in HEK293 cells expressing the hOPN5 (WT). The light sensitivity was determined with the parameter eLi50, similar to the EC50 used in the pharmacological context. The eLi50 of hOPN5 (WT) in the HEK293 cell lines was ~3.4 μW/mm^2 (Figure 16. a, and b). The light sensitivity of hOPN5 (WT) is at least 350 times more sensitive than the most commonly used ChR2 (1.1 mW/mm^2) in optogenetic research (Lin, 2010). To eliminate the possibility of any functional strain caused by the fusion of the eYFP fluorescent tag to the hOPN5, Ca^{2+} imaging was performed in a HEK293 cell line expressing hOPN5 (WT) and the fluorescent protein GFP as separate moieties. This was achieved using the IRES sequence (De Felipe et al., 2006) between the hOPN5 (WT) and the GFP gene sequences in the plasmid used for the protein expression. The eLi50 of hOPN5 (WT) in this cell line was ~3.2 μW/mm^2 (Figure 16. a, b, and c), which was very similar to that of the HEK293 cells in which hOPN5 was expressed as a fusion protein. The maximum Ca^{2+} transient amplitudes were also very similar, but they had a small significant increase in the case of the hOPN5 (WT) IRES cell line. This effect could possibly be due to better expression rate and strength in the hOPN5 (WT) IRES cell line compared to the hOPN5 (WT) fusion protein cell line. hOPN5 negative cells or cells with low expression of hOPN5 could lead to the reduced average of the maximal Ca^{2+} transients in the cells expressing the hOPN5 fusion protein, leading to this difference. In this case, to quantify the expression strength, a hOPN5 antibody staining protocol for the hOPN5 IRES cell line is necessary. However, there is no specific hOPN5 antibody commercially available. Also, efforts to produce custom-made hOPN5 antibodies did not yield a positive outcome. On the whole, the light sensitivity and maximum Ca^{2+} transients' comparison between two hOPN5 cell lines with either fusion protein or individually expressed hOPN5 protein excludes the possibility of any functional strain created by the fusion of the fluorescent tag to hOPN5 (WT).

The bistable nature was first explored by Kojima and colleagues with spectroscopic analysis of purified protein from HEK293 cells performed at a non-physiological temperature of 0 °C and it revealed absorption maxima at 380 and 470 nm (Kojima et al., 2011). The wavelength maxima for hOPN5 (WT) obtained from Ca^{2+} imaging experiments performed in the lab of Philipp Sasse were ~406 nm for activation and ~510 nm for deactivation respectively, (Figure 17). The light intensities (≥1.2 mW/mm^2) used in the specific wavelength determination experiments were very high as compared to the light sensitivity (eLI50 of ~3.4 μW/mm^2) of the hOPN5 (WT). The use of high light intensities (~400 times more than eLi50) would lead to a broader activation spectrum since longer wavelengths of light can still activate hOPN5. Therefore, the light intensity of different wavelengths has to be as low as possible to still evoke sufficient Ca^{2+} transients.

DAG is the other second messenger produced after the lysis of the PIP_2 by PLC-β (Dietrich et al., 2005b; Hofmann et al., 1999; Rhee, 2001). DAG is a lipid moiety that stays in the cell membrane and activates its specific downstream effectors, which have a DAG sensing domain in the vicinity. DAG is known to activate the non-selective cation channels TRPC3/6/7 and presents as a good target to analyze the G_q protein activation (Hofmann et al., 1999). I chose to use the TRPC6 channel because of its low constitutive activity, which clearly distinguishes between the G_q protein-activated and inactive states of the TRPC6 channel (Dietrich et al., 2005a). I recorded the activity of the TRPC6 channels using the patch clamp technique in HEK293 cells expressing both TRPC6 and hOPN5 (WT) to prove its coupling to the $G_{q\alpha}$ protein. UV stimulation of the cells led to a characteristic TRPC6 specific trace, the 'S' shaped trace with flattening close to reversal potential from 0 to +20 mV was obtained. Along with the dual rectification of the channels with a greater influx of positive ions at more negative membrane potentials (≥-20 mV), whereas at more positive membrane potentials (≥40 mV), there is an amplified outward efflux of positive ions produced the characteristic 'S' shaped TRPC6 trace (Dietrich et al., 2003; Dryer and Kim, 2018; Tu et al., 2009). The relative increase of the inward and outward currents was 5 and 8 times compared to the basal levels at -60 mV and +60 mV. The activation of the TRPC6 channel by UV light-mediated increase of DAG via the G_q signaling pathway also supports the claim that there is UV light-mediated hOPN5 (WT) coupling to the G_q signaling cascade leading to TRPC6 channel opening (Figure 19). In the future, TRPC6 assay should be performed in the presence of a G_q blocker to assess if the UV stimulation effect is abolished. This effect would further justify that the DAG produced via hOPN5-mediated G_q activation of PLC-β is the cause for TRPC6 channel activation. The use of G_q specific blocker FR900359 is quite critical as it is not commercially available, and it was a kind gift from Evi Kostenis (University of Bonn). Recently, a commercially available G_q specific blocker YM-254890, was used for experiments with cOPN5 (Dai et al., 2022), and I will use YM-254890 in my future experiments to evaluate the G_q blocking effect in the TRPC6 experiments as well as adapt to Ca^{2+} imaging experiments.

All of the above described experiments gave valuable information on the hOPN5 coupling to G_q proteins in HEK293 cells. To explore hOPN5 coupling to G_q proteins in other cellular systems, members of the Philip Sasse group generated transgenic hOPN5 mouse embryonic stem cells to explore hOPN5's G_q protein coupling abilities in other cellular systems as well. Embryoid bodies generated from transgenic hOPN5 mouse embryonic stem cells displayed UV light (385 nm, 300 μW/mm^2, 5 s) stimulation-dependent increase in spontaneous beating, and it was compared to the endothelin-1 (ET-1, 100 nM) stimulation of G_q coupled ET-1 receptors. An apparent increase in spontaneous beating rate was observed in both cases. An instantaneous increase in beating rate

was observed with UV light stimulation compared to the perfusion-dependent ET-1 stimulation effect. It was apparent that light stimulation provided a high temporal control in comparison to the stimulation by ET-1 perfusion. With the use of the G_q specific blocker FR9000359, the light-mediated effect was fully abolished. Thus, this experiment supports hOPN5 mediated activation of G_q proteins to increase the chronotropic effect upon UV light illumination in embryoid bodies from mouse stem cell-derived cardiomyocytes. A transgenic hOPN5 mouse model was developed in our lab, which expresses hOPN5 (WT)/eYFP using the same expression cassette used in HEK293 cells. Contractility experiments performed using in-house coded online myocyte contraction analyzer software with adult ventricular cardiomyocytes demonstrated a UV light-mediated increase in contractility. This effect was abolished with the use of G_q specific blocker FR900539, and no light-mediated effect was observed in WT adult ventricular cardiomyocytes. This again shows the coupling of G_q proteins to hOPN5, which leads to an increase in the contractility of adult ventricular cardiomyocytes (Wagdi et al., 2022).

With the above discussed results, there is a clear evidence of hOPN5 (WT) coupling to the G_q signaling cascade, along with the evidence of the bistable nature of hOPN5, explored with functional experiments like Ca^{2+} imaging. However, the activation of the G_q signaling cascade alone does not exclude the possibility of hOPN5 (WT) coupling to other G_i proteins. Therefore, I looked into assays that can address the coupling selectivity of a GPCR more concretely.

4.1.2. Excluding the hOPN5 (WT) coupling to G_i proteins

Previous reports from Kojima et al., 2011; Sugiyama, Suzuki, & Takahashi, 2014; Yamashita et al., 2010, 2014 suggested the coupling of hOPN5 (WT) to G_i protein. To address the former observations, firstly with the help of Berivan Mansurogulu (University of Bonn), the cAMP GloSensor assay (Promega) was performed with HEK293 cells expressing hOPN5 (WT) very similar to the experiments performed by Kojima et al., 2011. Also, a HEK293 cell line expressing strictly G_i specific M2 receptors was generated as a G_i control. No apparent light-mediated decay of cAMP levels in hOPN5 (WT) HEK293 cells was observed despite using supramaximal intensities of UV light (500 ms, 110 µW/mm^2). However, a sharp reduction in cAMP levels was observed in M2-expressing HEK293 cells after stimulation with CCh (100 µM, Figure 20). The observations obtained by the previous report can be explained by differences in OPN5 expression techniques or long exposure (1 min) of UV light (2.2 mW/mm^2) that possibly led to G_q-dependent Ca^{2+} mediated inhibition of Adenylyl cyclases 5 and 6 (Sunahara and Taussig, 2002),

the main isoforms in HEK293 cells (Atwood et al., 2011) or by activation of certain Ca^{2+} sensitive phosphodiesterases which reduces cAMP levels (Brzezinska et al., 2021). Also, Sugiyama et al., 2014 reported an increase in Ca^{2+} levels and a decrease in cAMP levels after UV light illumination, further supporting the hypothesis of Ca^{2+} release-induced cAMP decrease.

None of the previous reports performed Ca^{2+} imaging in HEK293 cells with genetic ablation of either G_i (Hisano et al., 2019) or $G_{q/11}$ proteins (Schrage et al., 2015) expressing hOPN5 (WT). This experiment is important to explore if the Ca^{2+} increase displayed by the hOPN5 (WT) HEK293 cells occurs primarily due to hOPN5 (WT) coupling to Gq proteins. UV stimulation produced a significant Ca^{2+} transient in the G_i KO cells, which was even more pronounced than in HEK293 cells with intact endogenous G proteins, but the UV light-induced Ca^{2+} transient was completely abolished in the case of $G_{q/11}$ KO cells (Figure 21. a. and b.). The use of CPA which blocks SERCA in these experiments, also proved that there were no problems associated with Ca^{2+} homeostasis in all the hOPN5-expressing cell lines with or without the genetic ablation of specific G_α proteins. UV light-mediated Ca^{2+} increase was completely abolished in $G_{q/11}$ KO cells, while Ca^{2+} increase was observed in the other two cell lines, which occurs only because of the coupling of hOPN5 (WT) to G_q proteins after light stimulation. Hence, this experiment clearly portrays the requirement of functional G_q proteins by hOPN5 to produce Ca^{2+} transients.

The next experiment was done with the GIRK channel assay. which is an ideal technique to determine the promiscuity of a certain GPCR (Breitwieser, 2005; Lüscher and Slesinger, 2010). This assay can clearly distinguish the GPCR coupling to either G_i or G_q proteins or both. The activation of G_i proteins will increase GIRK currents by the $G_{\beta\gamma}$ subunits binding to the GIRK channels, whereas G_q signaling will inhibit the channels by PIP_2 depletion needed for channel stability as well as by the phosphorylation of the GIRK 1/2 subunits by the PKC, both these processes are triggered by the activation of G_q signaling cascade (Breitwieser, 2005). Hence, this patch clamp-based assay was used to assess the specific and selective activation of G_q proteins by hOPN5 (WT). Daniela Malan (University of Bonn) performed the experiments with HEK293 cells expressing GIRK 1/2 channels and hOPN5 (WT) in addition to the control group HEK293 cells expressing only the GIRK 1/2 channels. The electrophysiology recordings showed a clear UV light-mediated reduction in the GIRK currents, and there was no observable reduction in the control group of HEK293 cells expressing GIRK channels. Also, no significant difference in the GIRK current reduction was seen when PTX, a G_i specific blocker was used, but the reduction in GIRK current was abolished with the use of G_q specific blocker, proving that the GIRK reduction was mediated only by the activation of G_q proteins (Figure 22. a. and b.). If there were any promiscuous coupling to G_i proteins there would

have been a direct increase in GIRK currents upon the use of G_q blocker. Thereby, the GIRK assay excludes any Gi protein coupling by hOPN5 (WT) in HEK293 cells.

In order to explore the G protein selectivity of hOPN5 (WT) in other cellular systems, the transgenic hOPN5 (WT) mouse model developed in our lab was used. *Ex vivo* experiments with UV light stimulation of Langendorf-perfused adult mouse hearts expressing hOPN5 (WT) were performed and subsequently compared to the UV light stimulation in control mice hearts without hOPN5 expression. An adult mouse heart is an ideal cellular system to exclude the promiscuity of hOPN5 because the adult heart is prone to G_i signaling. In the adult heart, G_i signaling is mediated by parasympathetic pathways, which are responsible for heart rate deceleration at rest (Mika and Fischmeister, 2021). If hOPN5 (WT) couples to G_i protein as described by previous reports, it will decrease the beating rate. In stark contrast, a UV light-dependent increase in the beating rate of the heart was observed when the sinoatrial node region was illuminated with UV light. My colleagues also performed this experiment in OPN4-expressing mouse model, where light stimulation of the OPN4-expressing heart led to a significant decrease in the beating rate rather than accelerating it. Light stimulation on both OPN4 and OPN5 expressing adult mouse hearts concretely proves that OPN5 shows selective activation of the G_q signaling cascade in adult mouse hearts while OPN4 couples to Gi proteins in this model (Figure 37).

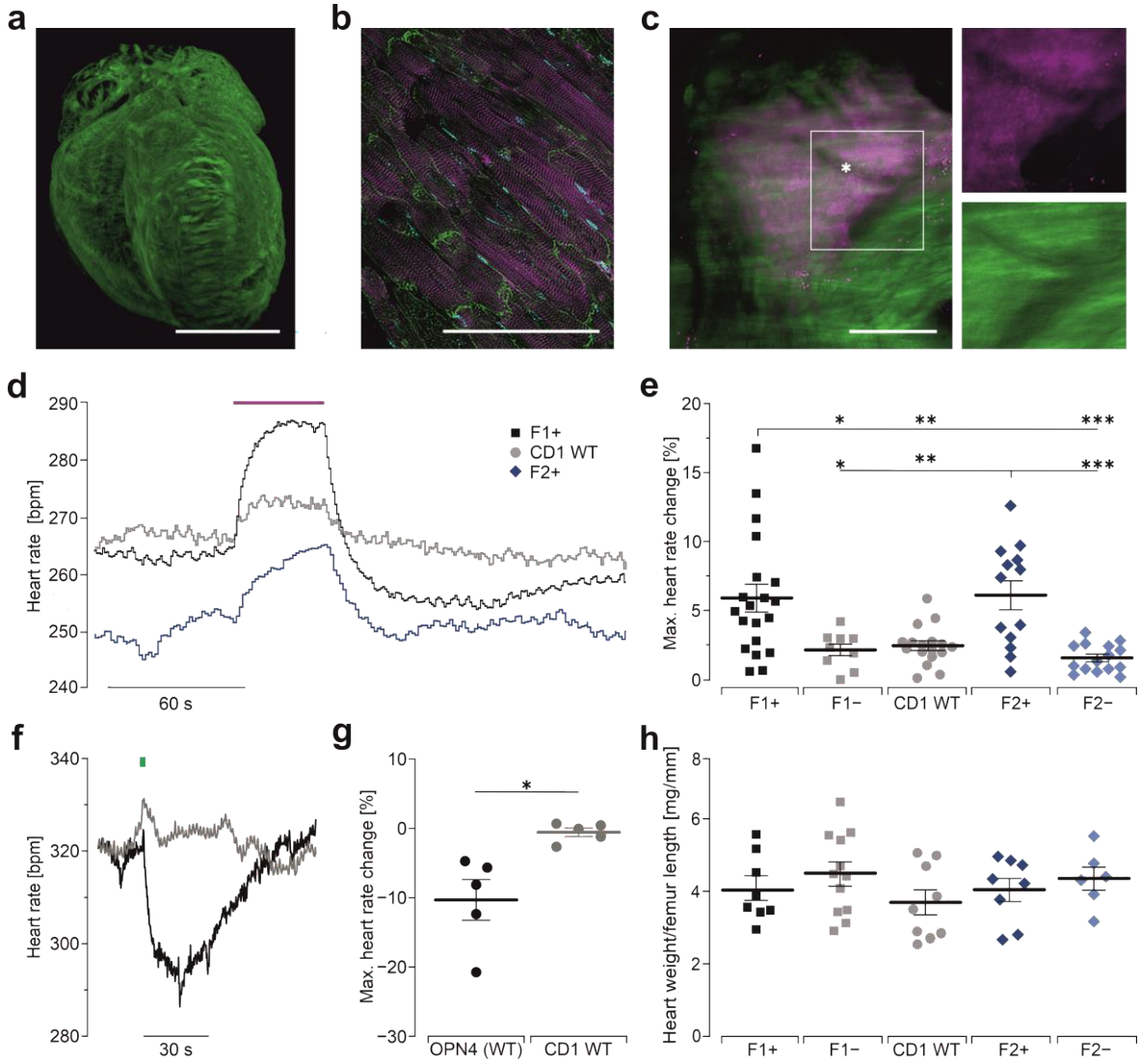

Figure 37: Modulation of heart rate in hOPN5 (WT)/eYFP and OPN4 (WT)/eGFP transgenic hearts.

a. hOPN5 (WT) /eYFP (green) expression in the whole heart. **b.** A ventricular section of cardiomyocytes with expressed hOPN5 (WT)/eYFP (green), α-actinin staining (purple), and DAPI stained nuclei (cyan). **c.** Sinus node identified by HCN4 staining (purple) along with the expressed hOPN5 (WT)/eYFP (green). **c*.** Sinus nodal artery as a classical landmark. Bars = 3mm (**a.**), 100 µm (**b.**), 300 µm (**c.**). **d.** Representative heart rate traces from hOPN5 (WT) hearts from founder lines #1 and #2 (F1+, F2+), and control mice (CD1 WT) after UV illumination of the dorsal right atrium (385 nm, 1 mW/mm^2,10 s). **e.** Statistical analysis of the light-induced increase in maximum heart rate of hOPN5 (WT) hearts (F1+, F2+) and WT hearts (CD1 WT) as well as hOPN5 (WT) negative littermates (F1−, F2−). Each symbol is the average from one heart. Statistical analysis was performed with a one-way non-parametric ANOVA test with Tukey's multiple comparison post-test (All p values ≥ 0.91). **f.** Representative time course of beating rate in an OPN4 (WT) (black) and a CD1 WT heart (gray) after blue light illumination (460 nm, 1 s, 1.4 mW/mm^2). **g.** Statistical analysis of maximal change in heart rate using two-sided unpaired Student's t test. **h.** Analysis of the heart weight to femur length in 2-months-old hOPN5 (WT) mice with

an ordinary one-way ANOVA test with Tukey's multiple comparison post-test (All p values more than ≥ 0.37). Each dot represents the result from one heart. All values are presented as mean ± SEM. *p < 0.05, **p < 0.01, ***p < 0.001. Adapted from Wagdi *et al.*, 2022.

The functional experiments performed in this project are superior to the assays used previously for proving the G protein coupling, especially with simplified radioactive ligand binding assays in a rather non-physiological context (Tarttelin et al., 2003; Yamashita et al., 2014, 2010) with high abundance of individual G proteins and neglecting essential differences in the affinity for other G proteins. Furthermore, these *in vitro* reconstitution assays using purified proteins lack the endogenous cellular environment with no phosphorylation or glycosylation and the microdomain influence on ions and other native protein interactors.

To summarize, the assays performed for this thesis work prove the specificity of hOPN5 (WT) towards G_q proteins, and there was no indication of G_i protein activation in HEK293 cells, which was concretely proven using specific blockers for G_i and G_q proteins as well as performing Ca^{2+} imaging using G_i or $G_{q/11}$ protein knock-out HEK293 cells. It is worthwhile to explore the specificity of hOPN5 towards G_q proteins in other cell types owing to differential cell type specific post-translational modifications that might affect coupling selectivity, but also the mere expression difference of certain G proteins in a particular cell type or even microdomains.

4.1.3 hOPN5's optogenetic potential to control G_q signaling

UV light-mediated selective activation of G_q signaling cascade by hOPN5 (WT) can be favorable for experiments in different cells or organs as it allows parallel optical recording of intracellular Ca^{2+} dynamics and other second messengers with the use of red-shifted indicators to avoid cross-activation. In Ca^{2+} imaging experiments performed for this work, there were no observable hOPN5 activation effects with low-intensity imaging light (~200 µW/mm^2, 550 nm), but the impact of the imaging light cannot be completely excluded as it might affect the duration of the activated state and could accelerate the inactivation of hOPN5. One notable advantage of using hOPN5 is its light sensitivity, as it was observed that during the experiments with normal laboratory light conditions, it did not cause the activation of hOPN5. Thus, there will be no need for special dark rooms with dim red light to avoid the activation of hOPN5. The required light intensities and pulse durations for hOPN5 activation are below toxic light levels, and the UV light levels used for the experiments did not negatively affect the HEK293 cells. During the paired UV pulse protocols on HEK293 cells, there was an observable desensitization of G_q stimulation, which depended on the pulse duration used. However, the recovery time from desensitization was not directly

dependent on the pulse duration but rather depended on the Ca^{2+} depletion in cells after the light stimulation (Figure.18). This desensitization effect observed here can be attributed to the emptying of the Ca^{2+} stores from the ER rather than the desensitization of OPN5 itself. Desensitization experiments done on smooth muscle stripes from hOPN5 (WT) transgenic mouse by measuring isometric force in our lab (Figure 38) displayed a faster recovery of 50% at ~4 s after the first UV light stimulation pulse due to faster refill of the Ca^{2+} store in smooth muscle cells compared to HEK293 cells (Wagdi et al., 2022).

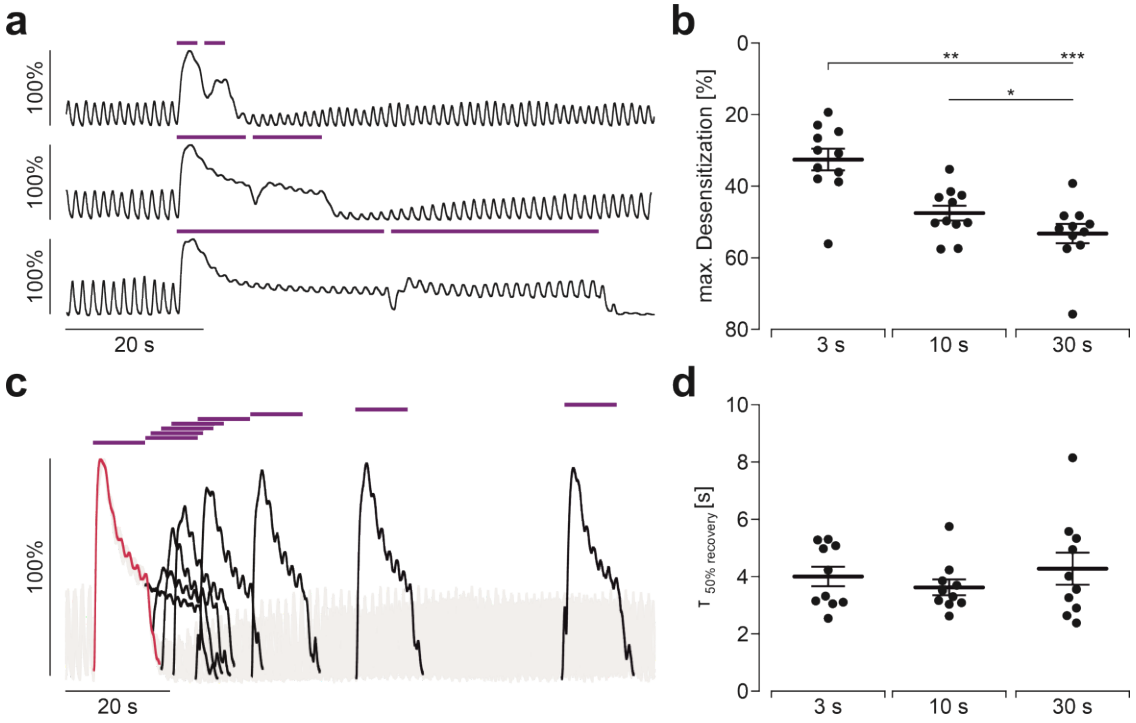

Figure 38: Desensitization and recovery from desensitization of UV light-induced isometric force in OPN5 expressing small intestinal strips.

a. Representative traces and **b.** aggregated data of isometric force measurements of small intestine strips showing the maximum desensitization to UV light-induced isometric force in dependence to the pulse duration (violet bars, 1 mW/mm^2, 3 s, 10 s, 30 s from top to bottom). Statistical analysis was performed with one-way ANOVA with Tukey's multiple comparison test (N=4). **c.** Overlay of representative traces of the isometric force generated after a paired-pulse protocol with 10 s long UV light pulses (violet bars, 1 mW/mm^2, with pulse increasing pulse intervals 0.1 s, 1 s, 3 s, 5 s, 10 s, 20 s, 40 s, 80 s). Force trace from the first pulse is shown in red, and the force trace from the second light pulse is shown in black. **d.** Aggregated data showing the half-maximal recovery time at different pulse durations. Statistical analysis was performed with ordinary one-way ANOVA (N= 4, n = 10, p = 0.56). All values are presented as mean ± SEM (Wagdi et al., 2022).

UV light-induced contractions in smooth muscles from the transgenic hOPN5 mouse intestine proved the potential to use of hOPN5 (WT) to control contractility in smooth muscle cells. It was also observed that hOPN5 (WT) expression was also present in the uterus and bladder of the transgenic OPN5 mice and displayed UV light-induced force generation. Therefore, light-mediated stimulation of the G_q signaling in smooth muscle cells to induce contractility using ectopic hOPN5 expression might pave the way to treat diseases like gastroparesis (Vogt et al., 2021). Also, owing to the similarity between OPN5 in mice and humans, the mouse model generated in our lab with hOPN5 did not reveal any visible side effects related with regards to heart physiology, as the electrocardiogram recordings were similar to the control mice. As known from the literature, chronic G_q activation leads to cardiac hypertrophy, the heart weight to femur length was compared in two months old mice. No significant differences were observed between the hOPN5 mice, sibling controls and WT mice controls from the same background. Therefore, there are no significant side effects on ectopic over-expression in the mouse model, thereby excluding the dark activity of the hOPN5 and alterations made to native G_q signaling. Thus, the analysis of the possible side effects already addressed one main criterion to consider for hOPN5s future translational use in humans. Using a human origin receptor, it is expected to have fewer chances of triggering an immune reaction during ectopic overexpression (Berry et al., 2019; Gundelach et al., 2020; Wagdi et al., 2022). As hOPN5 has been shown to be expressed in the brain, eye, skin, and other tissues in humans and mice (Nakane et al., 2010; Tarttelin et al., 2003).

Recently, our lab collaborated with Bayer AG to use OPN5 as a tool for investigating potential TRPC6 channel inhibitors with all optical high throughput screening (HTS). All optical HTS technique provides a unique advantage of discovering potential drugs for specific proteins involved in distinct intracellular signaling steps without causing undesired effects upstream of the protein of interest. For instance, if a tested drug compound affects the receptor used for triggering a signaling cascade under investigation, it leads to several non-specific positive hits, which needs a comprehensive evaluation of all the positive hits acquired during the process, increasing the overall time and overhead costs for the drug discovery process. Thus, a tool for the activation step not affected by the tested drug compounds would improve the reliability of the positive hits and improve drug screening efficiency significantly. This all-optical screening assay revealed that hOPN5 (WT) was not affected by 218,064 compounds which included compounds classified as frequent hitters and PAN assay interference compounds (PAINS). Taken together, the outcome of an all-optical HTS assay strengthens the idea of hOPN5's use as an ideal activator for Gq/ PLC-β dependent HTS assays (Wagdi et al., 2022).

Even though the bistability of hOPN5 was proved with different wavelengths using Ca^{2+} imaging, the intrinsic relaxation from the activated state to the deactivated state was very fast even without illumination with longer wavelengths of light (yellow) (Kojima et al., 2011). Therefore, to use hOPN5 as an optimal bi-stable optogenetic tool, amino acid mutations targeting the responsible regions to decelerate spontaneous inactivation are desired (Mattis et al., 2011; Wietek et al., 2017). One future perspective will be to engineer hOPN5 chimeras with other desired animal opsins (Airan et al., 2009; Kleinlogel, 2016) to shift the activation wavelength towards the red spectrum.

On the whole, there is strong evidence for the high specificity of hOPN5 towards G_q proteins, raising a persuasive outlook for its use as an effective optogenetic tool to control G_q signaling in cells, organs and also for drug screening. Several strategies and ideas have been put forward for enhancing specific characteristics of hOPN5 optimized for distinct optogenetic applications, which would finally lead to the creation of a hOPN5 optogenetic toolbox.

4.2. Development of enhanced OPN5 variants

Specific characteristics are desired for the effective usage of an optogenetic GPCR in research, including narrow peak wavelengths for activation and deactivation for bistable opsins, enhanced retinal retention, improved receptor kinetics, and red-shifted peak wavelengths for activation. Also, it is necessary to build a foundation to facilitate the improvement of the desired characteristics, like in the case of the development of ChR variants. In this project, I present the basic groundwork required to develop enhanced OPN5 variants for specific optogenetic applications.

To understand the important amino acid positions of OPN5 and their relevance in structure-retinal relationships for predicting mutations to improve OPN5 are briefly discussed here. OPN5 has a lysine residue at the amino acid position 296, which forms covalent Schiff base linkage with retinal (Tarttelin et al., 2003). Positively charged Schiff base is balanced by a negatively charged amino acid (glutamate) which acts as counterion in the third transmembrane domain similar in most vertebrate visual opsins (Terakita et al., 2004), but a tyrosine residue is present in hOPN5 at the counterion position 109 (Tarttelin et al., 2003), and this substitution is likely the source of the OPN5 bistability. In turn, glutamate at position 177 in extracellular loop 2 might serve as the Schiff base counterion in OPN5s (Terakita et al., 2004). Also, it was suggested that the presence of alanine and serine at position 192 -193 in the extracellular loop might assist

the rapid turnover of the inactivated state based on the similar amino acids found in visual rod opsins (Tarttelin et al., 2003).

Till Rudack (University of Bochum) designed the *in silico* elucidation for the OPN5 structure and its retinal interaction using molecular dynamics simulations (Figure 39). The models based on the amino acid information of OPN5s, along with the protein crystal structure from bovine rhodopsin and squid rhodopsin helped to gain atomistic insights into the structural dynamics underlying protein function and its relationship with the retinal chromophore. Furthermore, these simulations serve as a foundation for quantum chemical calculations to predict the light absorption features and the structure-wavelength relationship of OPN5. A conserved sequence of 35 amino acids forming the retinal binding pocket was deduced from various OPN5s and sequence alignment analysis with other opsin similar to the work done in OPN4 (Hankins et al., 2008).

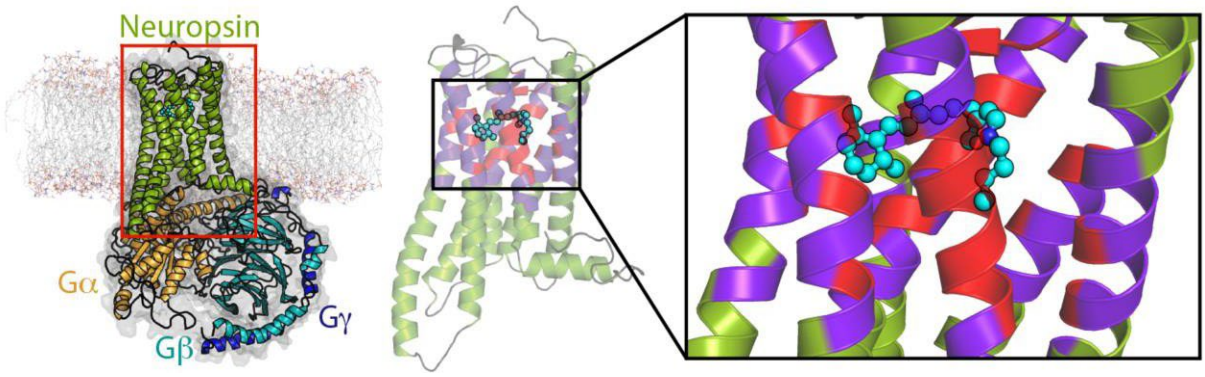

Figure 39: Simulation of hOPN5 bound to the heterotrimer G_q heterotrimer with the enlarged retinal binding pocket.
The amino acids in red and purple are in the 5 Å and 10 Å radius of retinal, respectively. Molecular dynamics simulations were performed by Till Rudack from the University of Bochum.

Color tuning of rhodopsin has been an important research topic in retinal proteins. The amino acid changes made in the retinal binding pocket environment would allow to tune the absorption spectra by altering the charge of the retinal electronic ground states and photoexcited states (Ernst et al., 2014; Katayama et al., 2012; Shichida and Imai, 1998; Thoen et al., 2014; Tsutsui and Shichida, 2010). Using the simulations, tyrosine at position 174 in the second extracellular loop was identified as a critical amino acid, and when exchanged with the non-polar amino acid phenylalanine, a left shift in activation was observed. In addition, phenylalanine at 217 when exchanged with polar amino acids leucine, isoleucine or valine would lead to a red shift in the deactivation wavelength. Amino acids phenylalanine at 114, isoleucine at 203, serine at 218,

tyrosine at 268 and 301 within a 10 Å radius of retinal was targeted for mutation based on simulations for a blue shift in the activation (Figure 40). These predictions were made based on the evidence from previous simulation studies that an increase in negative charge around the retinal Schiff base will lead to a stabilization of the electronic ground state of retinal, while an increase in positive charge around the ionone ring of retinal close to helices 5 and 6 would destabilize its photoexcited state (Thoen et al., 2014; Tsutsui and Shichida, 2010). T164A mutation in previous studies displayed direct binding to all-trans retinal, which was lost during evolution in mammals (Yamashita et al., 2014). In MD simulations, T164A mutation was predicted to cause a right shift towards the longer wavelengths. Also, cOPN5 (WT) which naturally contains the alanine substitution at position 164 was recently reported to have high light sensitivity when overexpressed in HEK293 (Dai et al., 2022).

Thus, a few amino acids involved in the color tuning of hOPN5 were predicted with insights from multiple sequence alignments and structure-based models along with molecular dynamics simulations. These predicted amino acid substitutions were used for the generation of mutant hOPN5s, which were expressed in HEK293 cell lines, and characterized for their light sensitivity and wavelength specificity using Ca^{2+} imaging. I also considered using the cOPN5 (WT) to explore the characteristics of cOPN5 (WT) with our experimental conditions as it was also reported to couple to G_q proteins (Dai et al., 2022; Tomonari et al., 2008). It was also intriguing to compare the light sensitivities of cOPN5 (~4.8 μW/mm^2) (Dai et al., 2022) and hOPN5 (~4 μW/mm^2), they displayed similar light sensitivities even though they belonged to different species.

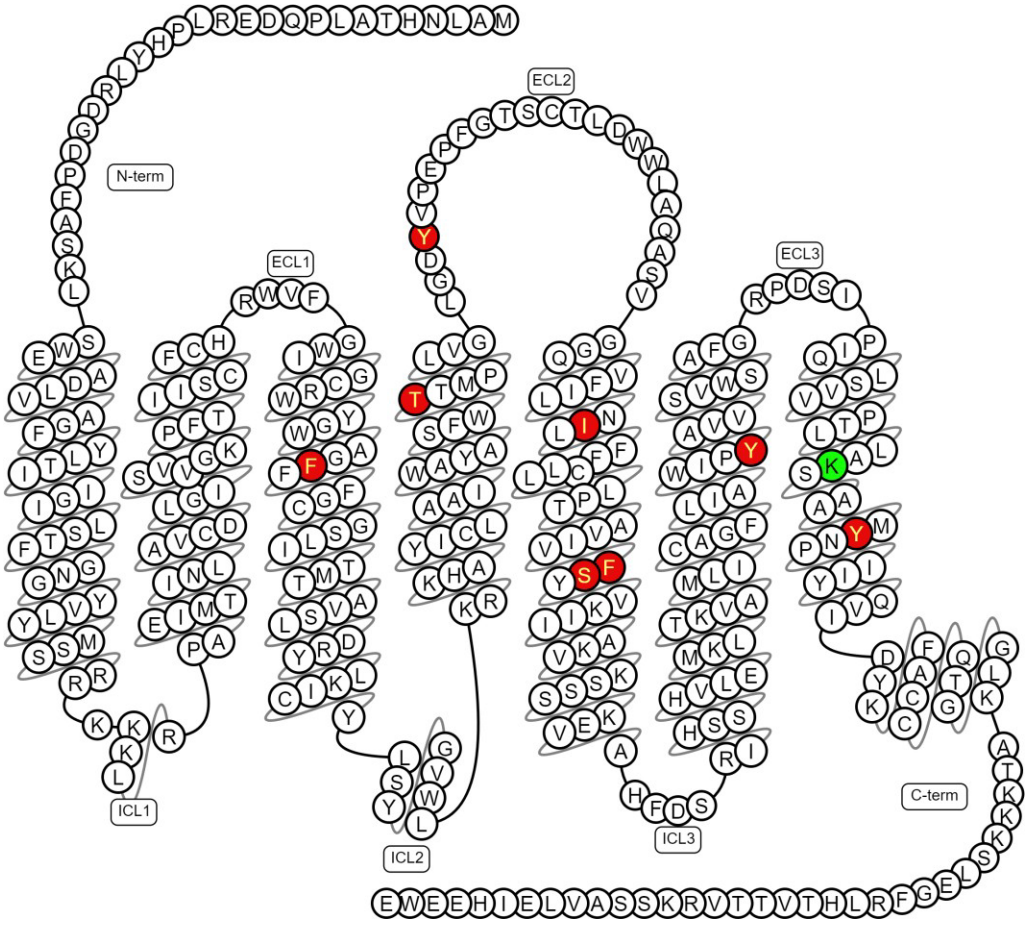

Figure 40: Schematic representation of the hOPN5 (WT) amino acid sequence with target positions for mutation.
The amino acid sequence of hOPN5 (WT) assembled in their predicted domain structures. Amino acid target positions for mutation are marked in red. Lysine (K, green) which forms a non-covalent Schiff base linkage with retinal. Generated using https://gpcrdb.org with amino acid sequence of hOPN5 (WT).

The HEK293 cell lines which expressed different OPN5 variants were first analyzed for their expression rate and expression strength, as it is important to assess the variability of the ectopic protein expression stably maintained with G418 antibiotic pressure. The expression rate (Figure 25 and 26) shows high variability among different OPN5 variants compared to the expression of hOPN5 (WT). The mutant OPN5s Y268F and Y301H had similar expression rates of ~60 % compared to hOPN5 (WT) and F114S displayed a slightly higher expression rate of 68%. The cOPN5 (WT) had an expression rate of 75% and was significantly higher than hOPN5 (WT). The hOPN5 mutants T164A, F217V, F217L, F217I, and S218C had strong expression rates which was highly significant with ≥ 80 %, out of which T164A had the

highest expression rate of 98%. These variabilities can be attributed to several factors including technical aspects like plasmid purity, transfection efficiency, and biochemical aspects of overexpressed proteins like three-dimensional stability and toxicity. The mutant I203D was not able to be generated even after three separate transfection trials to produce a viable cell line with ectopic expression of the desired protein.

Next, the expression strength was analyzed using ELISA for the different cell lines, which provided valuable information on the amount of the OPN5 protein expression per total proteins expressed in the cell lines (Figure 27). Expression strength and expression rate are important factors to be considered to assess impartially the results obtained from different OPN5 variants, as the expression of a certain OPN5 variant could affect the outcome of the individual cell line. The expression strength was normalized with the expression rate to determine the approximate OPN5 expression levels in the HEK293 cell lines. The normalized expression strength of mutant hOPN5 T164A was the highest with 280 pg per ng of total protein, followed by S218C (215 pg per ng of total protein) and F217L (150 pg per ng of total protein). The normalized expression strength of hOPN5 (WT) was 135 pg per ng of total protein, whereas cOPN5 (WT), hOPN5 mutants F217V and Y268F had similar levels (110 pg per ng of total protein). The hOPN5 mutants Y174F and F217I had similar levels (95 pg per ng of total protein). The lowest was found in both hOPN5 mutants F114S and Y301H (50 pg per ng of total protein). This normalization of expression strength to expression rate is important in a polyclonal HEK293 cell line as some cells do not express the protein of interest but survive antibiotic selection and variability in expression levels from cell to cell, which affects the average expression level per cell when taken as a whole. Therefore, normalizing the expression strength to the expression rate when comparing different mutant proteins is necessary.

The light sensitivity of OPN5 variants with Ca^{2+} imaging revealed that there were some OPN5 variants significantly improved than the others even though they had similar expression levels of the protein. It proved beneficial to categorize the different OPN5 variants on their light sensitivity after the UV light stimulation protocol with increasing light intensities (385 nm, 100 ms), as their light sensitivities varied from 2 to 160 $\mu W/mm^2$. The cOPN5 (WT) was quite an outlier with the highest light sensitivity of 2 $\mu W/mm^2$, but the maximum Ca^{2+} transient amplitude reached only 1.1 $\Delta F/F_0$ compared to 1.6 $\Delta F/F_0$ for hOPN5 (WT) with an eLi50 4 $\mu W/mm^2$ (Figure 28 a, d and Figure 29 a, b). Even though cOPN5 (WT) and hOPN5 (WT) expressing cell lines had quite similar normalized OPN5 expression strengths of 135 and 110 pg of fusion protein per ng of total protein, there was variability in light sensitivity and efficiency to induce Ca^{2+} transients. These effects hinted at the efficiency of the intracellular signal amplification process to induce Ca^{2+}

transients in these OPN5s as they are from different organisms. The light sensitivity for cOPN5 (WT) was reported as 4.8 µW/mm2 when stimulated with blue light (470 nm, 10 ms) (Dai et al., 2022), whereas with my experimental conditions, the light sensitivity was 2 µW/mm^2 with the use of UV (385 nm) and 100 ms pulse duration. Although the light sensitivity information cannot be directly compared owing to different experimental conditions used for generating the data. The information on the high light sensitivity of cOPN5 (WT) is consistent. I will explore 470 nm light illumination on cOPN5 (WT) with my Ca^{2+} imaging experimental conditions in the future.

The hOPN5 (T164A) mutant displayed higher light sensitivity (3 µW/mm^2) than hOPN5 (WT), which can be attributed to direct all-trans retinal binding which led to better receptor stability as the apoprotein of hOPN5 is unstable (Yamashita et al., 2014). It had a maximum Ca^{2+} increase of 1.6 $\Delta F/F_0$ same as that of hOPN5 (WT). The hOPN5 mutants Y174F, F217L, F217I, and S218C displayed similar light sensitivities (eLi50 in the range of 4 to 7 µW/mm 2), but the maximum Ca^{2+} increase was very similar to hOPN5 (WT). The light sensitivity and maximum Ca^{2+} increase of these mutants were not different from hOPN5 (WT). The hOPN5 mutant F217V had similar eLi50 to hOPN5 (WT) but displayed a lower average maximum Ca^{2+} increase of 1.3 $\Delta F/F_0$, which might be due to the possible destabilization of the photoexcited state leading to a change in efficiency to produce Ca^{2+} transients. The hOPN5 mutant Y268F displayed three times lower light sensitivity than the hOPN5 (WT) and an average maximum Ca^{2+} increase of 0.9 $\Delta F/F_0$, which was significantly less compared to hOPN5 (WT). Y268F mutant had a normalized expression strength of 110 pg of fusion protein per ng of total protein comparable to hOPN5 (WT), and still had a lower response than hOPN5 (WT) which indicates either a problem with retinal binding or G_q protein interaction that arose due to mutation related OPN5 conformation changes. The hOPN5 mutants F114S and Y301H were the mutants with very low light sensitivity (Figure 28. j, k) with eLi50s 80 and 160 µW/mm^2 and average maximum Ca^{2+} increase of 0.8 and 0.4 $\Delta F/F_0$ (Figure 29. a, b). They both displayed evident problems with OPN5 expression with 45 pg of fusion protein per ng of total protein. Thus, their lowered efficiency in producing Ca^{2+} transients in HEK293 cells could be attributed to protein folding challenges of the mutant OPN5s and issues with retinal binding. To assess the maximum Ca^{2+} increase of low light sensitive mutants, a pharmacologic stimulation protocol using ATP (2 mM) similar to the protocol used for the hOPN5 (WT) experiment described above should be performed to exclude that the G_q mediated Ca^{2+} increase is not affected in these cell lines. Further, new HEK293 transfections with these low light-sensitive mutants should be performed to re-confirm these findings.

The light sensitivity information was very important to perform the wavelength specificity experiments for all OPN5 variants. For the stimulation protocol, a fixed light intensity value for each wavelength was planned, and I decided to adapt the fixed light intensity value from the eLi80 values for each OPN5 variant (Figure 30). As discussed briefly in section 4.1.1., it is necessary to use wavelengths adapted to eLi80 for each OPN5 variant because a broad activation spectrum when using higher light intensities will lead to imprecise determination of the specific wavelength. Adapting the light intensity of each wavelength to the eLi80 values would produce a narrow activation spectrum, which will lead to a more precise determination of specific wavelength for activation. This method is technically more precise than the technique used for the generation of preliminary wavelength specificity data of hOPN5 (WT) performed in Bonn, as the new CAIRN monochromator (U.K.) has the advantage of having better control over the intensities of the required wavelengths.

With the above experiments, only two hOPN5 mutants Y174F (380.8 nm, Figure 31. d) and F217I (381.4 nm, Figure 31. e) displayed a significant left shift of ~7 nm from that of the hOPN5 (WT) which was 387.8 nm (Figure 32). The other hOPN5 mutants did not have any significant difference compared to the specific activation wavelength of hOPN5 (WT) (Figure 32). As predicted with the simulations, the replacement of tyrosine by phenylalanine affected the charge in the retinal binding pocket, which probably led to the left shift towards UV. A red shift in the deactivation wavelength for the mutant F217I was anticipated, but a left shift for the activation wavelength towards UV was observed. cOPN5 (WT) displayed an average activation wavelength of 407 nm (Figure 31. k), a 20 nm right shift from the UV, the report from Dai *et al.*, 2022 mentions 488 nm as the specific activation wavelength, which is an 80 nm right shift from the wavelength determined in my experiments. This discrepancy could be attributed to the experimental conditions as Dai *et al.*, 2022 did not use the same light intensities for each wavelength to compare the efficiencies to induce Ca2+ transients for each wavelength. There was still a broad activation spectrum for cOPN5 (WT) compared to the hOPN5 (WT), and the right shift in the specific wavelength is probably due to this broad spectrum. The next step will be to reduce the light intensity to check if there is a narrowing of the activation spectrum and to assess if the right shift is preserved.

Due to technical constraints with the stimulation protocol for deactivation wavelength determination, it is currently being implemented, and I plan to use a near infra-red fluorescent Ca^{2+} indicator Calbryte 630, AM which has excitation maxima at 609 nm which is at least 30 nm red-shifted than X-Rhod-1. Thus, Ca^{2+} imaging with Calbryte 630 will be more

preferable to explore the deactivation wavelengths as there is a very low chance of activating or deactivating OPN5 with the imaging light of Calbryte 630.

The retinal retention was explored in the HEK293 expressing OPN5 variants using Ca^{2+} imaging. The fetal bovine serum consists of vitamin A in the range of 2 mg/mL (Napoli, 1986), and the common HEK293 culture medium consists of 10% FCS. Therefore, each mL of DMEM supplemented with 10% FCS contains about 0.67 µM of Vitamin A. Also, HEK293 cells are known to possess the functional retinoid processing machinery with which they can produce 11-cis retinal needed for the ectopically expressed rhodopsins (Brueggemann and Sullivan, 2002). The Ca^{2+} imaging experiment performed with the three OPN5 variants with the highest light sensitivity cOPN5 (WT), hOPN5 (T164A), and hOPN5 (WT) also displayed that there was no observable difference with or without the use of all-trans retinal supplementation before the experiment (Figure 33. a, b and c). This indicates that for the experiments with HEK293 cells expressing OPN5, which were cultured with DMEM-supplemented FCS, the cells do not require retinal supplementation in order to have a light response. To explore the retinal retention in detail, the HEK293 cells expressing OPN5 variants were subjected to serum starvation using Panserin 401 serum-free medium, and Ca^{2+} imaging was performed after different starvation durations. The hOPN5 (WT) HEK293 cell lines displayed a significant drop in light sensitivity (Figure 33. a left) from the second day of starvation, and a drastic drop in light sensitivity was observed by day eight of starvation. This possibly could occur due to the loss of retinal levels with no replenishment from inside as well as outside of the cell. The effectiveness to induce Ca^{2+} transients also declined drastically from the second day of starvation (Figure 33. a right). In the case of hOPN5 (T164A), the light sensitivity dropped to a significant level only on the fourth day of starvation (Figure 33. b left) compared to hOPN5 (WT) at a similar starvation duration (Figure 34). However, hOPN5 (T164A) displayed significantly higher light sensitivity, and effectiveness to induce Ca^{2+} transients (Figure 34) compared to hOPN5 (WT). The improvement can be attributed to the mutation T164A, which allowed the direct binding of all-trans retinal in the retinal binding pocket. Also, reports on bistable rhodopsins' ability to thermally isomerize all-trans retinal to 11-cis retinal in the dark can further explain the improved protein stability seen in the T164A mutant of hOPN5 (Sakai et al., 2022). This direct all-trans retinal binding would have improved hOPN5s protein stability in the HEK293 cells. Thereby, hOPN5 (T164A) was more efficient than hOPN5 (WT) when compared at similar starvation durations. cOPN5 (WT) displayed better light sensitivities compared to both hOPN5 (WT) and hOPN5 (T164A) under similar starvation durations (Figure 34). Also, cOPN5 (WT) displayed a significant drop in effectiveness to induce Ca^{2+} transients only after day eight of starvation (Figure 33. c right), whereas the light sensitivity presented a slight drop after the second

day of starvation and significantly declined from the fourth day of starvation (Figure 33. c left). These effects can be attributed to the reason that cOPN5 (WT) already contains alanine at the equivalent amino acid position 164, and it seems to be better equipped for retinal retention. It was also reported to function in several cell types without exogenous retinal application (Dai et al., 2022). However, the amino acid alanine at position 164 was replaced with threonine in mammalian OPN5s during evolution (Yamashita et al., 2014). Further, alanine at 164 position, along with other amino acids which are responsible for providing the retinal stability in the retinal binding pocket of cOPN5 (WT) will be explored in MD simulations to enhance hOPN5 to better equip for future optogenetic applications.

4.3. Conclusion and Outlook

In the first part of the thesis, I characterized and proved selective G_q protein coupling of hOPN5 (WT) in HEK293 cells. In addition, I explored its high light sensitivity and bistable nature with Ca^{2+} imaging. The vital finding of hOPN5 coupling to G_q proteins changes the prevailing knowledge as previous reports on OPN5 provided mixed information on G protein coupling, with many reports suggesting G_i coupling. The selective G protein coupling of hOPN5 was proved with GIRK assay and Ca^{2+} imaging in knock-out HEK293 cells. The other experiments performed proved the G_q protein activation that sequentially addressed each second messenger produced during the G_q signaling cascade. The experiments used for the thesis are far superior to the previously reported, for experimenting with G protein selectivity, as most of them were performed in non-physiological conditions and did not use specific G protein blockers to prove their claim. The assays that were used to prove the G protein coupling selectivity of hOPN5 included the Ca^{2+} imaging with G_i and $G_{q/11}$ knock out of HEK293 cells and the GIRK channel assay, which is the ideal assay to exclude promiscuous G protein binding because of its ability to detect the even minimal changes.

In the second part of the thesis, a platform to develop enhanced OPN5 variants suited for specific optogenetic applications was laid out. The hOPN5 mutant T164A was by far the best mutant generated in this project, with improved light sensitivity compared to hOPN5 (WT). The future mutants should be engineered to integrate the T164A mutation due to its direct all-trans binding abilities. The information I obtained on light sensitivity and wavelength specificity from newly generated hOPN5 mutants will be used to train the MD simulations. Also, new amino acid predictions to create better OPN5 variants are planned from the trained models of MD simulations. The Ca^{2+} imaging with cOPN5 (WT) proved its high light sensitivity, and in the future,

OPN5s from other species will also be characterized with the assays established during this thesis. The information on light sensitivity and wavelength specificity from other OPN5s will be highly beneficial to understanding the OPN5 structure-retinal relationship to fine-tune the wavelength specificity.

In addition, I plan to use spectroscopic analysis of OPN5 variants, which would support the wavelength specificity information of the new OPN5 variants generated with Ca^{2+} imaging. X-ray crystallography structures of OPN5 in the dark state or photo-intermediate states will help to further the understanding of the interaction of the retinal with the native environment of the retinal binding pocket. As current MD simulations of OPN5 still rely on bovine and squid rhodopsin crystal structures, which are evolutionarily distant from OPN5. Also, prevailing knowledge on OPN5 deactivation, arrestin binding, and its microdomain environment is very limited. Also, 3D cryo-electron micrograph structures of OPN5 will improve our interpretation of the molecular mechanisms underlying their function and specialized regions for G protein interaction and other interaction partners that might affect OPN5. To conclude, all the experiments and ideas mentioned will pave the way for a rational design to engineer enhanced OPN5 variants to selectively control G_q signaling in different cells and organs.

5 References

Abe-Yoshizumi, R., Inoue, K., Kato, H.E., Nureki, O., Kandori, H., 2016. Role of Asn112 in a Light-Driven Sodium Ion-Pumping Rhodopsin. Biochemistry 55, 5790–5797. https://doi.org/10.1021/acs.biochem.6b00741

Airan, R.D., Thompson, K.R., Fenno, L.E., Bernstein, H., Deisseroth, K., 2009. Temporally precise in vivo control of intracellular signalling. Nature 458, 1025–1029. https://doi.org/10.1038/NATURE07926

Arendt, D., 2003. Evolution of eyes and photoreceptor cell types. Int. J. Dev. Biol. https://doi.org/10.1387/IJDB.14756332

Armbruster, B.N., Li, X., Pausch, M.H., Herlitze, S., Roth, B.L., 2007. Evolving the lock to fit the key to create a family of G protein-coupled receptors potently activated by an inert ligand. Proc. Natl. Acad. Sci. U. S. A. 104, 5163–5168. https://doi.org/10.1073/pnas.0700293104

Attwood, T.K., Findlay, J.B.C., 1994. Fingerprinting G-protein-coupled receptors. Protein Eng. 7, 195–203. https://doi.org/10.1093/protein/7.2.195

Atwood, B.K., Lopez, J., Wager-Miller, J., Mackie, K., Straiker, A., 2011. Expression of G protein-coupled receptors and related proteins in HEK293, AtT20, BV2, and N18 cell lines as revealed by microarray analysis. BMC Genomics 12, 14. https://doi.org/10.1186/1471-2164-12-14

Avelar, G.M., Schumacher, R.I., Zaini, P.A., Leonard, G., Richards, T.A., Gomes, S.L., 2014. A Rhodopsin-Guanylyl cyclase gene fusion functions in visual perception in a fungus. Curr. Biol. 24, 1234–1240. https://doi.org/10.1016/j.cub.2014.04.009

Bailes, H.J., Lucas, R.J., 2013. Human melanopsin forms a pigment maximally sensitive to blue light (λmax ≈ 479 nm) supporting activation of Gq/11 and Gi/o signalling cascades. Proc. R. Soc. B Biol. Sci. 280, 20122987. https://doi.org/10.1098/rspb.2012.2987

Balashov, S.P., Imasheva, E.S., Dioumaev, A.K., Wang, J.M., Jung, K.H., Lanyi, J.K., 2014. Light-driven Na(+) pump from Gillisia limnaea: a high-affinity Na(+) binding site is formed transiently in the photocycle. Biochemistry 53, 7549–7561. https://doi.org/10.1021/BI501064N

Beiert, T., Bruegmann, T., Sasse, P., 2014. Optogenetic activation of Gq signalling modulates pacemaker activity of cardiomyocytes. Cardiovasc. Res. 102, 507–516. https://doi.org/10.1093/cvr/cvu046

Berndt, A., Yizhar, O., Gunaydin, L.A., Hegemann, P., Deisseroth, K., 2009. Bi-stable neural state switches. Nat. Neurosci. 12, 229–234. https://doi.org/10.1038/nn.2247

Berry, M.H., Holt, A., Salari, A., Veit, J., Visel, M., Levitz, J., Aghi, K., Gaub, B.M., Sivyer, B., Flannery, J.G., Isacoff, E.Y., 2019. Restoration of high-sensitivity and adapting vision with a cone opsin. Nat. Commun. 10, 1221. https://doi.org/10.1038/s41467-019-09124-x

Berson, D.M., Dunn, F.A., Takao, M., 2002. Phototransduction by retinal ganglion cells that set the circadian clock. Science (80-.). 295, 1070–1073. https://doi.org/10.1126/science.1067262

Blackshaw, S., Snyder, S.H., 1997. Parapinopsin, a novel catfish opsin localized to the parapineal organ, defines a new gene family. J. Neurosci. 17, 8083–8092. https://doi.org/10.1523/jneurosci.17-21-08083.1997

Bohm, M., Gierschik, P., Jakobs, K.H., Pieske, B., Schnabel, P., Ungerer, M., Erdmann, E., 1990. Increase of Gi alpha in human hearts with dilated but not ischemic cardiomyopathy. Circulation 82, 1249–1265. https://doi.org/10.1161/01.CIR.82.4.1249

Bos, J.L., Rehmann, H., Wittinghofer, A., 2007. GEFs and GAPs: Critical Elements in the Control of Small G Proteins. Cell. https://doi.org/10.1016/j.cell.2007.05.018

Boyden, E.S., Zhang, F., Bamberg, E., Nagel, G., Deisseroth, K., 2005. Millisecond-timescale, genetically targeted optical control of neural activity. Nat. Neurosci. 8, 1263–8. https://doi.org/10.1038/nn1525

Breitwieser, G.E., 2005. GIRK channels: Hierarchy of control. Focus on “PKC-δ sensitizes Kir3.1/3.2 channels to changes in membrane phospholipid levels after M 3 receptor activation in HEK-293 cells.” Am. J. Physiol. - Cell Physiol. https://doi.org/10.1152/ajpcell.00237.2005

Brodde, O.E., Michel, M.C., 1999. Presence, distribution and physiological function of adrenergic and muscarinic receptors in the human heart. Pharmacol. Rev. 51, 651–90.

Brueggemann, L.I., Sullivan, J.M., 2002. HEK293S cells have functional retinoid processing machinery. J. Gen. Physiol. 119, 593–612. https://doi.org/10.1085/jgp.20018495

Brunet, T., Larson, B.T., Linden, T.A., Vermeij, M.J.A., McDonald, K., King, N., 2019. Light-regulated collective contractility in a multicellular choanoflagellate. Science 366, 326–334. https://doi.org/10.1126/science.aay2346

Bruysters, M., Jongejan, A., Akdemir, A., Bakker, R.A., Leurs, R., 2005. A Gq/11-coupled mutant histamine H1 receptor F435A activated solely by synthetic ligands (RASSL). J. Biol. Chem. 280, 34741–34746. https://doi.org/10.1074/jbc.M504165200

Brzezinska, P., Simpson, N.J., Hubert, F., Jacobs, A.N., Umana, M.B., MacKeil, J.L., Burke-Kleinman, J., Payne, D.M., Ferguson, A. V., Maurice, D.H., 2021. Phosphodiesterase 1C integrates store-operated calcium entry and cAMP signaling in leading-edge protrusions of migrating human arterial myocytes. J. Biol. Chem. 296, 100606. https://doi.org/10.1016/j.jbc.2021.100606

Buhr, E.D., Yue, W.W.S., Ren, X., Jiang, Z., Liao, H.W.R., Mei, X., Vemaraju, S., Nguyen, M.T., Reed, R.R., Lang, R.A., Yau, K.W., Van Gelder, R.N., 2015. Neuropsin (OPN5)-mediated photoentrainment of local circadian oscillators in mammalian retina and cornea. Proc. Natl. Acad. Sci. U. S. A. 112, 13093–13098. https://doi.org/10.1073/pnas.1516259112

Chen, X., Choo, H., Huang, X.P., Yang, X., Stone, O., Roth, B.L., Jin, J., 2015. The first structure-activity relationship studies for designer receptors exclusively activated by designer drugs. ACS Chem. Neurosci. 6, 476–484. https://doi.org/10.1021/cn500325v

Chew, K.S., Schmidt, T.M., Rupp, A.C., Kofuji, P., Trimarchi, J.M., 2014. Loss of Gq/11 genes does not abolish melanopsin phototransduction. PLoS One 9. https://doi.org/10.1371/journal.pone.0098356

Chow, B.Y., Han, X., Dobry, A.S., Qian, X., Chuong, A.S., Li, M., Henninger, M.A., Belfort, G.M., Lin, Y.,

Monahan, P.E., Boyden, E.S., 2010. High-performance genetically targetable optical neural silencing by light-driven proton pumps. Nature 463, 98–102. https://doi.org/10.1038/nature08652

Christie, J.M., Swartz, T.E., Bogomolni, R.A., Briggs, W.R., 2002. Phototropin LOV domains exhibit distinct roles in regulating photoreceptor function. Plant J. 32, 205–19. https://doi.org/10.1046/j.1365-313x.2002.01415.x

Claeysen, S., Joubert, L., Sebben, M., Bockaert, J., Dumuis, A., 2003. A single mutation in the 5-HT4 receptor (5-HT4-R D100(3.32)A) generates a Gs-coupled receptor activated exclusively by synthetic ligands (RASSL). J. Biol. Chem. 278, 699–702. https://doi.org/10.1074/jbc.C200588200

Conklin, B.R., Hsiao, E.C., Claeysen, S., Dumuis, A., Srinivasan, S., Forsayeth, J.R., Guettier, J.M., Chang, W.C., Pei, Y., McCarthy, K.D., Nissenson, R.A., Wess, J., Bockaert, J., Roth, B.L., 2008. Engineering GPCR signaling pathways with RASSLs. Nat. Methods 5, 673–678. https://doi.org/10.1038/nmeth.1232

Coward, P., Wada, H.G., Falk, M.S., Chan, S.D.H., Meng, F., Akil, H., Conklin, B.R., 1998. Controlling signaling with a specifically designed Gi-coupled receptor. Proc. Natl. Acad. Sci. U. S. A. 95, 352–357. https://doi.org/10.1073/pnas.95.1.352

Cunha, R.A., Ribeiro, J.A., 2000. Adenosine A2A receptor facilitation of synaptic transmission in the CA1 area of the rat hippocampus requires protein kinase C but not protein kinase A activation. Neurosci. Lett. 289, 127–30. https://doi.org/10.1016/s0304-3940(00)01295-7

Dai, R., Yu, T., Weng, D., Li, H., Cui, Y., Wu, Z., Guo, Q., Zou, H., Wu, W., Gao, X., Qi, Z., Ren, Y., Wang, S., Li, Y., Luo, M., 2022. A neuropsin-based optogenetic tool for precise control of Gq signaling. Sci. China. Life Sci. https://doi.org/10.1007/s11427-022-2122-0

Das, J., Rahman, G.M., 2014. C1 domains: structure and ligand-binding properties. Chem. Rev. 114, 12108–31. https://doi.org/10.1021/cr300481j

De Felipe, P., Luke, G.A., Hughes, L.E., Gani, D., Halpin, C., Ryan, M.D., 2006. E unum pluribus: multiple proteins from a self-processing polyprotein. Trends Biotechnol. 24, 68–75. https://doi.org/10.1016/J.TIBTECH.2005.12.006

Dhanasekaran, N., Dermott, J.M., 1996. Signaling by the G12 class of G proteins. Cell. Signal. 8, 235–245. https://doi.org/10.1016/0898-6568(96)00048-4

Díaz, N.M., Lang, R.A., van Gelder, R.N., Buhr, E.D., 2020. Wounding induces facultative opn5-dependent circadian photoreception in the murine cornea. Investig. Ophthalmol. Vis. Sci. 61, 2–5. https://doi.org/10.1167/IOVS.61.6.37

Dietrich, A., Kalwa, H., Rost, B.R., Gudermann, T., 2005a. The diacylgylcerol-sensitive TRPC3/6/7 subfamily of cation channels: functional characterization and physiological relevance. Pflugers Arch. 451, 72–80. https://doi.org/10.1007/s00424-005-1460-0

Dietrich, A., Mederos Y Schnitzler, M., Emmel, J., Kalwa, H., Hofmann, T., Gudermann, T., 2003. N-Linked Protein Glycosylation Is a Major Determinant for Basal TRPC3 and TRPC6 Channel Activity. J. Biol. Chem. 278, 47842–47852. https://doi.org/10.1074/jbc.M302983200

Dietrich, A., Mederos Y Schnitzler, M., Kalwa, H., Storch, U., Gudermann, T., 2005b. Functional characterization and physiological relevance of the TRPC3/6/7 subfamily of cation channels. Naunyn. Schmiedebergs. Arch. Pharmacol. 371, 257–265. https://doi.org/10.1007/s00210-005-1052-8

Dryer, S.E., Kim, E.Y., 2018. Permeation and Rectification in Canonical Transient Receptor Potential-6 (TRPC6) Channels. Front. Physiol. 9, 1055. https://doi.org/10.3389/fphys.2018.01055

Dutt, P., Nguyen, N., Toksoz, D., 2004. Role of Lbc RhoGEF in Gα12/13-induced signals to Rho GTPase. Cell. Signal. 16, 201–209. https://doi.org/10.1016/S0898-6568(03)00132-3

Eickelbeck, D., Rudack, T., Tennigkeit, S.A., Surdin, T., Karapinar, R., Schwitalla, J.-C., Mücher, B., Shulmann, M., Scherlo, M., Althoff, P., Mark, M.D., Gerwert, K., Herlitze, S., 2019. Lamprey Parapinopsin ("UVLamP"): a bistable UV-sensitive optogenetic switch for ultrafast control of GPCR pathways. Chembiochem 1, 104–111. https://doi.org/10.1002/cbic.201900485

Ernst, O.P., Lodowski, D.T., Elstner, M., Hegemann, P., Brown, L.S., Kandori, H., 2014. Microbial and animal rhodopsins: structures, functions, and molecular mechanisms. Chem. Rev. 114, 126–63. https://doi.org/10.1021/cr4003769

Flesch, M., Schwinger, R.H.G., Schnabel, P., Schiffer, F., Van Gelder, I., Bavendiek, U., Südkamp, M., Kuhn-Regnier, F., Böhm, M., 1996. Sarcoplasmic reticulum Ca2+ATPase and phospholamban mRNA and protein levels in end-stage heart failure due to ischemic or dilated cardiomyopathy. J. Mol. Med. (Berl). 74, 321–332. https://doi.org/10.1007/BF00207509

Fredriksson, R., Lagerström, M.C., Lundin, L.-G., Schiöth, H.B., 2003. The G-protein-coupled receptors in the human genome form five main families. Phylogenetic analysis, paralogon groups, and fingerprints. Mol. Pharmacol. 63, 1256–72. https://doi.org/10.1124/mol.63.6.1256

Fukuharaa, S., Chikumi, H., Silvio Gutkind, J., 2001. RGS-containing RhoGEFs: The missing link between transforming G proteins and Rho? Oncogene. https://doi.org/10.1038/sj.onc.1204182

Govardovskii, V.I., Fyhrquist, N., Reuter, T., Kuzmin, D.G., Donner, K., 2000. In search of the visual pigment template. Vis. Neurosci. 17, 509–528. https://doi.org/10.1017/S0952523800174036

Govorunova, E.G., Sineshchekov, O.A., Li, H., Spudich, J.L., 2017. Microbial rhodopsins: Diversity, mechanisms, and optogenetic applications. Annu. Rev. Biochem. 86, 845–872. https://doi.org/10.1146/annurev-biochem-101910-144233

Gradinaru, V., Thompson, K.R., Deisseroth, K., 2008. eNpHR: A Natronomonas halorhodopsin enhanced for optogenetic applications. Brain Cell Biol. 36, 129–139. https://doi.org/10.1007/s11068-008-9027-6

Graham, D.M., Wong, K.Y., Shapiro, P., Frederick, C., Pattabiraman, K., Berson, D.M., 2008. Melanopsin ganglion cells use a membrane-associated rhabdomeric phototransduction cascade. J. Neurophysiol. 99, 2522–2532. https://doi.org/10.1152/jn.01066.2007

Guettier, J.M., Gautam, D., Scarselli, M., De Azua, I.R., Li, J.H., Rosemond, E., Ma, X., Gonzalez, F.J., Armbruster, B.N., Lu, H., Roth, B.L., Wess, J., 2009. A chemical-genetic approach to study G protein regulation of β cell function in vivo. Proc. Natl. Acad. Sci. U. S. A. 106, 19197–19202. https://doi.org/10.1073/pnas.0906593106

Gundelach, L.A., Hüser, M.A., Beutner, D., Ruther, P., Bruegmann, T., 2020. Towards the clinical translation of optogenetic skeletal muscle stimulation. Pflugers Arch. 472, 527–545. https://doi.org/10.1007/s00424-020-02387-0

Gurevich, V. V., Gurevich, E. V., 2019. GPCR signaling regulation: The role of GRKs and arrestins. Front. Pharmacol. 10, 125. https://doi.org/10.3389/fphar.2019.00125

Gurevich, V. V., Gurevich, E. V., 2015. Arrestins: Critical Players in Trafficking of Many GPCRs. Prog. Mol. Biol. Transl. Sci. 132, 1–14. https://doi.org/10.1016/bs.pmbts.2015.02.010

Haltaufderhyde, K., Ozdeslik, R.N., Wicks, N.L., Najera, J.A., Oancea, E., 2015. Opsin Expression in Human Epidermal Skin. Photochem. Photobiol. 91, 117–123. https://doi.org/10.1111/php.12354

Hankins, M.W., Peirson, S.N., Foster, R.G., 2008. Melanopsin: an exciting photopigment. Trends Neurosci. 31, 27–36. https://doi.org/10.1016/j.tins.2007.11.002

Hao, W., Fong, H.K.W., 1999. The endogenous chromophore of retinal G protein-coupled receptor opsin from the pigment epithelium. J. Biol. Chem. 274, 6085–90. https://doi.org/10.1074/jbc.274.10.6085

Helgerson, S.L., Stoeckenius, W., 1985. Transient proton inflows during illumination of anaerobic Halobacterium halobium cells. Arch. Biochem. Biophys. 241, 616–627. https://doi.org/10.1016/0003-9861(85)90588-0

Henderson, R., Unwin, P.N.T., 1975. Three-dimensional model of purple membrane obtained by electron microscopy. Nature 257, 28–32. https://doi.org/10.1038/257028a0

Hisano, Y., Kono, M., Cartier, A., Engelbrecht, E., Kano, K., Kawakami, K., Xiong, Y., Piao, W., Galvani, S., Yanagida, K., Kuo, A., Ono, Y., Ishida, S., Aoki, J., Proia, R.L., Bromberg, J.S., Inoue, A., Hla, T., 2019. Lysolipid receptor cross-talk regulates lymphatic endothelial junctions in lymph nodes. J. Exp. Med. 216, 1582–1598. https://doi.org/10.1084/jem.20181895

Hofmann, T., Obukhov, A.G., Schaefer, M., Harteneck, C., Gudermann, T., Schultz, G., 1999. Direct activation of human TRPC6 and TRPC3 channels by diacylglycerol. Nature 397, 259–263. https://doi.org/10.1038/16711

Hollborn, M., Ulbricht, E., Rillich, K., Dukic-Stefanovic, S., Wurm, A., Wagner, L., Reichenbach, A., Wiedemann, P., Limb, G.A., Bringmann, A., Kohen, L., 2011. The human Müller cell line MIO-M1 expresses opsins. Mol. Vis. 17, 2738–2750.

Hubbard, K.B., Hepler, J.R., 2006. Cell signalling diversity of the Gqα family of heterotrimeric G proteins. Cell. Signal. 18, 135–150. https://doi.org/10.1016/j.cellsig.2005.08.004

Hughes, S., Jagannath, A., Hickey, D., Gatti, S., Wood, M., Peirson, S.N., Foster, R.G., Hankins, M.W., 2014. Using siRNA to define functional interactions between melanopsin and multiple G Protein partners. Cell. Mol. Life Sci. 72, 165–179. https://doi.org/10.1007/s00018-014-1664-6

Inoue, A., Raimondi, F., Kadji, F.M.N., Singh, G., Kishi, T., Uwamizu, A., Ono, Y., Shinjo, Y., Ishida, S., Arang, N., Kawakami, K., Gutkind, J.S., Aoki, J., Russell, R.B., 2019. Illuminating G-Protein-Coupling Selectivity of GPCRs. Cell 177, 1933-1947.e25. https://doi.org/10.1016/j.cell.2019.04.044

Inoue, K., Ono, H., Abe-Yoshizumi, R., Yoshizawa, S., Ito, H., Kogure, K., Kandori, H., 2013. A light-driven sodium ion pump in marine bacteria. Nat. Commun. 4, 1678. https://doi.org/10.1038/ncomms2689

Jacobson, K.A., Gao, Z.-G., Liang, B.T., 2007. Neoceptors: reengineering GPCRs to recognize tailored ligands. Trends Pharmacol. Sci. 28, 111–6. https://doi.org/10.1016/j.tips.2007.01.006

Jacobson, K.A., Gao, Z.G., Chen, A., Barak, D., Kim, S.A., Lee, K., Link, A., Van Rompaey, P., Van Calenbergh, S., Liang, B.T., 2001. Neoceptor concept based on molecular complementarity in GPCRs: A mutant adenosine A3 receptor with selectively enhanced affinity for amine-modified nucleosides. J. Med. Chem. 44, 4125–4136. https://doi.org/10.1021/jm010232o

Jagannath, A., Hughes, S., Abdelgany, A., Pothecary, C.A., Di Pretoro, S., Pires, S.S., Vachtsevanos, A., Pilorz, V., Brown, L.A., Hossbach, M., MacLaren, R.E., Halford, S., Gatti, S., Hankins, M.W., Wood, M.J.A., Foster, R.G., Peirson, S.N., 2015. Isoforms of Melanopsin Mediate Different Behavioral Responses to Light. Curr. Biol. 25, 2430–2434. https://doi.org/10.1016/j.cub.2015.07.071

Joshi, J., Rubart, M., Zhu, W., 2020. Optogenetics: Background, Methodological Advances and Potential Applications for Cardiovascular Research and Medicine. Front. Bioeng. Biotechnol. https://doi.org/10.3389/fbioe.2019.00466

Jost, M., Fernández-Zapata, J., Polanco, M.C., Ortiz-Guerrero, J.M., Chen, P.Y.-T., Kang, G., Padmanabhan, S., Elías-Arnanz, M., Drennan, C.L., 2015. Structural basis for gene regulation by a B12-dependent photoreceptor. Nature 526, 536–41. https://doi.org/10.1038/nature14950

Kankanamge, D., Ratnayake, K., Samaradivakara, S., Karunarathne, A., 2018. Melanopsin (Opn4) utilizes Gαi and Gβγ as major signal transducers. J. Cell Sci. 131. https://doi.org/10.1242/JCS.212910

Katayama, K., Furutani, Y., Imai, H., Kandori, H., 2012. Protein-Bound Water Molecules in Primate Red- and Green-Sensitive Visual Pigments. https://doi.org/10.1021/bi201676y

Kateriya, S., Nagel, G., Bamberg, E., Hegemann, P., 2004. “Vision” in single-celled algae. News Physiol. Sci. 19, 133–137. https://doi.org/10.1152/NIPS.01517.2004

Kato, H.E., Inoue, K., Abe-Yoshizumi, R., Kato, Y., Ono, H., Konno, M., Hososhima, S., Ishizuka, T., Hoque, M.R., Kunitomo, H., Ito, J., Yoshizawa, S., Yamashita, K., Takemoto, M., Nishizawa, T., Taniguchi, R., Kogure, K., Maturana, A.D., Iino, Y., Yawo, H., Ishitani, R., Kandori, H., Nureki, O., 2015. Structural basis for Na(+) transport mechanism by a light-driven Na(+) pump. Nature 521, 48–53. https://doi.org/10.1038/NATURE14322

Kato, H.E., Nureki, O., 2013. Crystal structure of channelrhodopsin, a light-gated cation channel - All cations lead through the monomer. Biophys. 9, 57–61. https://doi.org/10.2142/biophysics.9.57

Kawano-Yamashita, E., Koyanagi, M., Wada, S., Tsukamoto, H., Nagata, T., Terakita, A., 2015. Activation of transducin by bistable pigment parapinopsin in the pineal organ of lower vertebrates. PLoS One 10, e0141280. https://doi.org/10.1371/journal.pone.0141280

Kim, J.-M., Hwa, J., Garriga, P., Reeves, P.J., RajBhandary, U.L., Khorana, H.G., 2005. Light-driven activation of beta 2-adrenergic receptor signaling by a chimeric rhodopsin containing the beta 2-adrenergic receptor cytoplasmic loops. Biochemistry 44, 2284–92. https://doi.org/10.1021/bi048328i

King, N., Hittinger, C.T., Carroll, S.B., 2003. Evolution of key cell signaling and adhesion protein families predates animal origins. Science (80-.). 301, 361–363. https://doi.org/10.1126/science.1083853

Kleinlogel, S., 2016. Optogenetic user’s guide to Opto-GPCRs. Front. Biosci. - Landmark 21, 794–805. https://doi.org/10.2741/4421

Kojima, D., Mori, S., Torii, M., Wada, A., Morishita, R., Fukada, Y., 2011. UV-sensitive photoreceptor protein OPN5 in humans and mice. PLoS One 6, e26388. https://doi.org/10.1371/journal.pone.0026388

Kojima, K., Sudo, Y., 2023. Convergent evolution of animal and microbial rhodopsins. RSC Adv. 13, 5367–5381. https://doi.org/10.1039/d2ra07073a

Kojima, K., Yamashita, T., Imamoto, Y., Kusakabe, T.G., Tsuda, M., Shichida, Y., 2017. Evolutionary steps involving counterion displacement in a tunicate opsin. Proc. Natl. Acad. Sci. U. S. A. 114, 6028–6033. https://doi.org/10.1073/pnas.1701088114

Kottke, T., Xie, A., Larsen, D.S., Hoff, W.D., 2018. Photoreceptors Take Charge: Emerging Principles for Light Sensing. Annu. Rev. Biophys. 47, 291–313. https://doi.org/10.1146/ANNUREV-BIOPHYS-070317-033047

Koyanagi, M., Kawano, E., Kinugawa, Y., Oishi, T., Shichida, Y., Tamotsu, S., Terakita, A., 2004. Bistable UV pigment in the lamprey pineal. Proc. Natl. Acad. Sci. U. S. A. 101, 6687–6691. https://doi.org/10.1073/pnas.0400819101

Koyanagi, M., Takano, K., Tsukamoto, H., Ohtsu, K., Tokunaga, F., Terakita, A., 2008. Jellyfish vision starts with cAMP signaling mediated by opsin-G(s) cascade. Proc. Natl. Acad. Sci. U. S. A. 105, 15576–80. https://doi.org/10.1073/pnas.0806215105

Lander, E.S., Linton, L.M., Birren, B., Nusbaum, C., Zody, M.C., Baldwin, J., Devon, K., Dewar, K., Doyle, M., Fitzhugh, W., Funke, R., Gage, D., Harris, K., Heaford, A., Howland, J., Kann, L., Lehoczky, J., Levine, R., McEwan, P., McKernan, K., Meldrim, J., Mesirov, J.P., Miranda, C., Morris, W., Naylor, J., Raymond, Christina, Rosetti, M., Santos, R., Sheridan, A., Sougnez, C., Stange-Thomann, N., Stojanovic, N., Subramanian, A., Wyman, D., Rogers, J., Sulston, J., Ainscough, R., Beck, S., Bentley, D., Burton, J., Clee, C., Carter, N., Coulson, A., Deadman, R., Deloukas, P., Dunham, A., Dunham, I., Durbin, R., French, L., Grafham, D., Gregory, S., Hubbard, T., Humphray, S., Hunt, A., Jones, M., Lloyd, C., McMurray, A., Matthews, L., Mercer, S., Milne, S., Mullikin, J.C., Mungall, A., Plumb, R., Ross, M., Shownkeen, R., Sims, S., Waterston, R.H., Wilson, R.K., Hillier, L.W., McPherson, J.D., Marra, M.A., Mardis, E.R., Fulton, L.A., Chinwalla, A.T., Pepin, K.H., Gish, W.R., Chissoe, S.L., Wendl, M.C., Delehaunty, K.D., Miner, T.L., Delehaunty, A., Kramer, J.B., Cook, L.L., Fulton, R.S., Johnson, D.L., Minx, P.J., Clifton, S.W., Hawkins, T., Branscomb, E., Predki, P., Richardson, P., Wenning, S., Slezak, T., Doggett, N., Cheng, J.F., Olsen, A., Lucas, S., Elkin, C., Uberbacher, E., Frazier, M., Gibbs, R.A., Muzny, D.M., Scherer, S.E., Bouck, J.B., Sodergren, E.J., Worley, K.C., Rives, C.M., Gorrell, J.H., Metzker, M.L., Naylor, S.L., Kucherlapati, R.S., Nelson, D.L., Weinstock, G.M., Sakaki, Y., Fujiyama, A., Hattori, M., Yada, T., Toyoda, A., Itoh, T., Kawagoe, C., Watanabe, H., Totoki, Y., Taylor, T., Weissenbach, J., Heilig, R., Saurin, W., Artiguenave, F., Brottier, P., Bruls, T., Pelletier, E., Robert, C., Wincker, P., Rosenthal, A., Platzer, M., Nyakatura, G., Taudien, S., Rump, A., Smith, D.R., Doucette-Stamm, L., Rubenfield, M., Weinstock, K., Hong, M.L., Dubois, J., Yang, H., Yu, J., Wang, J., Huang, G., Gu, J., Hood, L., Rowen, L., Madan, A., Qin, S., Davis, R.W., Federspiel, N.A., Abola, A.P., Proctor, M.J., Roe, B.A., Chen, F., Pan, H., Ramser, J., Lehrach, H., Reinhardt, R., McCombie, W.R., De La Bastide, M., Dedhia, N., Blöcker, H., Hornischer, K., Nordsiek, G., Agarwala, R., Aravind, L., Bailey, J.A., Bateman, A., Batzoglou, S., Birney, E., Bork, P., Brown, D.G., Burge, C.B., Cerutti, L., Chen, H.C., Church, D., Clamp, M., Copley, R.R., Doerks, T., Eddy, S.R., Eichler, E.E., Furey, T.S., Galagan, J., Gilbert, J.G.R., Harmon, C., Hayashizaki, Y., Haussler, D., Hermjakob, H., Hokamp, K., Jang, W., Johnson, L.S., Jones, T.A., Kasif, S., Kaspryzk, A., Kennedy, S., Kent, W.J., Kitts, P., Koonin, E. V, Korf, I., Kulp, D., Lancet, D., Lowe, T.M., McLysaght, A., Mikkelsen, T., Moran, J. V, Mulder, N., Pollara, V.J., Ponting, C.P., Schuler, G., Schultz, J., Slater, G., Smit, A.F.A., Stupka, E., Szustakowki, J., Thierry-Mieg, D., Thierry-Mieg, J., Wagner, L., Wallis, J., Wheeler, R., Williams, A., Wolf, Y.I., Wolfe, K.H., Yang, S.P., Yeh, R.F., Collins, F., Guyer, M.S., Peterson, J., Felsenfeld, A., Wetterstrand, K.A., Myers, R.M., Schmutz, J., Dickson, M., Grimwood, J., Cox, D.R., Olson, M. V, Kaul, R., Raymond, Christopher, Shimizu, N., Kawasaki, K., Minoshima, S., Evans, G.A., Athanasiou, M., Schultz, R., Patrinos, A., Morgan, M.J., 2001. Initial sequencing and analysis of the human genome. Nature 409, 860–921. https://doi.org/10.1038/35057062

Lanyi, J.K., 1986. Halorhodopsin: a light-driven chloride ion pump. Annu. Rev. Biophys. Biophys. Chem. https://doi.org/10.1146/annurev.bb.15.060186.000303

Leung, N.Y., Montell, C., 2017. Unconventional Roles of Opsins. Annu. Rev. Cell Dev. Biol. 33, 241–264. https://doi.org/10.1146/annurev-cellbio-100616-060432

Leung, T., Manser, E., Tan, L., Lim, L., 1995. A novel serine/threonine kinase binding the ras-related RhoA GTPase which translocates the kinase to peripheral membranes. J. Biol. Chem. 270, 29051–

29054. https://doi.org/10.1074/jbc.270.49.29051

Li, Q.-H., Yang, H.-Q., 2007. Cryptochrome signaling in plants. Photochem. Photobiol. 83, 94–101. https://doi.org/10.1562/2006-02-28-IR-826

Liccardo, F., Luini, A., Di Martino, R., 2022. Endomembrane-Based Signaling by GPCRs and G-Proteins. Cells 11. https://doi.org/10.3390/cells11030528

Lin, J.Y., 2010. A user's guide to channelrhodopsin variants: Features, limitations and future developments. Exp. Physiol. https://doi.org/10.1113/expphysiol.2009.051961

Logothetis, D.E., Kurachi, Y., Galper, J., Neer, E.J., Clapham, D.E., 1987. The βγ subunits of GTP-Binding proteins activate the muscarinic K+ channel in heart. Nature 325, 321–326. https://doi.org/10.1038/325321a0

Losi, A., Gardner, K.H., Möglich, A., 2018. Blue-Light Receptors for Optogenetics. Chem. Rev. 118, 10659. https://doi.org/10.1021/ACS.CHEMREV.8B00163

Losi, A., Gärtner, W., 2011. Old chromophores, new photoactivation paradigms, trendy applications: flavins in blue light-sensing photoreceptors. Photochem. Photobiol. 87, 491–510. https://doi.org/10.1111/j.1751-1097.2011.00913.x

Luck, M., Mathes, T., Bruun, S., Fudim, R., Hagedorn, R., Tran Nguyen, T.M., Kateriya, S., Kennis, J.T.M., Hildebrandt, P., Hegemann, P., 2012. A photochromic histidine kinase rhodopsin (HKR1) that is bimodally switched by ultraviolet and blue light. J. Biol. Chem. 287, 40083–90. https://doi.org/10.1074/jbc.M112.401604

Lüscher, C., Slesinger, P.A., 2010. Emerging roles for G protein-gated inwardly rectifying potassium (GIRK) channels in health and disease. Nat. Rev. Neurosci. https://doi.org/10.1038/nrn2834

Makowka, P., Bruegmann, T., Dusend, V., Malan, D., Beiert, T., Hesse, M., Fleischmann, B.K., Sasse, P., 2019. Optogenetic stimulation of Gs -signaling in the heart with high spatio-temporal precision. Nat. Commun. 10, 1281. https://doi.org/10.1038/s41467-019-09322-7

Maruyama, Y., Nishida, M., Sugimoto, Y., Tanabe, S., Turner, J.H., Kozasa, T., Wada, T., Nagao, T., Kurose, H., 2002. Gα12/13 mediates α1-adrenergic receptor-induced cardiac hypertrophy. Circ. Res. 91, 961–969. https://doi.org/10.1161/01.RES.0000043282.39776.7C

Matsuoka, D., Iwata, T., Zikihara, K., Kandori, H., Tokutomi, S., 2007. Primary processes during the light-signal transduction of phototropin. Photochem. Photobiol. 83. https://doi.org/10.1562/2006-03-29-RA-861

Mattis, J., Tye, K.M., Ferenczi, E.A., Ramakrishnan, C., O'Shea, D.J., Prakash, R., Gunaydin, L.A., Hyun, M., Fenno, L.E., Gradinaru, V., Yizhar, O., Deisseroth, K., 2011. Principles for applying optogenetic tools derived from direct comparative analysis of microbial opsins. Nat. Methods 9, 159–172. https://doi.org/10.1038/NMETH.1808

Melyan, Z., Tarttelin, E.E., Bellingham, J., Lucas, R.J., Hankins, M.W., 2005. Addition of human melanopsin renders mammalian cells photoresponsive. Nature 433, 741–5. https://doi.org/10.1038/nature03344

Mika, D., Fischmeister, R., 2021. Cyclic nucleotide signaling and pacemaker activity. Prog. Biophys. Mol. Biol. 166, 29–38. https://doi.org/10.1016/j.pbiomolbio.2021.07.007

Miura, Y., Senoo, A., Doura, T., Kiyonaka, S., 2022. Chemogenetics of cell surface receptors: Beyond genetic and pharmacological approaches. RSC Chem. Biol. https://doi.org/10.1039/d1cb00195g

Mukherjee, S., Hegemann, P., Broser, M., 2019. Enzymerhodopsins: novel photoregulated catalysts for optogenetics. Curr. Opin. Struct. Biol. 57, 118–126. https://doi.org/10.1016/j.sbi.2019.02.003

Nagai, Y., Miyakawa, N., Takuwa, H., Hori, Y., Oyama, K., Ji, B., Takahashi, M., Huang, X.P., Slocum, S.T., DiBerto, J.F., Xiong, Y., Urushihata, T., Hirabayashi, T., Fujimoto, A., Mimura, K., English, J.G., Liu, J., Inoue, K. ichi, Kumata, K., Seki, C., Ono, M., Shimojo, M., Zhang, M.R., Tomita, Y., Nakahara, J., Suhara, T., Takada, M., Higuchi, M., Jin, J., Roth, B.L., Minamimoto, T., 2020. Deschloroclozapine, a potent and selective chemogenetic actuator enables rapid neuronal and behavioral modulations in mice and monkeys. Nat. Neurosci. 23, 1157–1167. https://doi.org/10.1038/s41593-020-0661-3

Nagata, T., Inoue, K., 2021. Rhodopsins at a glance. J. Cell Sci. 134. https://doi.org/10.1242/jcs.258989

Nagata, T., Koyanagi, M., Lucas, R., Terakita, A., 2018. An all-trans-retinal-binding opsin peropsin as a potential dark-active and light-inactivated G protein-coupled receptor. Sci. Rep. 8, 3535. https://doi.org/10.1038/s41598-018-21946-1

Nagel, G., Szellas, T., Huhn, W., Kateriya, S., Adeishvili, N., Berthold, P., Ollig, D., Hegemann, P., Bamberg, E., 2003. Channelrhodopsin-2, a directly light-gated cation-selective membrane channel. Proc. Natl. Acad. Sci. U. S. A. 100, 13940–13945. https://doi.org/10.1073/pnas.1936192100

Nakajima, K., Wess, J., 2012. Design and functional characterization of a novel, arrestin-biased designer G protein-coupled receptor. Mol. Pharmacol. 82, 575–82. https://doi.org/10.1124/mol.112.080358

Nakane, Y., Ikegami, K., Ono, H., Yamamoto, N., Yoshida, S., Hirunagi, K., Ebihara, S., Kubo, Y., Yoshimura, T., 2010. A mammalian neural tissue opsin (Opsin 5) is a deep brain photoreceptor in birds. Proc. Natl. Acad. Sci. U. S. A. 107, 15264–15268. https://doi.org/10.1073/pnas.1006393107

Napoli, J.L., 1986. Quantification of Physiological Levels of Retinoic Acid. Methods Enzymol. 123, 112–124. https://doi.org/10.1016/S0076-6879(86)23015-3

Neves, S.R., Ram, P.T., Iyengar, R., 2002. G protein pathways. Science (80-.). 296, 1636–1639. https://doi.org/10.1126/science.1071550

Nguyen, M.T.T., Vemaraju, S., Nayak, G., Odaka, Y., Buhr, E.D., Alonzo, N., Tran, U., Batie, M., Upton, B.A., Darvas, M., Kozmik, Z., Rao, S., Hegde, R.S., Iuvone, P.M., Van Gelder, R.N., Lang, R.A., 2019. An opsin 5-dopamine pathway mediates light-dependent vascular development in the eye. Nat. Cell Biol. 21, 420–429. https://doi.org/10.1038/S41556-019-0301-X

Nieto, P.S., Valdez, D.J., Acosta-Rodríguez, V.A., Guido, M.E., 2011. Expression of novel opsins and intrinsic light responses in the mammalian retinal ganglion cell line RGC-5. Presence of Opn5 in the rat retina. PLoS One 6. https://doi.org/10.1371/journal.pone.0026417

Oesterhelt, D., Stoeckenius, W., 1971. Rhodopsin-like protein from the purple membrane of Halobacterium halobium. Nat. New Biol. 233, 149–152. https://doi.org/10.1038/newbio233149a0

Offermanns, S., Mancino, V., Revel, J.P., Simon, M.I., 1997. Vascular system defects and impaired cell chemokinesis as a result of Gα13 deficiency. Science (80-.). 275, 533–536. https://doi.org/10.1126/science.275.5299.533

Ota, W., Nakane, Y., Hattar, S., Yoshimura, T., 2018. Impaired Circadian Photoentrainment in Opn5-Null Mice. iScience 6, 299–305. https://doi.org/10.1016/j.isci.2018.08.010

Özgür, S., Sancar, A., 2006. Analysis of autophosphorylating kinase activities of Arabidopsis and human cryptochromes. Biochemistry 45, 13369–13374. https://doi.org/10.1021/BI061556N

Padmanabhan, S., Pérez-Castaño, R., Osete-Alcaraz, L., Polanco, M.C., Elías-Arnanz, M., 2022. Vitamin B12 photoreceptors, in: Vitamins and Hormones. Vitam Horm, pp. 149–184. https://doi.org/10.1016/bs.vh.2022.01.007

Palczewski, K., 2006. G protein-coupled receptor rhodopsin. Annu. Rev. Biochem. 75, 743–67. https://doi.org/10.1146/annurev.biochem.75.103004.142743

Panda, S., Nayak, S.K., Campo, B., Walker, J.R., Hogenesch, J.B., Jegla, T., 2005. Illumination of the melanopsin signaling pathway. Science (80-.). 307, 600–604. https://doi.org/10.1126/science.1105121

Pérez-Cerezales, S., Boryshpolets, S., Afanzar, O., Brandis, A., Nevo, R., Kiss, V., Eisenbach, M., 2015. Involvement of opsins in mammalian sperm thermotaxis. Sci. Rep. 5, 16146. https://doi.org/10.1038/srep16146

Pierce, K.L., Premont, R.T., Lefkowitz, R.J., 2002. Seven-transmembrane receptors. Nat. Rev. Mol. Cell Biol. https://doi.org/10.1038/nrm908

Plachetzki, D.C., Degnan, B.M., Oakley, T.H., 2007. The origins of novel protein interactions during animal opsin evolution. PLoS One 2, e1054. https://doi.org/10.1371/journal.pone.0001054

Pottie, E., Tosh, D.K., Gao, Z.G., Jacobson, K.A., Stove, C.P., 2020. Assessment of biased agonism at the A3 adenosine receptor using β-arrestin and miniGαi recruitment assays. Biochem. Pharmacol. 177, 113934. https://doi.org/10.1016/j.bcp.2020.113934

Provencio, I., Jiang, G., De Grip, W.J., Pär Hayes, W., Rollag, M.D., 1998. Melanopsin: An opsin in melanophores, brain, and eye. Proc. Natl. Acad. Sci. U. S. A. 95, 340–345. https://doi.org/10.1073/pnas.95.1.340

Provencio, I., Rodriguez, I.R., Jiang, G., Hayes, W.P., Moreira, E.F., Rollag, M.D., 2000. A novel human opsin in the inner retina. J. Neurosci. 20, 600–605. https://doi.org/10.1523/jneurosci.20-02-00600.2000

Raffelberg, S., Mansurova, M., Gärtner, W., Losi, A., 2011. Modulation of the photocycle of a LOV domain photoreceptor by the hydrogen-bonding network. J. Am. Chem. Soc. 133, 5346–5356. https://doi.org/10.1021/JA1097379

Rekas, A., Alattia, J.R., Nagai, T., Miyawaki, A., Ikura, M., 2002. Crystal structure of venus, a yellow fluorescent protein with improved maturation and reduced environmental sensitivity. J. Biol. Chem. 277, 50573–50578. https://doi.org/10.1074/JBC.M209524200

Rhee, S.G., 2001. Regulation of phosphoinositide-specific phospholipase C. Annu. Rev. Biochem. 70, 281–312. https://doi.org/10.1146/annurev.biochem.70.1.281

Rockman, H.A., Koch, W.J., Lefkowitz, R.J., 2002. Seven-transmembrane-spanning receptors and heart function. Nature 415, 206–12. https://doi.org/10.1038/415206a

Rost, B.R., Wietek, J., Yizhar, O., Schmitz, D., 2022. Optogenetics at the presynapse. Nat. Neurosci. 25, 984–998. https://doi.org/10.1038/s41593-022-01113-6

Sakai, K., Shichida, Y., Imamoto, Y., Yamashita, T., 2022. Creation of photocyclic vertebrate rhodopsin by single amino acid substitution. Elife 11. https://doi.org/10.7554/eLife.75979

Salazar, N.C., Chen, J., Rockman, H.A., 2007. Cardiac GPCRs: GPCR signaling in healthy and failing hearts. Biochim. Biophys. Acta 1768, 1006–18. https://doi.org/10.1016/j.bbamem.2007.02.010

Sanders, D., Hansen, U.P., Slayman, C.L., 1981. Role of the plasma membrane proton pump in pH regulation in non-animal cells. Proc. Natl. Acad. Sci. U. S. A. 78, 5903–5907. https://doi.org/10.1073/pnas.78.9.5903

Sato, K., Yamashita, T., Haruki, Y., Ohuchi, H., Kinoshita, M., Shichida, Y., 2016. Two UV-sensitive photoreceptor proteins, Opn5m and Opn5m2 in ray-finned fish with distinct molecular properties and broad distribution in the retina and brain. PLoS One 11, e0155339. https://doi.org/10.1371/journal.pone.0155339

Schihada, H., Shekhani, R., Schulte, G., 2021. Quantitative assessment of constitutive G protein–coupled receptor activity with BRET-based G protein biosensors. Sci. Signal. 14, 1653. https://doi.org/10.1126/scisignal.abf1653

Schiöth, H.B., Fredriksson, R., 2005. The GRAFS classification system of G-protein coupled receptors in comparative perspective, General and Comparative Endocrinology. Academic Press Inc. https://doi.org/10.1016/j.ygcen.2004.12.018

Schleicher, E., Kowalczyk, R.M., Kay, C.W.M., Hegemann, P., Bacher, A., Fischer, M., Bittl, R., Richter, G., Weber, S., 2004. On the reaction mechanism of adduct formation in LOV domains of the plant blue-light receptor phototropin. J. Am. Chem. Soc. 126, 11067–11076. https://doi.org/10.1021/JA049553Q

Schneider, J., Korshunova, K., Musiani, F., Alfonso-Prieto, M., Giorgetti, A., Carloni, P., 2018. Predicting ligand binding poses for low-resolution membrane protein models: Perspectives from multiscale simulations. Biochem. Biophys. Res. Commun. 498, 366–374. https://doi.org/10.1016/j.bbrc.2018.01.160

Schobert, B., Lanyi, J.K., 1982. Halorhodopsin is a light-driven chloride pump. J. Biol. Chem. 257, 10306–10313. https://doi.org/10.1016/s0021-9258(18)34020-1

Schrage, R., Schmitz, A.L., Gaffal, E., Annala, S., Kehraus, S., Wenzel, D., Büllesbach, K.M., Bald, T., Inoue, A., Shinjo, Y., Galandrin, S., Shridhar, N., Hesse, M., Grundmann, M., Merten, N., Charpentier, T.H., Martz, M., Butcher, A.J., Slodczyk, T., Armando, S., Effern, M., Namkung, Y., Jenkins, L., Horn, V., Stößel, A., Dargatz, H., Tietze, D., Imhof, D., Gales, C., Drewke, C., Müller, C.E., Hölzel, M., Milligan, G., Tobin, A.B., Gomeza, J., Dohlman, H.G., Sondek, J., Harden, T.K., Bouvier, M., Laporte, S.A., Aoki, J., Fleischmann, B.K., Mohr, K., König, G.M., Tüting, T., Kostenis, E., 2015. The experimental power of FR900359 to study Gq-regulated biological processes. Nat. Commun. 6, 10156. https://doi.org/10.1038/ncomms10156

Sekaran, S., Foster, R.G., Lucas, R.J., Hankins, M.W., 2003. Calcium imaging reveals a network of intrinsically light-sensitive inner-retinal neurons. Curr. Biol. 13, 1290–1298. https://doi.org/10.1016/S0960-9822(03)00510-4

Seong, J., Lin, M.Z., 2021. Optobiochemistry: Genetically Encoded Control of Protein Activity by Light. Annu. Rev. Biochem. 90, 475–501. https://doi.org/10.1146/annurev-biochem-072420-112431

Shatn, D., Yang, H., Mockler, T.C., Maymon, M., Guo, H., Whitelam, G.C., Lin, C., 2002. Regulation of Arabidopsis cryptochrome 2 by blue-light-dependent phosphorylation. Nature 417, 763–767. https://doi.org/10.1038/NATURE00815

Shcherbakova, D.M., Shemetov, A.A., Kaberniuk, A.A., Verkhusha, V. V., 2015. Natural Photoreceptors as a Source of Fluorescent Proteins, Biosensors, and Optogenetic Tools. Annu. Rev. Biochem. 84, 519–

550. https://doi.org/10.1146/annurev-biochem-060614-034411

Shichida, Y., Imai, H., 1998. Visual pigment: G-protein-coupled receptor for light signals. Cell. Mol. Life Sci. 54, 1299–1315. https://doi.org/10.1007/s000180050256

Shichida, Y., Matsuyama, T., 2009. Evolution of opsins and phototransduction. Philos. Trans. R. Soc. Lond. B. Biol. Sci. 364, 2881–95. https://doi.org/10.1098/rstb.2009.0051

Small, K.M., Brown, K.M., Forbes, S.L., Liggett, S.B., 2001. Modification of the β2-Adrenergic Receptor to Engineer a Receptor-Effector Complex for Gene Therapy. J. Biol. Chem. 276, 31596–31601. https://doi.org/10.1074/jbc.M102734200

Srinivasan, S., Santiago, P., Lubrano, C., Vaisse, C., Conklin, B.R., 2007. Engineering the melanocortin-4 receptor to control constitutive and ligand-mediated Gs signaling in vivo. PLoS One 2. https://doi.org/10.1371/journal.pone.0000668

Sriram, K., Insel, P.A., 2018. G protein-coupled receptors as targets for approved drugs: How many targets and how many drugs?, in: Molecular Pharmacology. pp. 251–258. https://doi.org/10.1124/mol.117.111062

Strader, C.D., Gaffney, T., Sugg, E.E., Rios Candelore, M., Keys, R., Patchett, A.A., Dixon, R.A.F., 1991. Allele-specific activation of genetically engineered receptors. J. Biol. Chem. 266, 5–8. https://doi.org/10.1016/s0021-9258(18)52392-9

Strathmann, M.P., Simon, M.I., 1991. Gα12 and Gα13 subunits define a fourth class of G protein α subunits. Proc. Natl. Acad. Sci. U. S. A. 88, 5582–5586. https://doi.org/10.1073/pnas.88.13.5582

Sugiyama, T., Suzuki, H., Takahashi, T., 2014. Light-induced rapid Ca^{2+} response and MAPK phosphorylation in the cells heterologously expressing human OPN5. Sci. Rep. 4, 5352. https://doi.org/10.1038/srep05352

Sunahara, R.K., Taussig, R., 2002. Isoforms of mammalian adenylyl cyclase: multiplicities of signaling. Mol. Interv. https://doi.org/10.1124/mi.2.3.168

Suzuki, N., Hajicek, N., Kozasa, T., 2009. Regulation and physiological functions of G12/13-mediated signaling pathways. NeuroSignals 17, 55–70. https://doi.org/10.1159/000186690

Tarttelin, E.E., Bellingham, J., Hankins, M.W., Foster, R.G., Lucas, R.J., 2003. Neuropsin (Opn5): A novel opsin identified in mammalian neural tissue. FEBS Lett. 554, 410–416. https://doi.org/10.1016/S0014-5793(03)01212-2

Terakita, A., 2005. The opsins. Genome Biol. 6, 213. https://doi.org/10.1186/gb-2005-6-3-213

Terakita, A., Koyanagi, M., Tsukamoto, H., Yamashita, T., Miyata, T., Shichida, Y., 2004. Counterion displacement in the molecular evolution of the rhodopsin family. Nat. Struct. Mol. Biol. 11, 284–9. https://doi.org/10.1038/nsmb731

Thoen, H.H., How, M.J., Chiou, T.-H., Marshall, J., 2014. A different form of color vision in mantis shrimp. Science 343, 411–3. https://doi.org/10.1126/science.1245824

Thompson, K.J., Khajehali, E., Bradley, S.J., Navarrete, J.S., Huang, X.P., Slocum, S., Jin, J., Liu, J., Xiong, Y., Olsen, R.H.J., Diberto, J.F., Boyt, K.M., Pina, M.M., Pati, D., Molloy, C., Bundgaard, C., Sexton, P.M., Kash, T.L., Krashes, M.J., Christopoulos, A., Roth, B.L., Tobin, A.B., 2018. DREADD Agonist 21 is an effective agonist for muscarinic-based DREADDs in vitro and in vivo. ACS Pharmacol.

Transl. Sci. 1, 61–72. https://doi.org/10.1021/acsptsci.8b00012

Tian, Y., Gao, S., von der Heyde, E.L., Hallmann, A., Nagel, G., 2018. Two-component cyclase opsins of green algae are ATP-dependent and light-inhibited guanylyl cyclases. BMC Biol. 16, 144. https://doi.org/10.1186/s12915-018-0613-5

Tichy, A.-M., Gerrard, E.J., Sexton, P.M., Janovjak, H., 2019. Light-activated chimeric GPCRs: limitations and opportunities. Curr. Opin. Struct. Biol. 57, 196–203. https://doi.org/10.1016/j.sbi.2019.05.006

Tomonari, S., Migita, K., Takagi, A., Noji, S., Ohuchi, H., 2008. Expression patterns of the opsin 5-related genes in the developing chicken retina. Dev. Dyn. 237, 1910–22. https://doi.org/10.1002/dvdy.21611

Tsukamoto, H., Terakita, A., 2010a. Diversity and functional properties of bistable pigments. Photochem. Photobiol. Sci. 9, 1435–43. https://doi.org/10.1039/c0pp00168f

Tsukamoto, H., Terakita, A., 2010b. Diversity and functional properties of bistable pigments. Photochem. Photobiol. Sci. 9, 1435–43. https://doi.org/10.1039/c0pp00168f

Tsutsui, K., Shichida, Y., 2010. Multiple functions of Schiff base counterion in rhodopsins. Photochem. Photobiol. Sci. 9, 1426–1434. https://doi.org/10.1039/C0PP00134A

Tu, P., Kunert-Keil, C., Lucke, S., Brinkmeier, H., Bouron, A., 2009. Diacylglycerol analogues activate second messenger-operated calcium channels exhibiting TRPC-like properties in cortical neurons. J. Neurochem. 108, 126–138. https://doi.org/10.1111/j.1471-4159.2008.05752.x

Vardy, E., Robinson, J.E., Li, C., Olsen, R.H.J., DiBerto, J.F., Giguere, P.M., Sassano, F.M., Huang, X.-P., Zhu, H., Urban, D.J., White, K.L., Rittiner, J.E., Crowley, N.A., Pleil, K.E., Mazzone, C.M., Mosier, P.D., Song, J., Kash, T.L., Malanga, C.J., Krashes, M.J., Roth, B.L., 2015. A New DREADD Facilitates the Multiplexed Chemogenetic Interrogation of Behavior. Neuron 86, 936–946. https://doi.org/10.1016/j.neuron.2015.03.065

Venter, J.C., Adams, M.D., Myers, E.W., Li, P.W., Mural, R.J., Sutton, G.G., Smith, H.O., Yandell, M., Evans, C.A., Holt, R.A., Gocayne, J.D., Amanatides, P., Ballew, R.M., Huson, D.H., Wortman, J.R., Zhang, Q., Kodira, C.D., Zheng, X.H., Chen, L., Skupski, M., Subramanian, G., Thomas, P.D., Zhang, J., Miklos, G.L.G., Nelson, C., Broder, S., Clark, A.G., Nadeau, J., Mckusick, V.A., Zinder, N., Levine, A.J., Roberts, R.J., Simon, M., Slayman, C., Hunkapiller, M., Bolanos, R., Delcher, A., Dew, I., Fasulo, D., Flanigan, M., Florea, L., Halpern, A., Hannenhalli, S., Kravitz, S., Levy, S., Mobarry, C., Reinert, K., Remington, K., Abu-Threideh, J., Beasley, E., Biddick, K., Bonazzi, V., Brandon, R., Cargill, M., Chandramouliswaran, I., Charlab, R., Chaturvedi, K., Deng, Z., Francesco, V. Di, Dunn, P., Eilbeck, K., Evangelista, C., Gabrielian, A.E., Gan, W., Ge, W., Gong, F., Gu, Z., Guan, P., Heiman, T.J., Higgins, M.E., Ji, R.-R., Ke, Z., Ketchum, K.A., Lai, Z., Lei, Y., Li, Z., Li, J., Liang, Y., Lin, X., Lu, F., Merkulov, G. V, Milshina, N., Moore, H.M., Naik, A.K., Narayan, V.A., Neelam, B., Nusskern, D., Rusch, D.B., Salzberg, S., Shao, W., Shue, B., Sun, J., Wang, Z.Y., Wang, A., Wang, X., Wang, J., Wei, M.-H., Wides, R., Xiao, C., Yan, C., Yao, A., Ye, J., Zhan, M., Zhang, W., Zhang, H., Zhao, Q., Zheng, L., Zhong, F., Zhong, W., Zhu, S.C., Zhao, S., Gilbert, D., Baumhueter, S., Spier, G., Carter, C., Cravchik, A., Woodage, T., Ali, F., An, H., Awe, A., Baldwin, D., Baden, H., Barnstead, M., Barrow, I., Beeson, K., Busam, D., Carver, A., Center, A., Cheng, M.L., Curry, L., Danaher, S., Davenport, L., Desilets, R., Dietz, S., Dodson, K., Doup, L., Ferriera, S., Garg, N., Gluecksmann, A., Hart, B., Haynes, J., Haynes, C., Heiner, C., Hladun, S., Hostin, D., Houck, J., Howland, T., Ibegwam, C., Johnson, J., Kalush, F., Kline, L., Koduru, S., Love, A., Mann, F., May, D., Mccawley, S., Mcintosh, T., Mcmullen, I., Moy, M., Moy, L., Murphy, B., Nelson, K., Pfannkoch, C., Pratts, E., Puri, V., Qureshi, H., Reardon, M., Rodriguez, R., Rogers, Y.-H., Romblad, D., Ruhfel, B., Scott, R., Sitter, C., Smallwood, M., Stewart, E., Strong, R.,

Suh, E., Thomas, R., Tint, N.N., Tse, S., Vech, C., Wang, G., Wetter, J., Williams, S., Williams, M., Windsor, S., Winn-Deen, E., Wolfe, K., Zaveri, J., Zaveri, K., Abril, J.F., Guigó, R., Campbell, M.J., Sjolander, K. V, Karlak, B., Kejariwal, A., Mi, H., Lazareva, B., Hatton, T., Narechania, A., Diemer, K., Muruganujan, A., Guo, N., Sato, S., Bafna, V., Istrail, S., Lippert, R., Schwartz, R., Walenz, B., Yooseph, S., Allen, D., Basu, A., Baxendale, J., Blick, L., Caminha, M., Carnes-Stine, J., Caulk, P., Chiang, Y.-H., Coyne, M., Dahlke, C., Mays, A.D., Dombroski, M., Donnelly, M., Ely, D., Esparham, S., Fosler, C., Gire, H., Glanowski, S., Glasser, K., Glodek, A., Gorokhov, M., Graham, K., Gropman, B., Harris, M., Heil, J., Henderson, S., Hoover, J., Jennings, D., Jordan, C., Jordan, J., Kasha, J., Kagan, L., Kraft, C., Levitsky, A., Lewis, M., Liu, X., Lopez, J., Ma, D., Majoros, W., Mcdaniel, J., Murphy, S., Newman, M., Nguyen, T., Nguyen, N., Nodell, M., Pan, S., Peck, J., Peterson, M., Rowe, W., Sanders, R., Scott, J., Simpson, M., Smith, T., Sprague, A., Stockwell, T., Turner, R., Venter, E., Wang, M., Wen, M., Wu, D., Wu, M., Xia, A., Zandieh, A., Zhu, X., 2001. The Sequence of the Human Genome.

Vögler, O., Barceló, J.M., Ribas, C., Escribá, P. V., 2008. Membrane interactions of G proteins and other related proteins. Biochim. Biophys. Acta - Biomembr. https://doi.org/10.1016/j.bbamem.2008.03.008

Vogt, M., Schulz, B., Wagdi, A., Lebert, J., van Belle, G.J., Christoph, J., Bruegmann, T., Patejdl, R., 2021. Direct optogenetic stimulation of smooth muscle cells to control gastric contractility. Theranostics 11, 5569–5584. https://doi.org/10.7150/thno.53883

Wada, S., Kawano-Yamashita, E., Koyanagi, M., Terakita, A., 2012. Expression of UV-sensitive parapinopsin in the iguana parietal eyes and its implication in UV-sensitivity in vertebrate pineal-related organs. PLoS One 7, e39003. https://doi.org/10.1371/journal.pone.0039003

Wada, S., Shen, B., Kawano-Yamashita, E., Nagata, T., Hibi, M., Tamotsu, S., Koyanagi, M., Terakita, A., 2018. Color opponency with a single kind of bistable opsin in the zebrafish pineal organ. Proc. Natl. Acad. Sci. U. S. A. 115, 11310–11315. https://doi.org/10.1073/pnas.1802592115

Wagdi, A., Malan, D., Sathyanarayanan, U., Beauchamp, J.S., Vogt, M., Zipf, D., Beiert, T., Mansuroglu, B., Dusend, V., Meininghaus, M., Schneider, L., Kalthof, B., Wiegert, J.S., König, G.M., Kostenis, E., Patejdl, R., Sasse, P., Bruegmann, T., 2022. Selective optogenetic control of Gq signaling using human Neuropsin. Nat. Commun. 13, 1765. https://doi.org/10.1038/s41467-022-29265-w

Wald, G., Hubbard, R., 1950. The Synthesis of Rhodopsin from Vitamin A(1). Proc. Natl. Acad. Sci. U. S. A. 36, 92–102. https://doi.org/10.1073/pnas.36.2.92

Wang, Huizhen, Han, H., Zhang, L., Shi, H., Schram, G., Nattel, S., Wang, Z., 2001. Expression of multiple subtypes of muscarinic receptors and cellular distribution in the human heart. Mol. Pharmacol. 59, 1029–1036. https://doi.org/10.1124/MOL.59.5.1029

Wang, H., Ma, L.G., Li, J.M., Zhao, H.Y., Xing Wang Deng, 2001. Direct interaction of Arabidopsis cryptochromes with COP1 in light control development. Science 294, 154–158. https://doi.org/10.1126/SCIENCE.1063630

Wietek, J., Rodriguez-Rozada, S., Tutas, J., Tenedini, F., Grimm, C., Oertner, T.G., Soba, P., Hegemann, P., Simon Wiegert, J., 2017. Anion-conducting channelrhodopsins with tuned spectra and modified kinetics engineered for optogenetic manipulation of behavior. Sci. Rep. 7. https://doi.org/10.1038/S41598-017-14330-Y

Xiang, Y., Kobilka, B.K., 2003. Myocyte adrenoceptor signaling pathways. Science 300, 1530–2. https://doi.org/10.1126/science.1079206

Xie, Z., Ho, W.T., Spellman, R., Cai, S., Exton, J.H., 2002. Mechanisms of regulation of phospholipase D1 and D2 by the heterotrimeric G proteins G13 and Gq. J. Biol. Chem. 277, 11979–11986.

https://doi.org/10.1074/jbc.M109751200

Xu, N., Voyno-Yasenetskaya, T., Silvio Gutkind, J., 1994. Potent transforming activity of the G13 α subunit defines a novel family of oncogenes. Biochem. Biophys. Res. Commun. 201, 603–609. https://doi.org/10.1006/bbrc.1994.1744

Yamashita, T., Ohuchi, H., Tomonari, S., Ikeda, K., Sakai, K., Shichida, Y., 2010. Opn5 is a UV-sensitive bistable pigment that couples with Gi subtype of G protein. Proc. Natl. Acad. Sci. U. S. A. 107, 22084–22089. https://doi.org/10.1073/pnas.1012498107

Yamashita, T., Ono, K., Ohuchi, H., Yumoto, A., Gotoh, H., Tomonari, S., Sakai, K., Fujita, H., Imamoto, Y., Noji, S., Nakamura, K., Shichida, Y., 2014. Evolution of mammalian Opn5 as a specialized UV-absorbing pigment by a single amino acid mutation. J. Biol. Chem. 289, 3991–4000. https://doi.org/10.1074/jbc.M113.514075

Yang, H.Q., Wu, Y.J., Tang, R.H., Liu, D., Liu, Y., Cashmore, A.R., 2000. The C termini of Arabidopsis cryptochromes mediate a constitutive light response. Cell 103, 815–827. https://doi.org/10.1016/S0092-8674(00)00184-7

Yang, S., Zhou, J., Li, D., 2021. Functions and Diseases of the Retinal Pigment Epithelium. Front. Pharmacol. 12. https://doi.org/10.3389/FPHAR.2021.727870

Yizhar, O., Fenno, L.E., Davidson, T.J., Mogri, M., Deisseroth, K., 2011. Optogenetics in Neural Systems. Neuron. https://doi.org/10.1016/j.neuron.2011.06.004

Yoshida, K., Tsunoda, S.P., Brown, L.S., Kandori, H., 2017. A unique choanoflagellate enzyme rhodopsin exhibits lightdependent cyclic nucleotide phosphodiesterase activity. J. Biol. Chem. 292, 7531–7541. https://doi.org/10.1074/jbc.M117.775569

Zhang, H., Fang, H., Liu, D., Zhang, Y., Adu-Amankwaah, J., Yuan, J., Tan, R., Zhu, J., 2022. Applications and challenges of rhodopsin-based optogenetics in biomedicine. Front. Neurosci. 16, 966772. https://doi.org/10.3389/fnins.2022.966772

Zhang, K.X., D'Souza, S., Upton, B.A., Kernodle, S., Vemaraju, S., Nayak, G., Gaitonde, K.D., Holt, A.L., Linne, C.D., Smith, A.N., Petts, N.T., Batie, M., Mukherjee, R., Tiwari, D., Buhr, E.D., Van Gelder, R.N., Gross, C., Sweeney, A., Sanchez-Gurmaches, J., Seeley, R.J., Lang, R.A., 2020. Violet-light suppression of thermogenesis by opsin 5 hypothalamic neurons. Nature 585, 420–425. https://doi.org/10.1038/s41586-020-2683-0

Acknowledgments

I want to express my most profound appreciation and gratitude to all those who have contributed to the successful completion of my Ph.D. thesis. Firstly, I extend my heartfelt thanks to my mentor and supervisor Prof. Dr. med. Dr. rer. nat. Tobias Brügmann, whose unwavering support and guidance have been invaluable throughout my doctoral research journey. His expertise, encouragement, and willingness to share scientific inputs have been instrumental in shaping the direction of this work.

I want to acknowledge the contributions of my thesis committee members Prof. Tobias Moser and Prof. Ralph Kehlenbach, who willingly dedicated their time and effort to provide valuable suggestions and insights. Their involvement has been crucial in shaping the outcomes of this research. I would also like to take this opportunity and thank my external examination board members, Prof. Oliver Schluter, Prof. Susanne Lutz, and Prof. Tim Gollisch for their readiness to be a part of the examination committee.

I am immensely grateful to all my research colleagues and fellow lab members for their cooperation and assistance during the entire time of my thesis work. I want to thank Melanie von Ahlen for her excellent technical support. I am glad to have been able to share the ups and downs of my doctoral journey with Svenja Kiehn, a fellow Ph.D. colleague and a good friend. I am thankful to her for being a great support in this journey. Dr. med. Marc Hüser, my best lab buddy, it was a pleasure to have him listen to my frustrations and share my positive milestones throughout the time spent in and outside the workplace. Other lab members including Carolin Radnik, Runzhu Shi, David Zipf, Marius Reichardt, Markus Vogt, Noelia Bellón, Lena Krause, Hiu Lam Wong and Martin Draband are the best lab members one can ask for during a Ph.D. expedition. Everyone's diverse perspectives, insightful discussions, and willingness to lend a helping hand have undoubtedly enriched this project and broadened my understanding of the subject matter. Also, a special thanks to Alexander Wenger for the IT support at times of need.

I am grateful to our neighboring labs, Prof. Dr. Dörthe M Katschinski, Head of the department, and Prof. Dr. Ivan Bogeski for allowing me to use their lab equipment as and when required for my project. It was and still will be a pleasure to meet all the neighboring fellow lab members over social gatherings or to pass by the corridor and have an informative chit-chat over coffee.

Finally, I am indebted to my family, friends, and loved ones for their unwavering support, encouragement, and understanding throughout this strenuous endeavor. My wife and soon-to-be mom, Dr. Maithily Nanadikar, also a neighboring lab member, is the strongest pillar to have by my side in the good and bad times during my career. This journey wouldn't be possible for me without her understanding, care, love and support over the past seven years. I am immensely thankful to my proud parents, grandparents, sister and my in-laws back in India who showed complete belief in me to conquer my dreams. A special thanks to my friends Amandeep Singh Arora, Shilpa Patil, Sandip Rath, Praveen Kumar Natramilarasu and Vignesh Gnanaskandan for their love, support and belief in me, which has driven my perseverance and determination.

This Ph.D. work wouldn't have been possible without all these individuals' collective support and collaboration. I am genuinely grateful for their contributions and for being an integral part of this meaningful journey.